Delta-Suisun Biogeochemical Model: Calibration and Validation (WY2016, WY2011)

Contributors:

Sienna R. White, Pradeep Mugunthan, Allie T. King, Farid Karimpour,
Lisa V. Lucas, David B. Senn

With technical assistance from:

Elizabeth B. Stumpner, Tamara E.C. Kraus, Brian A. Bergamaschi

September 2021

SFEI Contribution No. 1056

Table of Contents

1 Introduction 1

2 Methods 2

2.1 Overview of Coupled Hydrodynamic-Biogeochemical Model 2

2.2 Hydrodynamic Model Development and Validation 3

2.3 Biogeochemical Model Development 6

2.4 Biogeochemical Model Validation Data 14

2.5 Biogeochemical Model Validation Approach 21

3 Results 23

3.1 Discrete Data: Modeled-Measured Comparisons 23

3.2 High-Frequency Moorings 32

3.3 High-Frequency Flux Measurements 38

3.4 USGS Mapping Cruises 43

3.5 Grazing 56

4 Summary 61

5 References 63

APPENDICES

Appendix A: Hydrodynamic boundary conditions

Appendix B: POTW nutrient loading time series

Appendix C: Light attenuation field

Appendix D: USGS data processing methodology

Appendix E: Final Parameter Set

LIST OF FIGURES

Figure 2.1. Computational domain and full-resolution model grid..... 3

Figure 2.2. Hydrodynamic model boundary locations within the Suisun-Delta domain..... 4

Figure 2.3. Hydrodynamic model boundary conditions relevant to the interpretation of biogeochemical model results for WY2011 and WY2016.. 5
Figure 2.4. Sacramento River flow (near Verona), monthly averages, colored by water year. 5
Figure 2.5. San Joaquin River flow (near Vernalis), monthly averages, colored by water year. 6
Figure 2.6. Conceptual diagram illustrating the processes and state variables simulated in the current version of the SFE-BGCM. 7
Figure 2.7. Locations of point source inputs for the biogeochemical model. 10
Figure 2.9. Spatial maps of interpolated initial conditions for chlorophyll-a, nitrate, and phosphate. 11
Figure 2.10. Clam initial condition for *Corbicula* (freshwater clam) and *Potamocorbula* (saltwater clam). 12
Figure 2.11. Time series extracted from the interpolated turbidity grid. 13
Figure 2.12. Spatial maps of light attenuation coefficient (k_d) at timestamps in November and July 2016. 13
Figure 2.13. Shallow cells in Cache Slough with adjusted diatom growth rate during the simulation. 14
Figure 2.14. Map of the discrete sampling stations used for model validation. 15
Figure 2.15. Map of U.S. Geological Survey-operated continuous monitoring flow and water-quality stations in the Delta. 16
Figure 2.16. Map of sites sampled during a benthic survey on October 15, 2016. 19
Figure 2.17. Box plots of *Potamocorbula* biomass in Suisun Bay. 20
Figure 2.18. Boxplots of *Corbicula* biomass in Suisun Bay. 20
Figure 2.19. *Corbicula* Biomass in Cache Slough and the lower Sacramento River. 21
Figure 2.20. Zooplankton biomass time series. 21
Figure 2.21. Zooplankton biomass time series (Figure 2.20) converted to grazing rate using methodology defined by Lopez (2006). 21
Figure 3.1. WY2016 model validation of nitrate at discrete sampling sites. 23
Figure 3.2. WY2016 model validation of ammonium at discrete sampling sites. 24
Figure 3.3. WY2016 model validation of dissolved inorganic nitrogen at discrete sampling sites. 24
Figure 3.4. WY2016 model validation of phosphate at discrete sampling sites. 25
Figure 3.5. WY2016 model validation of silica at discrete sampling sites. 25
Figure 3.6. WY2016 model validation of dissolved oxygen at discrete sampling sites. 26
Figure 3.7. WY2016 model validation of chlorophyll-a at discrete sampling sites. 26
Figure 3.8. WY2011 model validation of nitrate at discrete sampling sites. 27
Figure 3.9. WY2011 model validation of ammonium at discrete sampling sites. 27

Figure 3.10. WY2011 model validation of dissolved inorganic nitrogen at discrete sampling sites. 28
Figure 3.11. WY2011 model validation of phosphate at discrete sampling sites. 28
Figure 3.12. WY2011 model validation of silica at discrete sampling sites. 29
Figure 3.13. WY2011 model validation of dissolved oxygen at discrete sampling sites. 29
Figure 3.14. WY2011 model validation of chlorophyll-a at discrete sampling sites. 30
Figure 3.15. Model validation with the high frequency mooring site at the Sacramento River at Freeport 33
Figure 3.16. Model validation with the high frequency mooring site at the Delta Cross Channel 34
Figure 3.17. Model validation with the high frequency mooring site at Cache Slough at Ryer Island 36
Figure 3.18. Model validation with the high frequency mooring site at Decker Island near Rio Vista 37
Figure 3.19. Plots of discharge, concentration, instantaneous and cumulative flux of both nitrate and chlorophyll-a at Freeport. 39
Figure 3.20. Plots of discharge, concentration, instantaneous and cumulative flux of both nitrate and chlorophyll-a above Delta Cross Channel near Walnut Grove. 40
Figure 3.21. Plots of discharge, concentration, instantaneous and cumulative flux of both nitrate and chlorophyll-a above Delta Cross Channel at Cache Slough near Ryer Island. 41
Figure 3.22. Plots of discharge, concentration, instantaneous and cumulative flux of both nitrate and chlorophyll-a at Decker Island. 42
Figure 3.23. Model validation with mapping cruise data on October 21, 2015 for nitrate. 44
Figure 3.24. Model validation with mapping cruise data on October 21, 2015 for chlorophyll-a. 45
Figure 3.25. Model validation with mapping cruise data on October 21, 2015 for DO. 46
Figure 3.26. Model validation with mapping cruise data on April 18, 2016 for nitrate. 47
Figure 3.27. Model validation with mapping cruise data on April 18, 2016 for chlorophyll-a. 48
Figure 3.28. Model validation with mapping cruise data on April 18, 2016 for dissolved oxygen. 49
Figure 3.29. Model validation with mapping cruise data on May 6, 2016 for nitrate. 50
Figure 3.30. Model validation with mapping cruise data on May 6, 2016 for chlorophyll-a 51
Figure 3.31. Model validation with mapping cruise data on May 6, 2016 for dissolved oxygen 52
Figure 3.32. Model validation with mapping cruise data on June 9, 2016 for nitrate. 53
Figure 3.33. Model validation with mapping cruise data on June 9, 2016 for chlorophyll-a. 54
Figure 3.34. Model validation with mapping cruise data on June 9, 2016 for dissolved oxygen. 55
Figure 3.35. WY2011 modelled grazing rates compared to U.S. Geological Survey CONSBL grazing rates (December 2010). 58
Figure 3.36. WY2011 modelled grazing rates compared to U.S. Geological Survey CONSBL grazing rates (April 2011). 59

Figure 3.37. WY2011 modelled grazing rates compared to U.S. Geological Survey CONSBL grazing rates (June 2011). 60

LIST OF TABLES

Table 2.1. Discrete sampling stations used for model validation. 15

Table 2.2. U.S. Geological Survey operated continuous monitoring flow and water-quality stations in the Delta. 16

Table 2.3. List of USGS high-resolution water-quality mapping dates, location, and associated project or event used for calibration and validation of WY2016 model. 18

Table 2.4. Final calibrated model parameter values. 22

ACRONYMS AND ABBREVIATIONS

ADVM	acoustic Doppler velocity meters
chl-a	chlorophyll-a
CTDEN	critical cut-off temperature
DCC	Delta Cross Channel
DEB	dynamic energy budget
Delta	Sacramento and San Joaquin River Delta
DFM	D-Flow Flexible Mesh
DIN	dissolved inorganic nitrogen levels
DO	dissolved oxygen
DWAQ	D-Water Quality
DWR	California Department of Water Resources
EMP	Environmental Monitoring Program
GRTS	generalized random tessellation stratified
Kd	light extinction
nSFE	northern San Francisco Estuary
nSFE-BGCM	northern San Francisco Estuary biogeochemical model
POTW	publicly-owned treatment work
SFB-BGCM	San Francisco Bay biogeochemical model
SFB-LSB-BGCM	Lower South Bay biogeochemical model
SFE-BGCM	San Francisco Estuary biogeochemical model
USGS	U.S. Geological Survey
WY2011	water year 2011
WY2016	water year 2016

ACKNOWLEDGEMENTS

The work presented in this report was supported by funding from the Delta Regional Monitoring Program, a grant from the California State Water Board, and funding from the San Francisco Bay Nutrient Management Strategy. Thank you to J. Thompson (USGS), and W. Kimmerer (SFSU) for sharing data and insights related to benthic and zooplankton grazing.

Suggested Citation:

SFEI (2021) Delta-Suisun Biogeochemical Model: Calibration and Validation (WY2016, WY2011). SFEI Contribution #1056. San Francisco Estuary Institute, Richmond, CA.

1 Introduction

The northern San Francisco Estuary (nSFE), including Suisun Bay and the Delta, serves as a critical aquatic habitat and vital water resource for both domestic consumption and irrigation. The nSFE receives large inputs of anthropogenic nutrients, resulting in elevated dissolved inorganic nitrogen levels (DIN; Jassby 2008; SFEI 2015) that exceed levels linked to adverse impacts in many other freshwater and estuarine systems (Paerl 2009; Dahm et al. 2016). The nSFE's nutrient-enriched status is a high-priority management issue, with regulators and environmental managers evaluating potential linkages between excess nutrients and several pressing ecological health issues (SFBRWQCB 2012; DSC 2013; CVRWQCB 2015; Cooke et al. 2018; SFEI 2020a). Quantitative, mechanistic understanding of nutrient cycling and nutrient-related ecosystem responses are needed to help inform on-going adaptive management and future management decisions in the Delta and San Francisco Bay. Given the physical and biogeochemical complexities of the nSFE, numerical models which are capable of simulating coupled hydrodynamics and biogeochemistry will be important tools in supporting science-based decision making.

Work has been underway over the past several years developing the San Francisco Estuary Biogeochemical Model (SFE-BGCM), a 3-D coupled hydrodynamic-biogeochemical model capable of simulating nutrient transport, nutrient cycling, and ecosystem responses (e.g., phytoplankton production). Initial work focused on model development, sensitivity analysis, and model calibration (SFEI 2018a,b; 2019a,b,c; 2020b,c).

This report describes recent (Sep 2020 – Aug 2021) improvements to the biogeochemical model and updates the model calibration and validation, which includes comparisons with additional observational data. This project's goals are summarized below:

- Set up a numerical biogeochemical simulation of the Delta and Suisun Bay systems for water year 2016 (WY2016) using the previously-developed version of the model that had been used to simulate WY2011.
- Implement refinements to the model, including improvements to boundary conditions, initial conditions, and key model inputs (e.g., light attenuation), along with refinements to sediment diagenesis, clam and zooplankton grazing, phytoplankton growth, and water column nutrient transformations.
- Incrementally refine the model to obtain the best "global" calibration for WY2016 and WY2011, two water years that differed considerably in both physical forcings (dry vs. wet) and biogeochemical responses.
- Evaluate model performance against additional observational data, including from high-frequency moorings and high-resolution biogeochemical mapping surveys from WY2016.

2 Methods

This section begins with an overview of the model platform and domain (Section 2.1-2.2), and then describes changes and improvements to the original model (nSFE-BGCM.v1; SFEI 2018, 2019) that have been incorporated into the current version (nSFE-BGCM.v2). The improvements include changes to: water column transformations and sediment diagenesis (Section 2.3.1); adjustments to clam and zooplankton initial conditions and grazing rates informed by comparisons with biomass and grazing data from a complementary modeling effort (Section 2.3.1, 2.4.5); refining boundary conditions for nutrient loading from both freshwater sources and publicly-owned treatment works (POTWs; Section 2.3.2); developing spatially varying initial conditions for nutrient concentrations (Section 2.3.3); and an interim fix of a wetting/drying-related issue within the Yolo Bypass (Section 2.3.6).

While the majority of this report's simulations and interpretations focused on WY2016, the model version, nSFE-BGCM.v2, represents the best "global" calibration currently available across WY2016 and WY2011. Compared to WY2016, WY2011 was a relatively wet year, without major bloom activity during the spring. Additionally, there are benthic grazing data available during WY2011 that enabled further refinements of the dynamic energy budget (DEB) grazing module.

2.1 Overview of Coupled Hydrodynamic-Biogeochemical Model

For this project, model development and WY2016 Delta-Suisun biogeochemical simulations were carried out using the San Francisco Estuary Biogeochemical Model (SFE-BGCM; SFEI 2018a,b, 2019a, 2020b), a 3D, process-based, spatially-explicit model that is externally coupled to the hydrodynamic model. The SFE-BGCM uses the public-domain/open-source models D-Flow Flexible Mesh (DFM; Deltares 2019a) to simulate hydrodynamics; D-Water Quality (DWAQ; Deltares 2019b) to simulate water quality; and a suite of Python-based utilities to facilitate model setup and post-processing (more info on the original open-source project can be found here: [https://www.usgs.gov/mission-areas/water-resources/science/cascade-computational-assessments-scenarios-change-delta]).

SFEI maintains three branches of the overarching SFE-BGCM, which focus on different regions of the San Francisco Estuary: the northern San Francisco Estuary model (Delta, Suisun; nSFE-BGCM); the San Francisco Bay model (SFB-BGCM); and the Lower South Bay model (SFB-LSB-BGCM). The biogeochemical modules for each of the regional models have the same baseline capabilities, and relevant updates or improvements made initially within one regional model are easily applied to other regional models. This project, which focuses on the Delta, utilized the northern San Francisco Estuary model.

The nSFE-BGCM grid and bathymetry were originally developed as part of the USGS CASCaDE project (Martyr-Koller et al. 2017). The nSFE-BGCM domain includes the Delta and San Francisco Bay and extends into the Pacific Ocean, about 20 km west of Point Reyes in the north and 40 km west of Half Moon Bay in the south, roughly encompassing the San Francisco Bight (Figure 2.1). The model employs a 3D unstructured grid with 75,019 horizontal cells and 10 vertical sigma layers. The grid has a higher resolution in the Delta and Suisun Bay and lower resolution in San Francisco Bay and the coastal ocean. Martyr-Koller et al. (2017) calibrated the hydrodynamics for March-September 2000 by adjusting spatially varying bottom friction to predict flow, water surface elevation, and salinity throughout the Delta and Suisun Bay. The model was then validated for WY2011 and WY2012. Vroom et al. (2017)

further developed the hydrodynamic model by incorporating a heat budget module and adding meteorological forcing to predict water temperature.

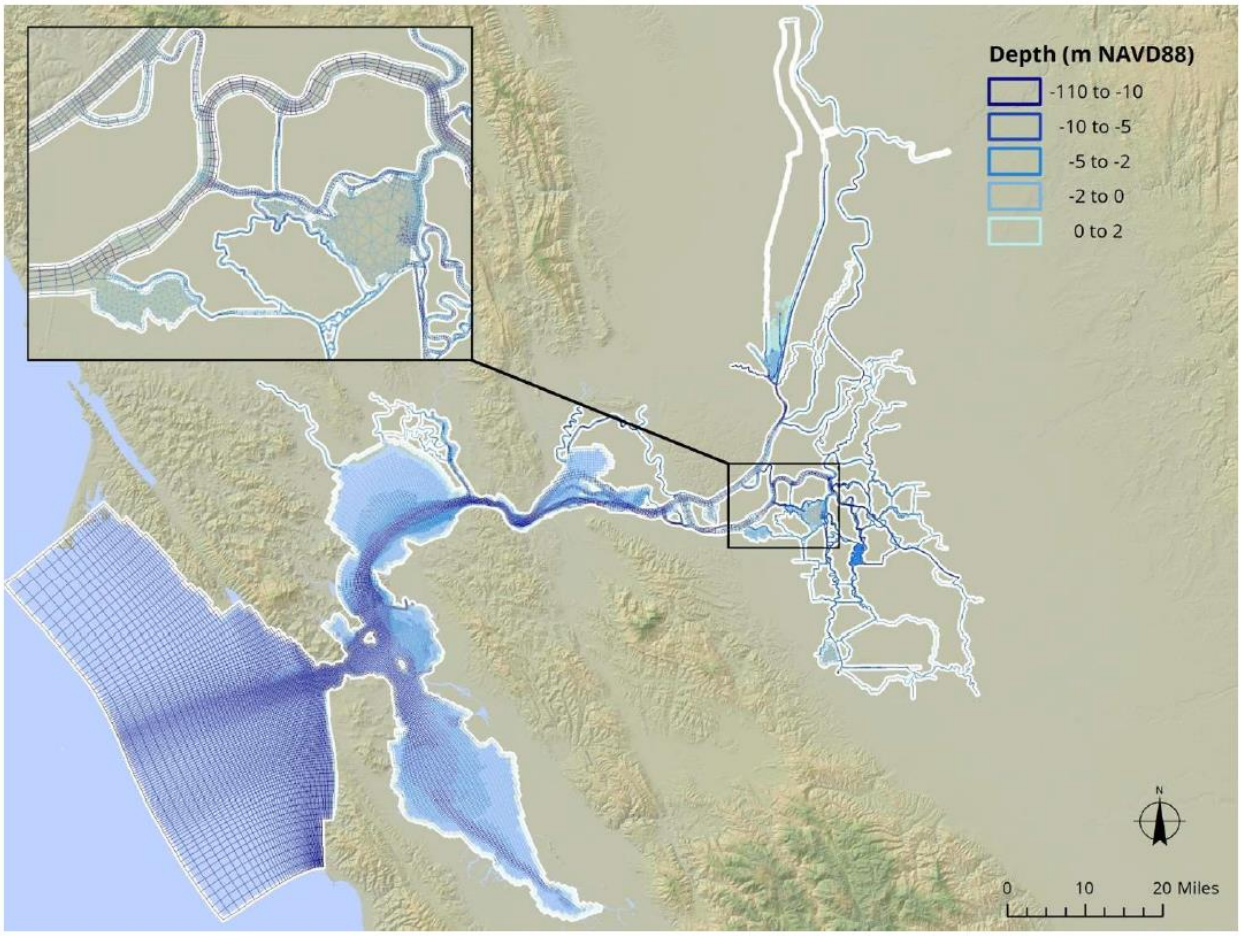

Figure 2.1. Computational domain and full-resolution model grid.

The first round of model development for the nSFE-BGCM focused on WY2011 (SFEI 2018b, 2019a). The updated biogeochemical module from the SFB-BGCM (SFEI 2018a) was applied to the WY2011 hydrodynamic model from Martyr-Koller et al. (2017) and calibrated for the Delta. A next major round of biogeochemical model development was carried out using the SFB-BGCM (SFEI 2020b).

2.2 Hydrodynamic Model Development and Validation

The hydrodynamic model was originally developed, calibrated, and validated for WY2011-WY2012 (Martyr-Koller et al. 2017). An early component of the current project involved refining and updating the model to simulate WY2016, including developing WY2016 boundary conditions and forcing datasets, and validating model output against observational data. The validation demonstrated good agreement between WY2016 predictions and observations, specifically continuous and tidally-averaged elevation, discharge, salinity, and temperature across locations in the Delta and Suisun Bay (SFEI 2019b). The WY2016 hydrodynamic output was used to drive this project's WY2016 biogeochemical simulations.

The locations of freshwater inflows, pumps, permanent structures, and temporary barriers for the hydrodynamic model within the Suisun-Delta domain are illustrated in Figure 2.2. Figure 2.3 shows a

time series of model boundary conditions most relevant to the interpretation of the biogeochemical model results, namely the freshwater inflows, the two largest withdrawals (from the State Water Project [at Clifton Court] and Central Valley Project), and the operation of the Delta Cross Channel (DCC). More complete hydrodynamic model boundary conditions are plotted in Appendix A.

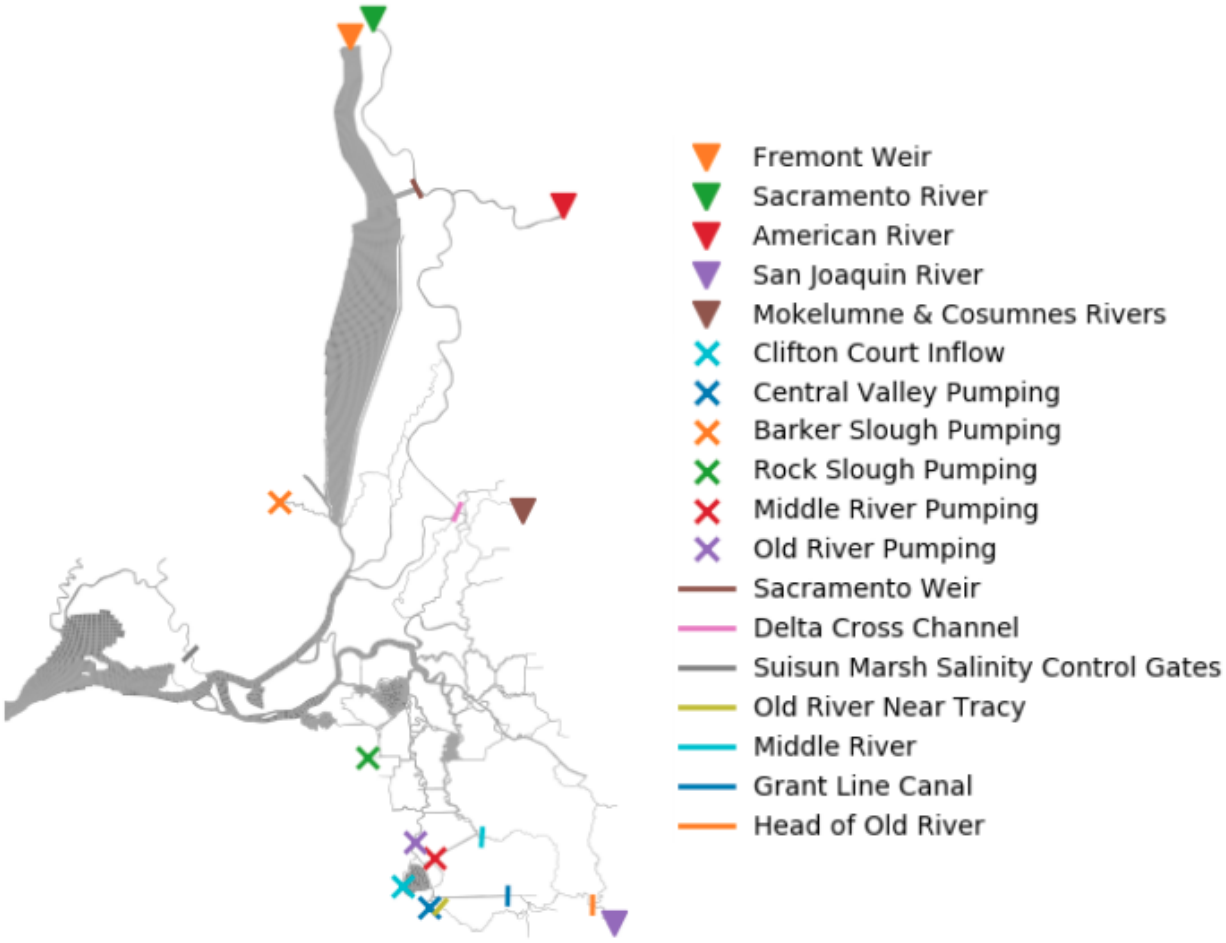

Notes: Tributaries (triangles), pumps (x), permanent structures (Sacramento Weir, Delta Cross Channel, Suisun Marsh Salinity Control Gates, indicated by short lines), and temporary barriers (remaining short lines)

Figure 2.2. Hydrodynamic model boundary locations within the Suisun-Delta domain.

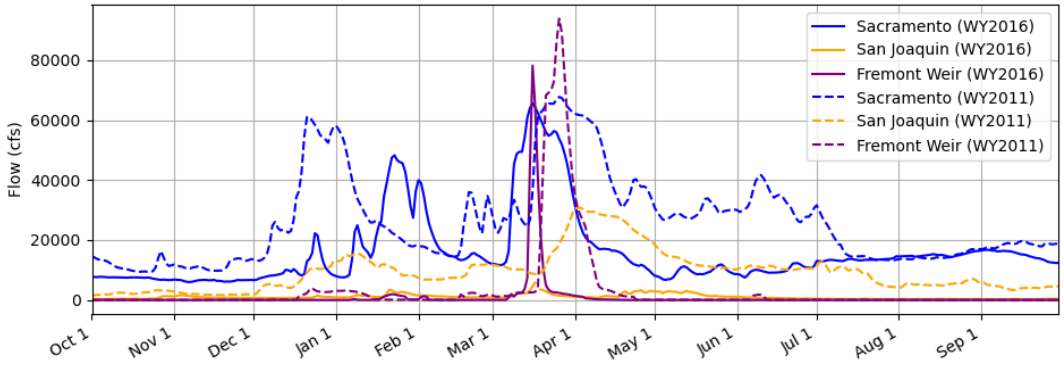

Figure 2.3. Hydrodynamic model boundary conditions relevant to the interpretation of biogeochemical model results for WY2011 and WY2016.

For WY2016, the California Department of Water Resources (DWR) runoff index was specified as "below normal" for the Sacramento Valley and "dry" for the San Joaquin Valley. Figures 2.4 and 2.5 show historical flow rates for the Sacramento River (at Verona) and the San Joaquin River (near Vernalis) by water year from 2001 through 2018, illustrating that in early WY2016 the Sacramento and San Joaquin River flows were moderately low and low, respectively. These figures also illustrate that the variance in San Joaquin River flows from year to year is high compared to the variance in Sacramento River flows, and while Sacramento River flows are typically much higher than San Joaquin River flows, as they were in WY2016 (by an order of magnitude), in some years, such as WY2011, the flows from the two rivers are more comparable. Note that while during the winter (Jan-April), the flow from the Sacramento River is comparable between water years (Figure 2.3), the flow over the Fremont Weir into the Yolo Bypass is significantly higher in WY2011. For the rest of the springtime, flows in the Sacramento are nearly 2x higher in WY2011 than WY2012.

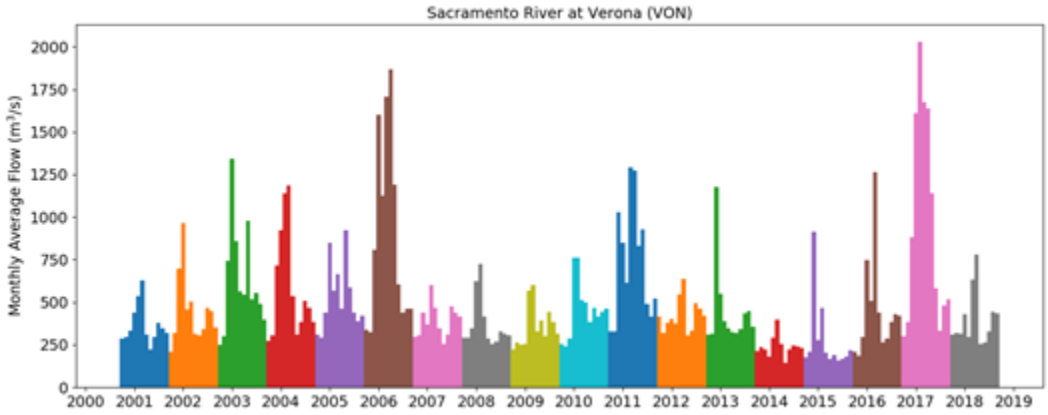

Figure 2.4. Sacramento River flow (near Verona), monthly averages, colored by water year.

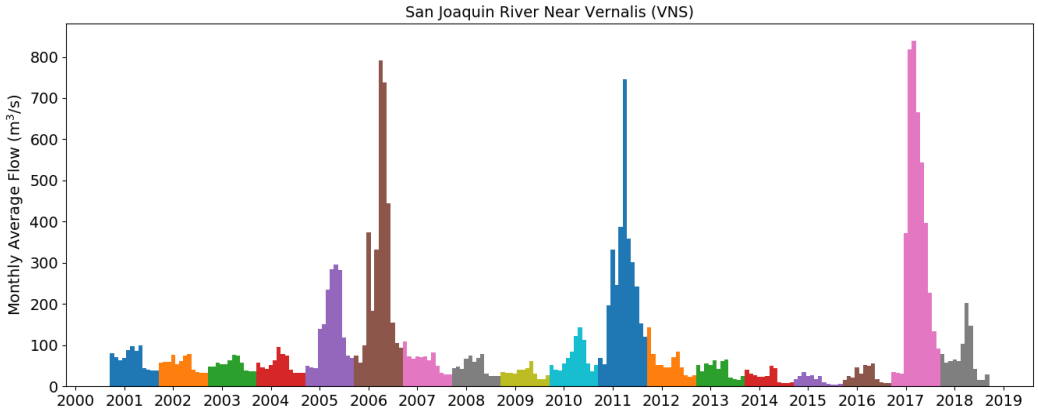

Figure 2.5. San Joaquin River flow (near Vernalis), monthly averages, colored by water year.

2.3 Biogeochemical Model Development

2.3.1 Model Framework and Processes Simulated

2.3.1.1 Water Column and Sediment Biogeochemical Process Framework

The conceptual diagram in Figure 2.6 provides an overview of the processes and state variables simulated within the current implementation of the SFE-BGCM. Equations for all processes included in the model (listed below) can be found in Deltares (2019b).

Water Column Processes

- Microbial water column processes: nitrification, respiration (DO consumption), and remineralization of organic matter (converting organic forms of nutrients, including dead phytoplankton, to inorganic forms)
- Phytoplankton: growth (including uptake/assimilation of nutrients, production of new biomass) and death
- Grazers: grazing (consumption of phytoplankton), excretion of nutrients, growth (increased biomass), and death
- Oxygen (O2) exchange between the water column and atmosphere
- Light attenuation by suspended sediment and phytoplankton

Sediment Processes

- Microbial sediment processes: nitrification, denitrification, aerobic respiration (DO consumption), and mineralization of organic matter (converting organic forms of nutrients to inorganic forms)
- Benthic grazing: filtration/consumption of phytoplankton and detritus, excretion of nutrients, growth (increased biomass), reproduction, and death
- Accumulation of organic matter (settling from the water column) and mixing/bioturbation of sediments
- Sediment-water exchanges: flux of ammonium (NH4), nitrate (NO3), phosphate (PO4), and silicon (Si) from the sediments to the water column; flux of nitrate and oxygen from the water column to the sediments; and denitrification and oxygen consumption at the sediment-water interface

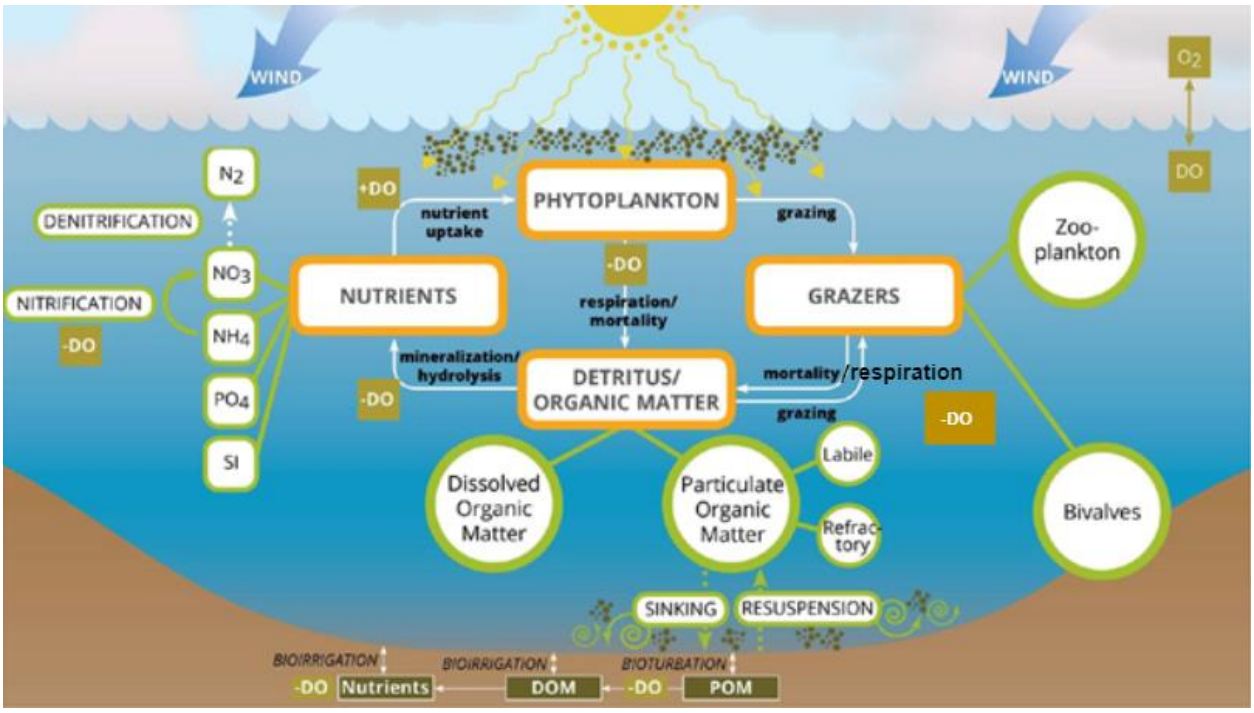

Figure 2.6. Conceptual diagram illustrating the processes and state variables simulated in the current version of the SFE-BGCM.

2.3.1.2 Dynamic Energy Budget Grazing Model

Grazing by both benthic (clams) and pelagic (zooplankton) grazers is thought to play a prominent and often dominant role in regulating primary production levels and activity throughout the Delta (Cloern 1982; Lucas et. al 2016; Crauder 2016; Lucas and Thompson 2012). Grazing is simulated in SFE-BGCM using DWAQ's DEB module for two species of clams: *Corbicula Fluminea*, a freshwater clam, and *Potamocorbula Amurensis*, a saltwater clam. Compared to other methodologies, where grazing is imposed as a boundary condition (via time and/or space varying grazing rates), the DEB module allows for clam and zooplankton biomass to react dynamically to changing food availability and environmental conditions. This means that grazing pressure at any point in time is a function of both current conditions as well as conditions over prior days to months within the system. The DEB approach complicates calibration/validation significantly, as the module requires calibration over a large parameter space and is difficult to validate with the limited data available. However, developing biogeochemical models with predictive/forecasting capacities remains an ongoing priority within the modeling project scope, and effort was invested into strengthening the application of the DEB model to improve the understanding of grazing throughout the system.

2.3.2 Boundary Conditions

2.3.2.1 Freshwater Inflows

The methodology used to derive nutrient loading for the WY2016 model is similar to that of the WY2011 Delta biogeochemical model (SFEI 2019a). The nitrate concentration time series imposed at the Sacramento River (at Verona) was estimated using high-frequency mooring data from Freeport (note the Freeport is downstream of Sacramento at Verona). The mooring data was down-sampled from 15-

minutes to a daily average. All other freshwater nitrate boundary conditions were estimated using concentration data from nearby DWR Environmental Monitoring Program (EMP) monthly discrete sampling sites. For WY2016, phosphate and silica data were not available for the Sacramento River. The Sacramento River phosphate load at Verona was estimated using a mass balance on the phosphate loads from the American River and the Sacramento River at Freeport (which is downstream of the confluence with the American River). The difference was assumed to be the phosphate load from the Sacramento River (at Verona) and the resulting mass was converted back into concentration. Silica data were not available at the American River and Sacramento River boundaries. Therefore, silica concentrations from the USGS discrete sampling station at Freeport were used for both boundaries. The Freemont Weir was assigned a constant dissolved silica concentration of 5.6 mg/L based on historical observations of background silica levels (Peterson 1978). Ammonium and DO loading data were available at discrete sampling sites for all boundaries. The resulting time series for nutrient loading from freshwater sources are shown in Figure 2.7. Chlorophyll-a is imposed at the San Joaquin and Sacramento River boundaries in units of algal biomass (gC/m^3), with data obtained from nearby DWR-EMP discrete sampling sites.

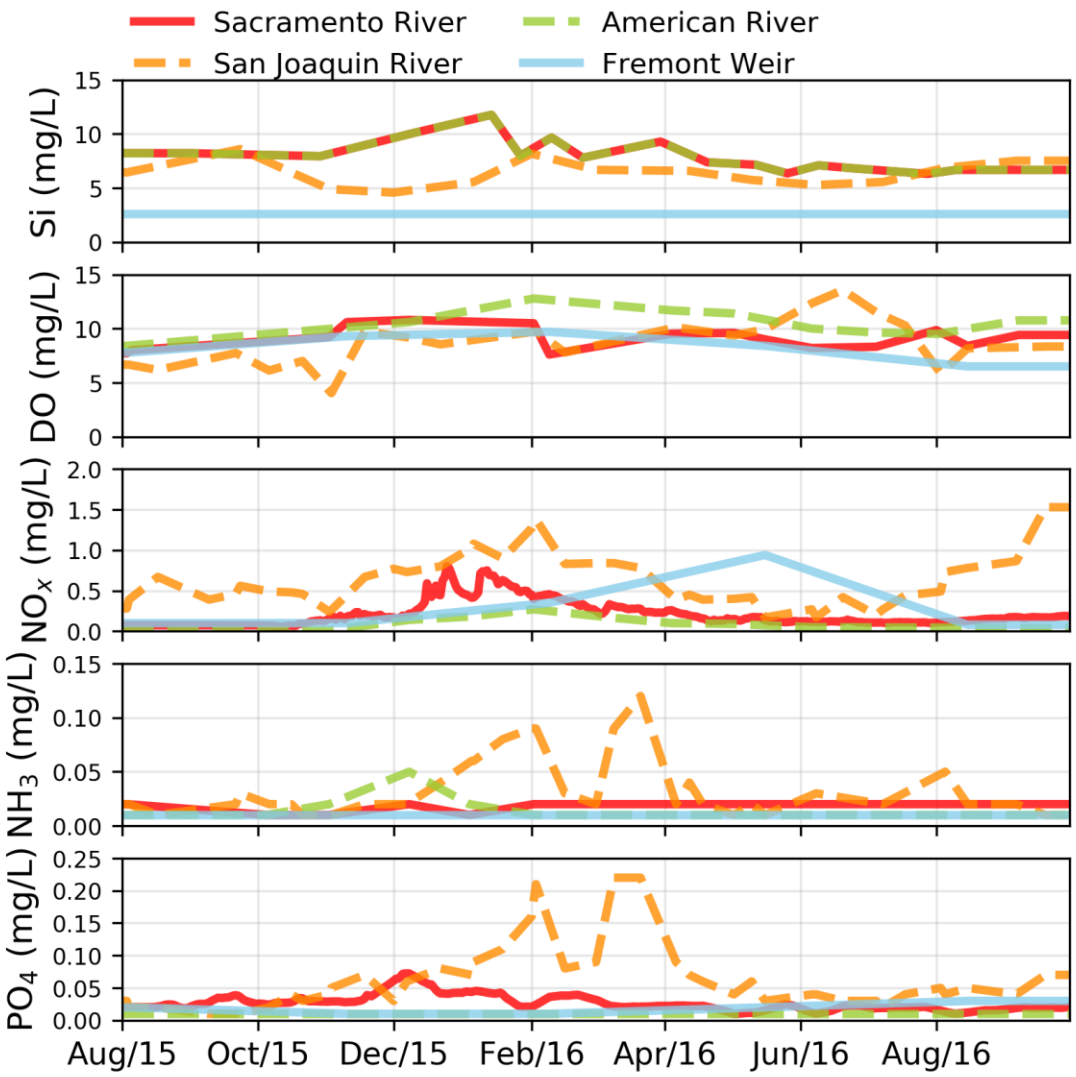

Figure 2.7. Time series of nutrient loadings at the freshwater boundary points for Sacramento @ Verona, San Joaquin near Mossdale, the American River and the Fremont Weir.

2.3.2.2 Point Sources

At point sources, including POTWs and refineries (Figure 2.8), influx (mass per unit time) of ammonia, nitrogen oxide, and phosphate is specified based on monitoring data (Figure 2.8). For sources with data gaps, long-term trend analysis was used to fill the gaps. Loads for the Stockton POTW were updated to use measurements rather than a long-term trend analysis, thereby increasing the accuracy of loading in the South Delta region. The resulting nutrient loading time series are shown in Appendix B.

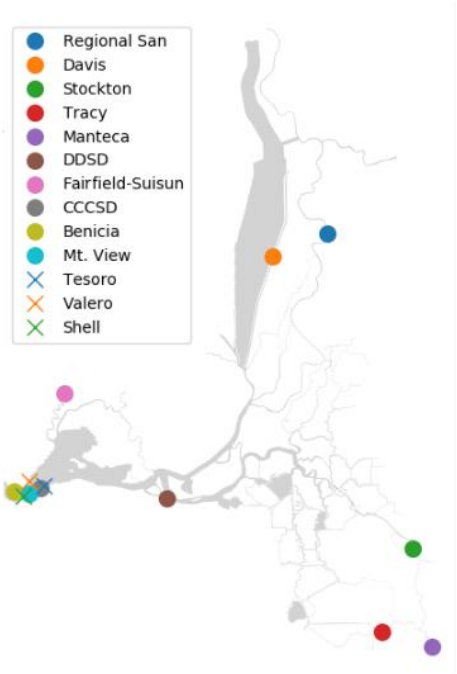

Note: Publicly-owned treatment works (circles) and refineries (x).

Figure 2.8. Locations of point source inputs for the biogeochemical model.

2.3.3 Initial Conditions

2.3.3.1 Water Column

Due to the drought conditions preceding WY2016, residence times in the Delta were likely longer than normal during the model spin-up (August 1-October 1) such that any uncertainty in the initial condition may not be fully resolved during spin-up. In order to account for the relatively long residence time, the model was initialized with spatially-varying concentrations for DO, ortho-phosphate, nitrate, ammonium, silica, and chl-a. These initial conditions were created by interpolating discrete (EMP) data across the grid and creating a 2D concentration field (Martinez and Perry 2021). The interpolation used the data collected closest to the start date of the simulation (i.e., August 1, 2015). By initializing the model based on data, any lingering effects of the initial concentrations that propagate into WY2016 (i.e., on October 1, 2015) are more representative of the actual concentrations that resulted from the low flow conditions. The initial concentrations used for a subset of model state variables are shown in Figure 2.9.

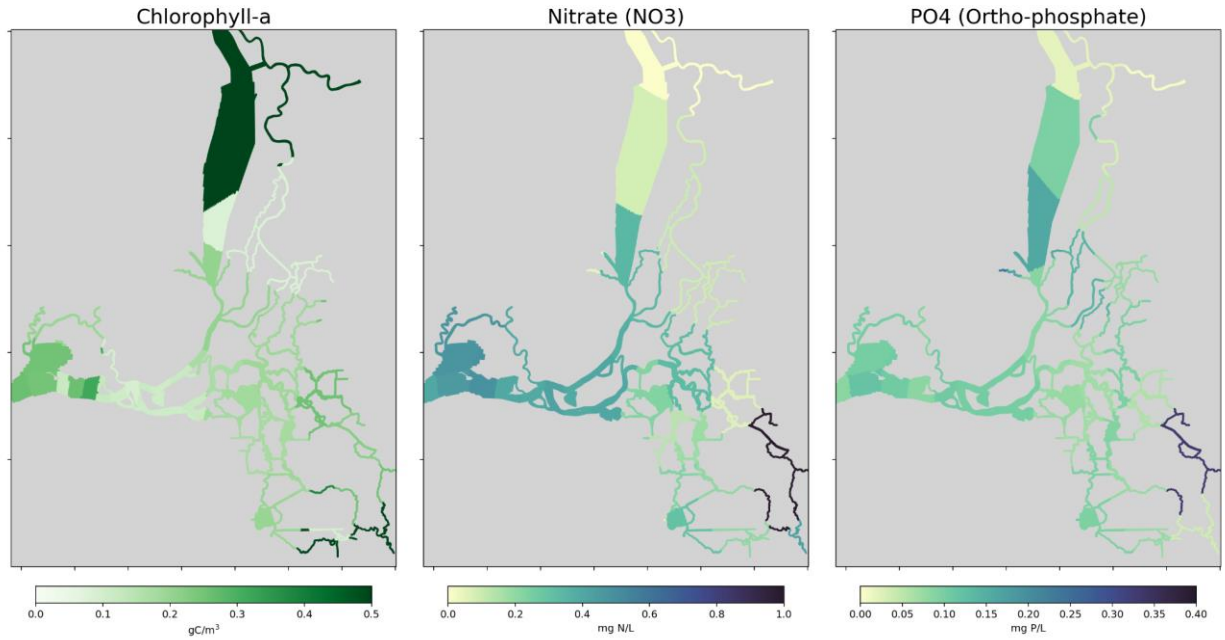

NOTE: Chlorophyll-a is depicted in units of gC/m³. For reference, 0.5 gC/m³ is equivalent to ~11.25 ug/L.

Figure 2.7. Spatial maps of interpolated initial conditions for chlorophyll-a, nitrate, and phosphate.

2.3.3.2 Sediments

The sediment model has two simplified layers, with the top layer representing the mineralization of labile—freshly deposited organic matter—and the bottom layer representing refractory organic matter. Sediment data within the Delta are limited. Therefore, the initial concentrations for carbon, nitrogen, and phosphorus within the sediments were derived from the improvements identified in the Open Bay biogeochemical model (SFEI 2020a). The sediment initial concentrations are spatially constant and were adjusted during calibration to provide reasonable sediment fluxes. The top layer sediment concentrations were approximately an order of magnitude lower than the second layer to reflect the rapid turnaround of freshly deposited labile organic matter.

2.3.3.3 Clams

In the DEB model, both clam species are initialized with biomass concentrations (gC/m^2) because they are treated as immobile state variables that are attached to a substrate (sediments). The initial conditions were derived from estimates of clam biomass provided by USGS (Jan Thompson, personal communication, May 12, 2021), which in-turn are derived from field measurements of clam density (Crauder et al. 2016), collected through the benthic component of DWR's Environmental Monitoring Program (EMP) (Zierdt et al. 2021). These data were collected as part of a generalized random tessellation stratified (GRTS) mapping survey and contain clam samples from approximately 50+ sites, which were collected roughly every 4 to 5 months. Data collected on October 15, 2015 (about 2 months after the start of the simulation) were used to initialize the WY2016 model. The clam data are interpolated across the grid in order to produce initial conditions for the model (Figure 2.10). This interpolation technique, used for several initial condition datasets, finds an iterative solution to the heat equation that approximates the input data, resulting in a smooth interpolated field that respects land

boundaries ("as the fish swims" vs. "as the bird flies"). More information about the benthic data, including the collection methodology, can be found in Crauder et al. (2016).

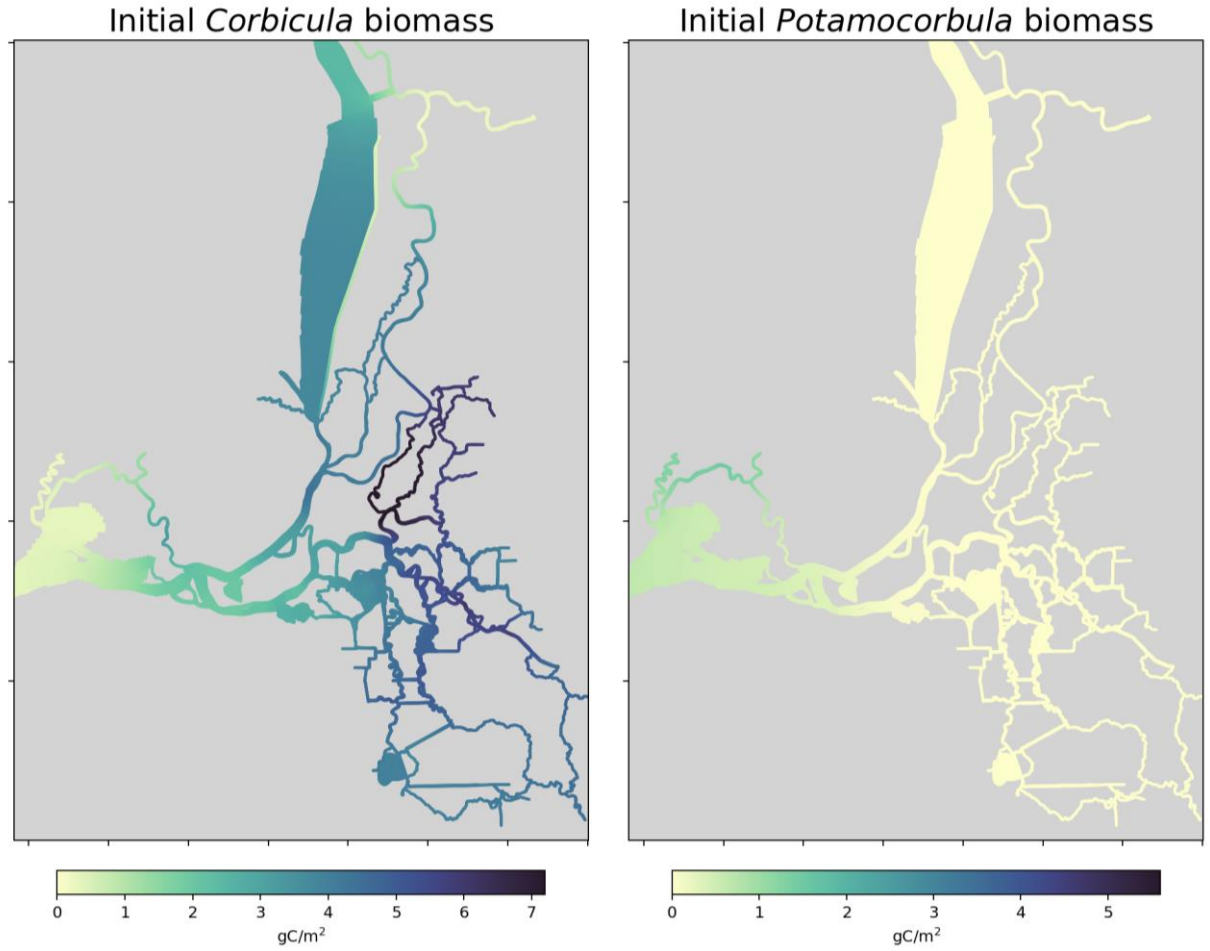

NOTE: Clam biomass in the figure above is depicted in units of gC/m². For reference, the conversion ratio between ash free dry weight (AFDW) and gC is ~0.4 gC per gAFDW.

Figure 2.8. Clam initial condition for *Corbicula* (freshwater clam) and *Potamocorbula* (saltwater clam).

2.3.4 Light Extinction

Accurately representing light attenuation in the nSFE is important for predicting phytoplankton production, because of the system's high suspended sediment concentrations (also highly variable in space and time), that can strongly regulate growth rates. However, without a mechanistic sediment transport model, representing short-term changes in the spatial gradients of turbidity is infeasible. To address this need, a spatially-interpolated, time-varying empirical light-extinction coefficient (K_D) field was developed using turbidity data from high-frequency sensors throughout the system and a relationship for turbidity:K_D based on nSFE data. Compared to the sparse spatial coverage of turbidity data in San Francisco Bay, the Delta contains a wealth of monitoring stations that collect turbidity data at 15-minute to monthly frequencies. There are 71 stations in the Delta that obtained turbidity data over WY2016. Daily-averaged turbidity data were interpolated over the model grid using the interpolation scheme described in Section 2.3.3.3. Examples of the daily-averaged turbidity data that were used in the interpolation are shown in Figure 2.11. These turbidity values were converted to

spatio-temporally variable light extinction inputs for the model using existing linear transformations derived from paired turbidity (FNU/NTU) and light extinction data (1/m) from the Delta (Figure 2.12 shows model light extinction inputs for two dates). Additional details about the light field data and the turbidity regression are provided in Appendix C.

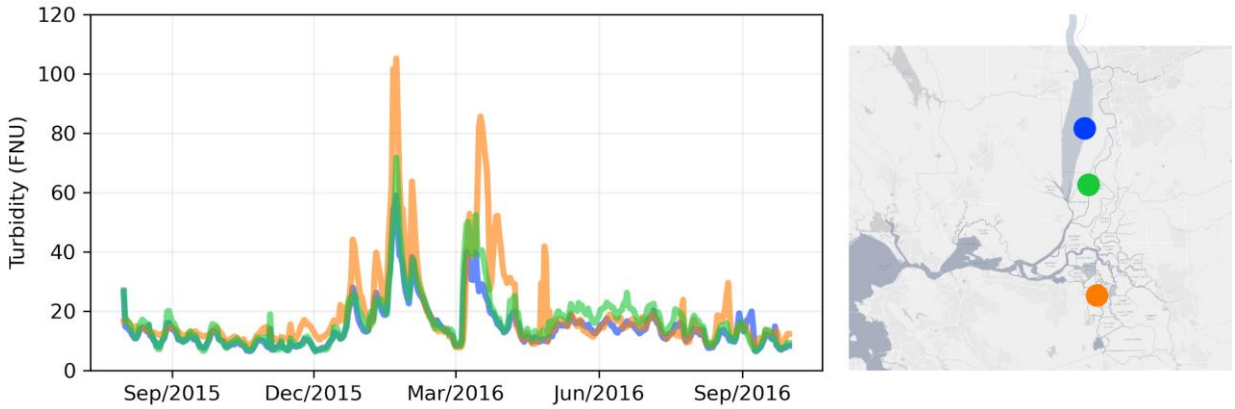

Note: Lines are color coded to match the stations in the right panel.

Figure 2.9. Time series extracted from the interpolated turbidity grid.

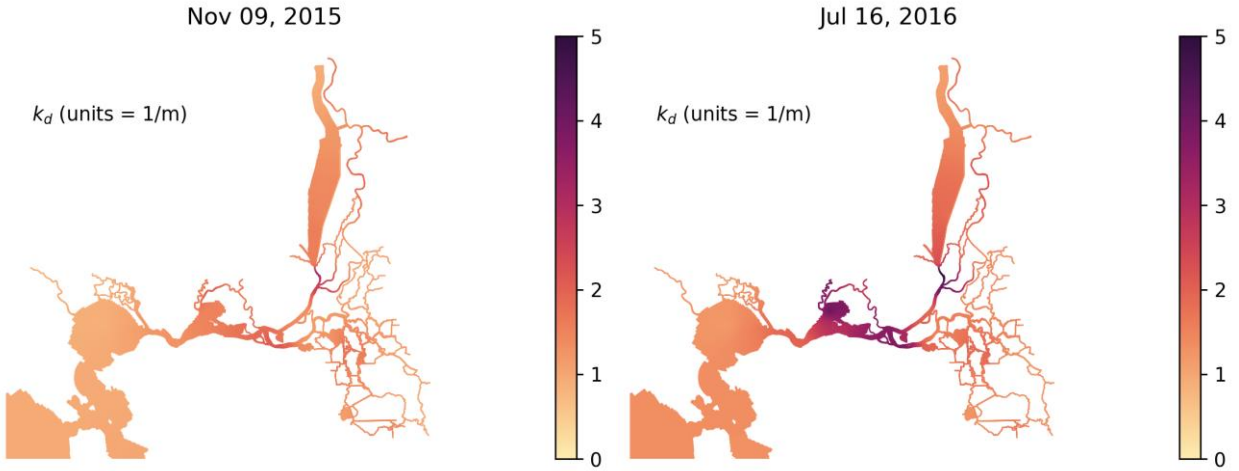

Figure 2.10. Spatial maps of light attenuation coefficient (k_d) at timestamps in November and July 2016.

2.3.5 Wind

Wind speed is used by DWAQ to parameterize oxygen flux across the water surface (reaeration rate). For WY2016 and WY2011, spatially and temporally varying wind speeds were derived from measurements at 52 stations across the San Francisco Bay-Delta region. The wind measurements were linearly interpolated using the SFEI_Wind package onto the model grid and provided as forcing to the SFE-BGCM (SFEI 2019c).

2.3.6 Other Model Updates

An apparent problem within the DWAQ code was identified during earlier runs through unrealistically high phytoplankton production and biomass and artificially elevated nutrient levels due to mineralization in some regions of the Yolo Bypass. The problem stemmed from wetting/drying in some grid cells that become shallowly and temporarily inundated. The issue was limited to the Yolo Bypass region and emerged after high flows are directed into the system from the Sacramento River. As waters drained from the Yolo Bypass floodplain (Figure 2.13, red hatched area) and some cells became disconnected from flow paths, DWAQ continued to treat those isolated, shallowly-inundated cells as active cells. In many of those cells, unrealistically-high phytoplankton biomass and nutrient concentrations accumulated. Because the cells were disconnected from major flow paths, the issue remained local, and did not substantially affect Cache Slough Complex nutrient net export or net transformations. However, it did exaggerate gross internal mass balance terms. As an interim fix, a local adjustment to phytoplankton growth (decreased phytoplankton growth rate by 80%) was implemented within those areas (Figure 2.13), which substantially mitigated the issue from a nutrient cycling perspective. Work is underway to more fully remedy the issue.

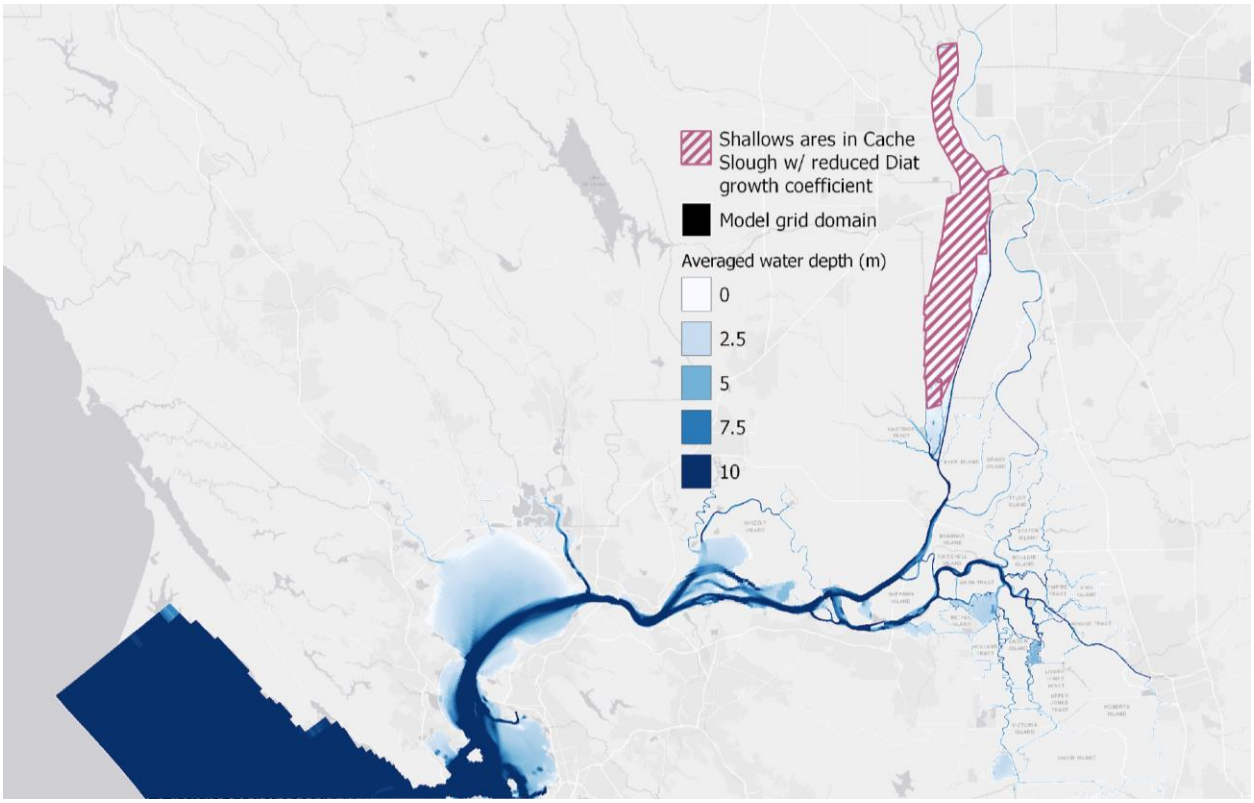

Figure 2.11. Shallow cells in the Yolo Bypass with adjusted diatom growth rate during the simulation.

2.4 Biogeochemical Model Validation Data

2.4.1 Discrete Data

Discrete monthly and semi-monthly data from nine sites in the Delta and Suisun Bay were used for comparisons of model predictions with field observations (Table 2.1, Figure 2.14). Data are from two

programs, the DWR EMP Interagency Ecological Program (Lesmeister and Martinez 2020) and the USGS San Francisco Bay Water Quality Program (Schraga and Cloern 2017; Schraga et al. 2020). Stations were selected to represent diverse regions, and selections were based on data availability, both in scope (parameters available) and range (time span of available parameters). In order to compare model output with these discrete data, each data site was specified as a monitoring location in the DWAQ model to generate outputs of surface-level time series of the state variables at each site.

Table 2.1. Discrete sampling stations used for model validation.

Site Name[1]	Station Number	Latitude	Longitude	Agency
D28A	B9D75821344	37.9705	-121.573	EMP
P8	B9D75871229	37.9782	-121.382	EMP
D19	B9D80261369	38.0438	-121.615	EMP
D6	E3B80272071	38.0444	-122.118	EMP
C3A-Hood	B9D82211312	38.3677	-121.521	EMP
D7	E0B80702024	38.1171	-122.0397	EMP
D8	E3B80361594	38.0599	-121.99	EMP
D26	B9D80461340	38.0766	-121.567	EMP
649	USGS-649	38.0617	-121.8	USGS Polaris/Peterson

Note:
1. Samples were collected at depth of 1 meter.

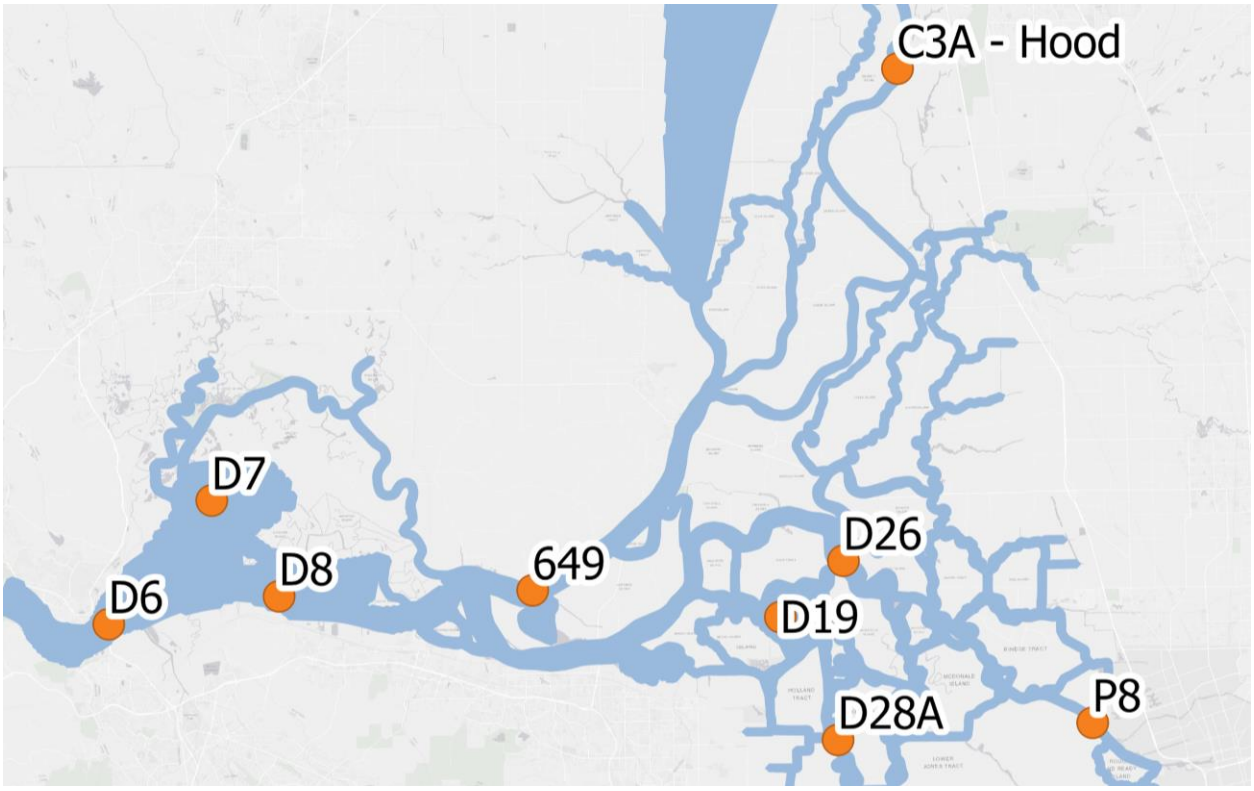

Figure 2.12. Map of the discrete sampling stations used for model validation.

2.4.2 High Frequency Mooring Data

Continuous water-quality and flow (Q) data were collected every quarter hour at USGS-operated fixed stations throughout the Delta during water years 2015 - 2016 (Figure 2.15, Table 2.2). Water-quality measurements were collected with a multiparameter water-quality sonde (YSI EXO2; Xylem Inc. (EXO), Rye Brook, NY) equipped with sensors to measure temperature, specific conductance (SpC), turbidity, pH, DO, dissolved organic matter fluorescence (fDOM), and chlorophyll fluorescence (fCHL). Nitrate measurements are collected with a submersible ultraviolet nitrate analyzer (SUNA V1; Sea-Bird Scientific, Bellevue, WA). Wipers clean the optical sensor windows of each instrument before every 15-minute sample interval. Data are collected over a 30 second sample period at the 15-minute timestamp following sensor warm-up and wiping and the median value of the bursts are reported. Instruments are deployed in 4-inch PVC pipes at a depth of 1 m at Mean Lower Low Water and operated according to the manufacturer's recommendations, USGS field manual (Wilde 2018), and Pellerin et al (2013). More continuous monitoring network specific considerations are described in Bergamaschi et al. (2017), Downing et al. (2017), and Kraus et al (2017). Most stations are also equipped with side-looking acoustic Doppler velocity meters (ADVM). Channel discharge from the ADVM data is computed using the index velocity method according to Ruhl and Simpson (2005) and Levesque and Oberg (2012).

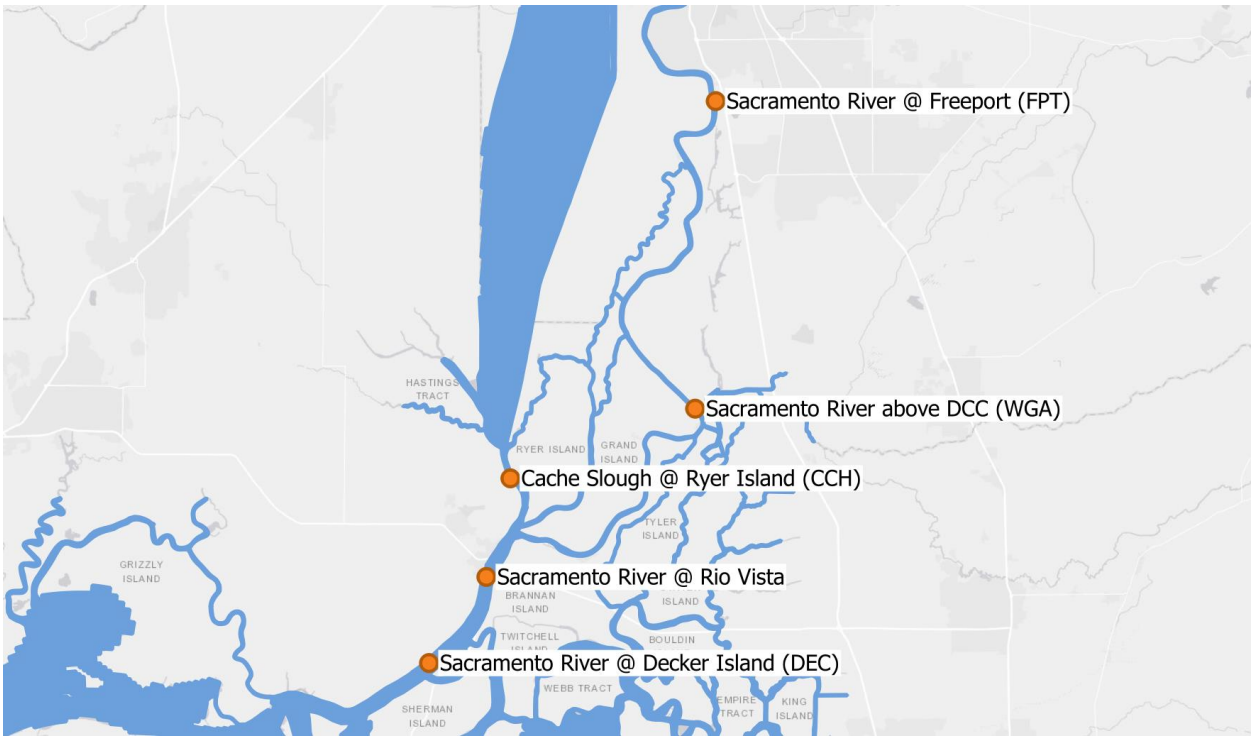

Figure 2.13. Map of U.S. Geological Survey-operated continuous monitoring flow and water-quality stations in the Delta.

Table 2.2. U.S. Geological Survey operated continuous monitoring flow and water-quality stations in the Delta.

USGS Site Abbreviation	Site ID	Site Name	Latitude	Longitude
CCH	11455350	Cache Slough at Ryer Island	38.212778	-121.66917
DEC	11455478	Sacramento River at Decker Island near Rio Vista CA	38.093333	-121.73611
FPT	11447650	Sacramento River at Freeport CA	38.456111	-121.50028
WGA	11447890	Sacramento River above Delta Cross Channel CA	38.257778	-121.51722

RIO	11455420	Sacramento River at Rio Vista (discharge used for flux calculations)	38.149044	-121.68894

Source: USGS National Water Information System database metadata

Water-quality station visits routinely occur for instrument maintenance and discrete sample collection. EXO sonde measurements are checked in native water before and after cleaning and compared to a gold-standard sonde used specifically for quality assurance purposes. Sensors are also checked in certified standards and calibrated when necessary. Data are reported to the National Water Information System database where lower and upper-level thresholds are applied, outliers are removed, and fouling and calibration drifts are corrected according to the USGS National Field Manual (Wilde 2018), Wagner et al (2006), and Pellerin et al. (2013). The 15-minute ADVM data is routinely compared to cross channel transects and a rating curve is generated to compute discharge using the cross-sectional area and channel average velocity that is further described in Ruhl and Simpson (2005). These data are also reported to the National Water Information System database.

Fixed-station water-quality and flow measurements are made under the assumption these data represent well-mixed vertical and lateral reaches of a channel. The data generated by algal and organic matter fluorescence and nitrate absorbance measurements have not been corrected by site-specific calibrations; dissolved organic matter fluorescence is adjusted by a temperature, turbidity, and inner-filter effect correction according to Downing et al. (2012). Whereas all federal scientific records generated by this project are managed and archived in accordance with Survey Manual Chapter 431.1, Records Management Program (https://www.usgs.gov/about/organization/science-support/survey-manual/4311-records-management-roles-and-responsibilities), the Water Resources Discipline Scientific Records Disposition Schedule 1400 and the USGS General Records Disposition Schedule, data at the time of this reporting is provisional. The local records officer at the USGS California Water Science Center will ensure scientific records are appropriately archived. Note that the high-frequency nitrate data at Freeport had not yet been regressed to discrete laboratory sample at the time of this report; however, based on previous experience, any changes to these values are expected to be inconsequentially small.

Model data for the mooring sites were produced by outputting data at each mooring site at 15-minute intervals. The model data were down-sampled to a daily average and averaged across the top meter of the water column.

2.4.3 High Frequency Flux Data

Flux-based monitoring is possible within the USGS station network as water-quality instruments are co-located with ADVM measurements. Flux measurements/estimates are calculated using the high frequency continuous monitoring station data described in Section 2.4.2. The stations identified in Figures 2.15 and Table 2.2 are used to compare field measurements with model output and to calculate fluxes for model validation. Discharge measurements from RIO are used to calculate fluxes at DEC because there is no ADVM located at DEC. Flux is estimated as a function of discharge and concentration. Modeled flux was output directly at the sampling sites every 15 minutes. Modeled fluxes at Rio Vista are used to compare to the DEC fluxes from USGS.

To compute tidally filtered and cumulative fluxes, it is first necessary to fill gaps in the observed discharge and concentration data. To fill gaps, the time series was smoothed using a simple running mean, where discharge was smoothed over one tidal cycle and concentration over a quarter tidal cycle.

The smoothed time series were then linearly interpolated and the interpolated values were used to fill gaps in the original, unsmoothed time series. These time series with gaps filled were then used to compute tidally filtered and cumulative fluxes. A Butterworth filter was used for tidal filtering.

2.4.4 U.S. Geological Survey Mapping Cruises

The USGS collected 17 high-resolution datasets aboard the R/V Mary Landsteiner between August 14, 2015 and September 30, 2016, according to methods described in Bergamaschi et al. (2020). The geographic extent of the data includes the western and central tidal zones and the Cache Slough Complex. The location of high-resolution data collections, dates, and event descriptions are described in Table 2.3. The datasets include underway measurements of nitrate, chlorophyll fluorescence, temperature, salinity, DO, pH, turbidity, and dissolved organic matter fluorescence. Briefly, sample water was continuously pumped onto the boat while underway at variable boat speeds up to 30 mph using a pick-up tube mounted at a fixed depth of 1 m below the surface. Sample water was pumped through a screen to remove large debris and into a pressure-compensated manifold, as described in Downing et al. (2016). Methods detailing the data quality assurance and quality control process are provided in Appendix D.

Table 2.3. List of USGS high-resolution water-quality mapping dates, location, and associated project or event used for calibration and validation of WY2016 model.

Water Year	Field Date	Geographical Location	Project
2015	8/14/2015	Lower Sac R – Central Delta	Emergency Drought Barrier
2015	9/10/2015	Lower Sac R – Central Delta	Emergency Drought Barrier
2015	9/14/2015	Lower Sac R – Central Delta	Emergency Drought Barrier
2016	10/5/2015	Cache Slough Complex	Zoop.-Kimmerer
2016	10/21/2015	Lower Sac R – Central Delta	Emergency Drought Barrier
2016	3/31/2016	Cache Slough Complex	CSC Mapping
2016	4/18/2016	Lower Sac R – Central Delta	Emergency Drought Barrier
2016	5/2/2016	Rio Visto to Golden Gate	Algae Bloom
2016	5/6/2016	Cache Slough Complex-Lower Sac R	Algae Bloom
2016	5/20/2016	Cache Slough Complex-Lower Sac R	Algae Bloom
2016	5/25/2016	Cache Slough Complex-Lower Sac R	Algae Bloom
2016	6/9/2016	Cache Slough Complex-Lower Sac R	Algae Bloom
2016	6/28/2016	Cache Slough Complex-Lower Sac R	Algae Bloom
2016	7/13/2016	Lower Sac R – Central Delta	Emergency Drought Barrier
2016	7/19/2016	Cache Slough Complex	North Delta Directed Flow Action
2016	8/3/2016	Cache Slough Complex	North Delta Directed Flow Action + Little Holland Tract Survey
2016	8/30/2016	Cache Slough Complex	CSC Mapping

Model data comparisons were made by taking the daily and depth-averaged value of each modeled constituent (nitrate, DO, etc.) on each cruise date and plotting the spatial map alongside the mapping cruise data. Daily averages were used to validate whether or not the model was properly capturing the general magnitude and gradient of each constituent as seen by the mapping cruise data collection.
Clams and Zooplankton

In order to improve the representation of grazing (both benthic and pelagic) in the model, additional field data and modeling insights from collaborators working on the USGS-led CASCaDE project were used to refine and improve the DEB model implementation (L Lucas, J Thompson, W Kimmerer, personal communication).

Benthic grazer field data is sparse in time and space. Biomass field surveys provided estimates of clam biomass (g/m^2) across sampling sites which were converted to a filtration rate ($m^3/m^2/day$) using empirical parameterizations developed by O'Riordan et al. (1995), described further by Crauder et. al (2016). An example of sites sampled during one such survey is provided in Figure 2.16.

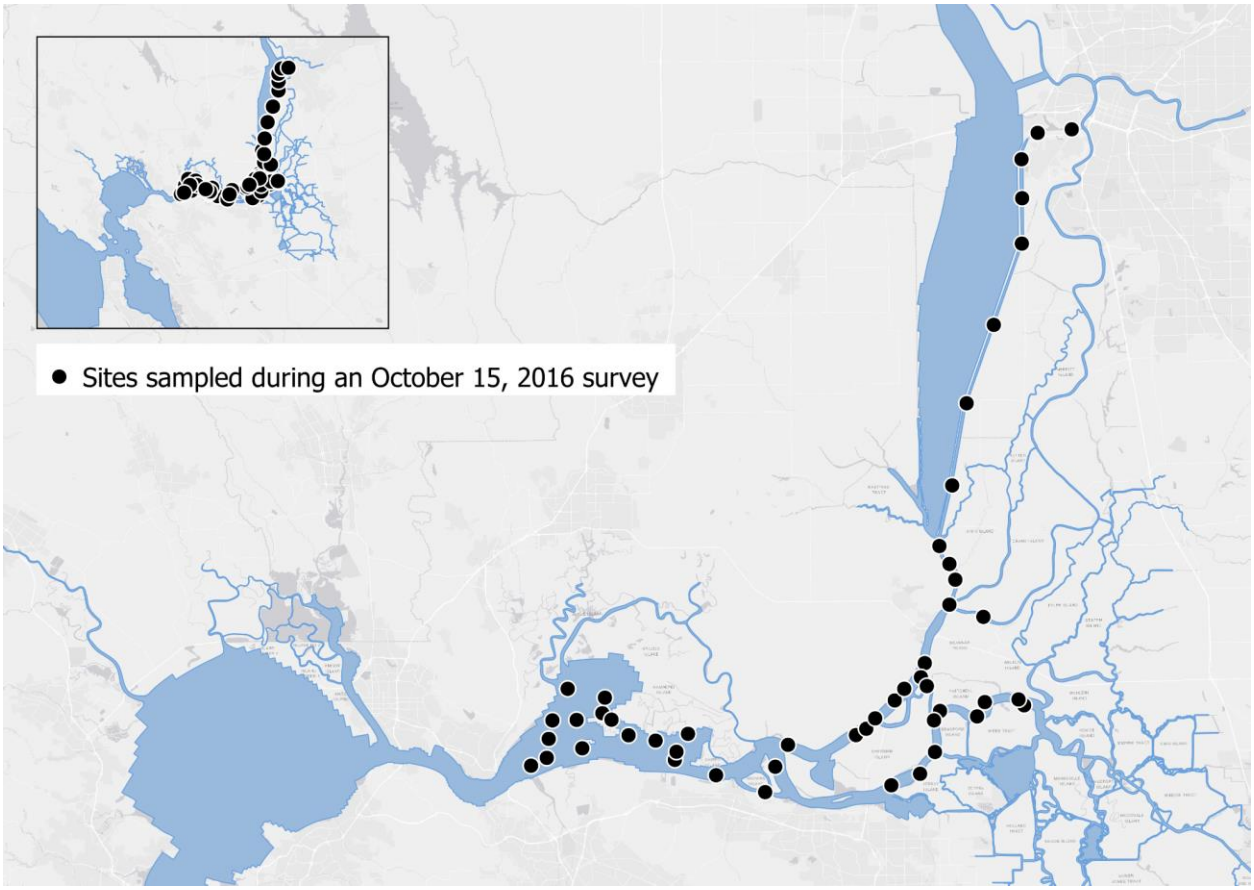

Figure 2.14. Map of sites sampled during a benthic survey on October 15, 2016.

USGS field data were used to create a greater understanding of the system as a whole in addition to guiding model validation. Figures 2.17 – 2.21 show different data processing methodologies used to inform understanding of grazing control on phytoplankton. Because the exact location and number of sites tend to vary survey to survey, to understand trends over time, biomass data was binned by region (Suisun Bay, lower and upper Cache Slough, Sacramento River stem, South Delta). The binned data was then plotted as a series of box plots in order to depict how clam biomass might vary across a region over a series of sampling dates. To give a rough idea of food availability, we also plot chlorophyll-a measured from a site within each polygon. This approach offers several interpretative findings. For example, Figure 2.17 shows the shifts in clam populations within Suisun Bay during 2017 when *Potamocorbula* biomass declined and *Corbicula* biomass increased, likely a result of the large freshwater runoff event in spring of 2017 that reduced salinity within Suisun Bay. Due to the complexity and heterogeneity of the system,

however, clear correlations and trends between chl-a and grazer biomass were less evident. Nonetheless, these boxplots provide an estimate of the general range of biomass expected in each region.

Empirically-based clam biomass and grazing estimates developed for the CASCaDE project were compared with DEB-predicted values from this work to refine DEB implementation. Unlike the DEB module approach used here (which simulates grazer biomass and grazing rates), the CASCaDE project incorporates benthic grazing into the model (also DFM-DELWAQ) by imposing empirically-derived grazing rates (as a model input or boundary condition). This provided an opportunity to compare the specified grazing rates in the USGS model to modeled grazing rates in the SFEI model (WY2011 only). Zooplankton grazing pressure in the USGS model simulated by supplying the model with a spatially uniform time series of zooplankton biomass. This biomass time series is then converted to a grazing pressure within the CONSBL model. USGS developed the zooplankton biomass time series (Figure 2.20) using measured data (Kimmerer 2006; Kimmerer et al. 2014). For a sense of magnitude, we converted the biomass time series into a grazing pressure (in $gC/m^3/day$) using the formulation set forth by Lopez (2006) in Figure 2.21. We referenced both the zooplankton biomass time series (and estimated zooplankton grazing pressure) alongside the maps of benthic grazing rate to validate the grazing pressure calculated by the SFEI model.

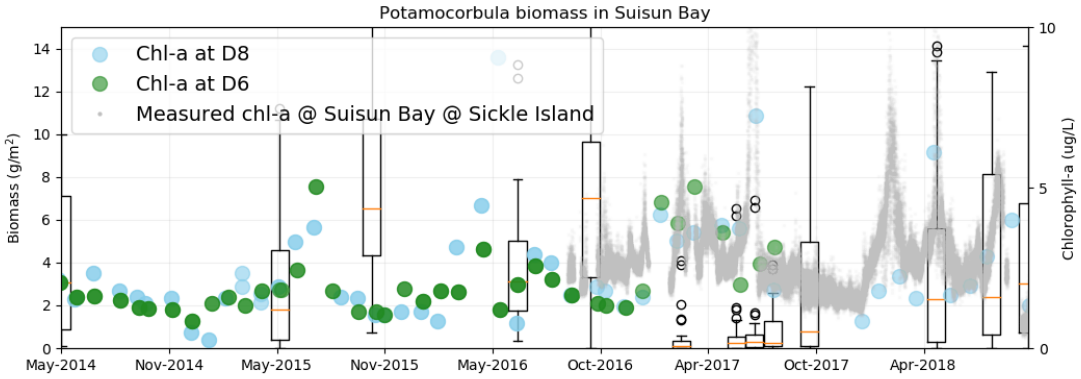

Note: Right-ordinate shows chlorophyll-a measured within Suisun Bay.

Figure 2.15. Box plots of *Potamocorbula* biomass in Suisun Bay.

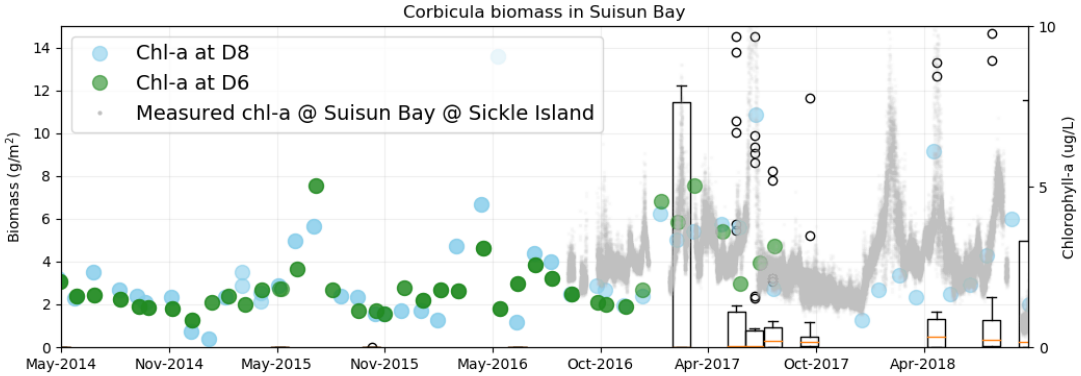

Note: Right-ordinate shows chlorophyll-a measured within Suisun Bay.

Figure 2.16. Boxplots of *Corbicula* biomass in Suisun Bay.

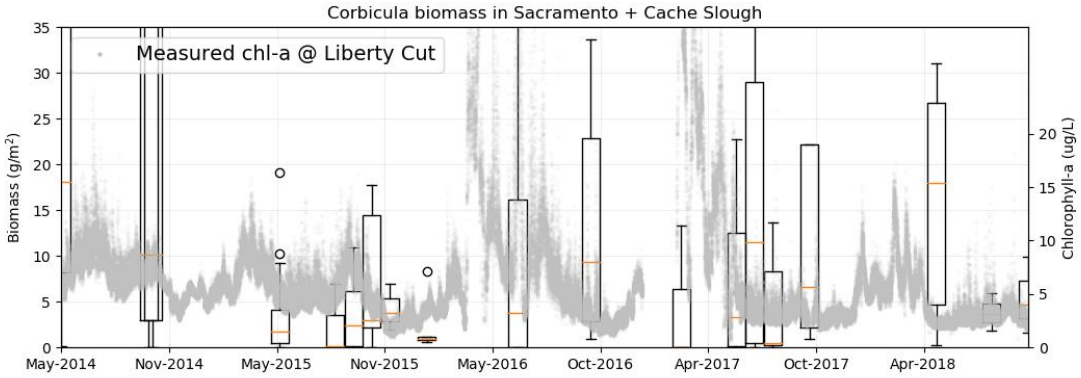

Figure 2.17. *Corbicula* Biomass in Cache Slough and the lower Sacramento River.

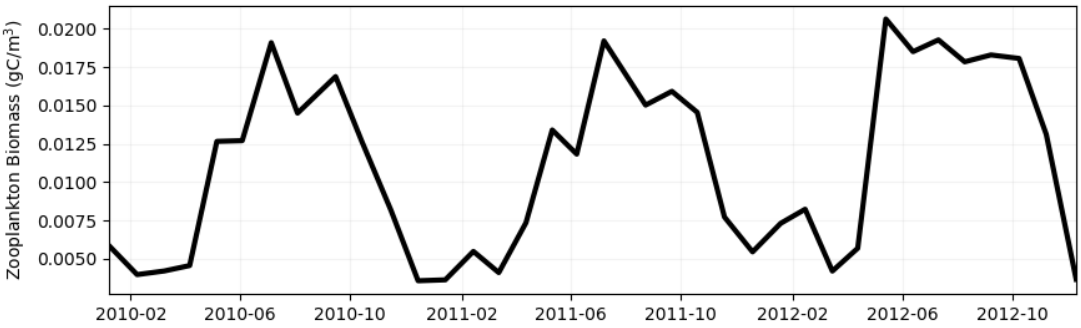

Source: Kimmerer (2014, 2006)

Figure 2.18. Zooplankton biomass time series.

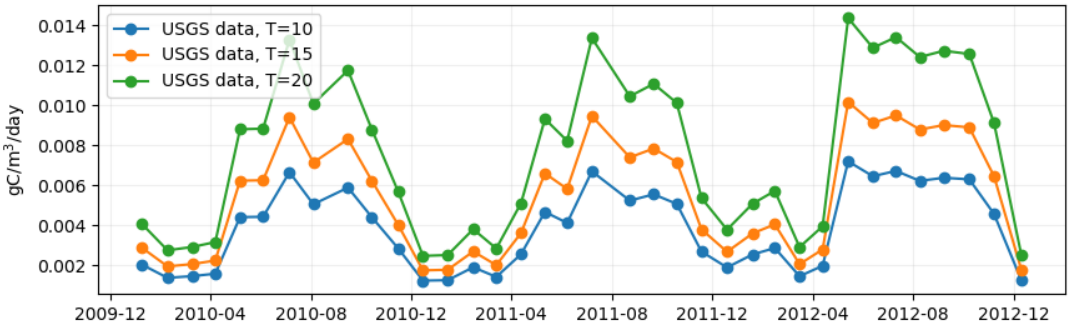

Figure 2.19. Zooplankton biomass time series (Figure 2.18) converted to grazing rate using methodology defined by Lopez (2006) at a variety of temperatures (10, 15, and 20 deg C).

2.5 Biogeochemical Model Validation Approach

With the biogeochemical processes (Section 2.4) included, the full resolution model takes approximately 7 days of wall clock time to complete a DWAQ simulation for a single water year, including 2 months of spin up (an approximately 14-month simulation). Because a large number of simulations (typically hundreds) are required to adequately explore the sensitivity of the biogeochemical model parameters, a horizontally aggregated grid with approximately 5,000 cells was developed for fast running biogeochemical model simulations. The aggregated grid model is capable of completing a full water year

simulation within 4 to 5 hours. After ensuring that the aggregated model predictions had sufficient fidelity relative to the full-resolution model predictions, the faster-running aggregated grid model was used to carry out approximately 100+ model simulations to explore the model parameter space.

Calibration of the model focused on denitrification, primary production, and DEB grazing module parameters. These parameters were selected based on an extended set of sensitivity runs done in the past and also reflect the key processes and state variables of interest. For denitrification, the calibration focused on the critical cut-off temperature (CTDEN), the temperature correction factor, and the first order denitrification rate. In calibrating the grazing module, a focus was placed on the maximum ingestion rate (j_xm) for both clam species. The "minimum food threshold" was also adjusted, which allows a small concentration of phytoplankton to persist such that when grazer levels decline phytoplankton can rebound without additional seeding from model boundaries. The final set of model parameters is presented in Table 2.4, and a complete list of parameter values can be found in Appendix E.

Table 2.4. Final calibrated model parameter values.

Parameter	Description	Unit	Model Value	Literature Values (Where Available)	Default DWAQ Values
z_shape	Shape coefficient for zooplankton DEB model	(-)	0.5	0.3143 (Troost et al. 2018)	0.314
j_xm (*Corbicula*)	Max ingestion rate for *Corbicula* grazer	$J/cm^2/d$	40	2660 (Petter et al. 2014)	196.8
j_xm (*Potamocorbula*)	Max ingestion rate for *Potamocorbula* grazer	$J/cm^2/d$	60	91.5 [*Cerastoderma edule*] (Troost et al. 2010), 273 [*Mytilus edulis*] (Troost et al. 2010)	196.8
minfood	Minimum food threshold for grazers (set individually for all grazer species)	gC/m^3	0.1		0.0
TCDEN	Temperature coefficient for denitrification	(-)	1.2		0.0
CTDEN	Critical temperature for denitrification	°C	2.0		2.0
RCDENsed	First-order denitrification rate in the sediments	m/d	0.1		0.1

3 Results and Discussion

Model performance was evaluated across a range of time and space scales using several different datasets for both WY2011 (discrete data) and WY2016 (discrete data, high frequency mooring and flux data, mapping cruises). The diversity of the validation datasets allowed model performance to be evaluated through different lenses. Monthly data from the EMP's long-term and region-wide network was well-suited for characterizing the model's ability to capture regional-scale water quality patterns, along with seasonal and inter-annual variability (Section 3.1). The high-frequency mooring data, including flux estimates, were used to examine tidal and tidally-averaged performance at intensively monitored fixed locations, and to assess the importance of deviations in terms of both concentrations and mass fluxes (Section 3.2-3.3). Lastly, the mapping cruises offered the opportunity to compare observed and modeled water quality over a range of spatial scales (sub-regional to regional), including locations of sharp biogeochemical gradients (Section 3.4). A brief exploration of grazing in the model and an assessment of modeled grazing pressure is also discussed in Section 3.5.

3.1 Discrete Data: Modeled-Measured Comparisons

Time series plots of model predictions and field observations at the discrete EMP + USGS sites (Figure 2.14) for a range of parameters (nitrate, ammonium, DIN, phosphate, silica, DO, and chl-a) for WY2016 and WY2011 are shown in Figures 3.1 - 3.7 and Figures 3.8 - 3.14, respectively. Model data represents the surface-level value and has been down-sampled to a daily average.

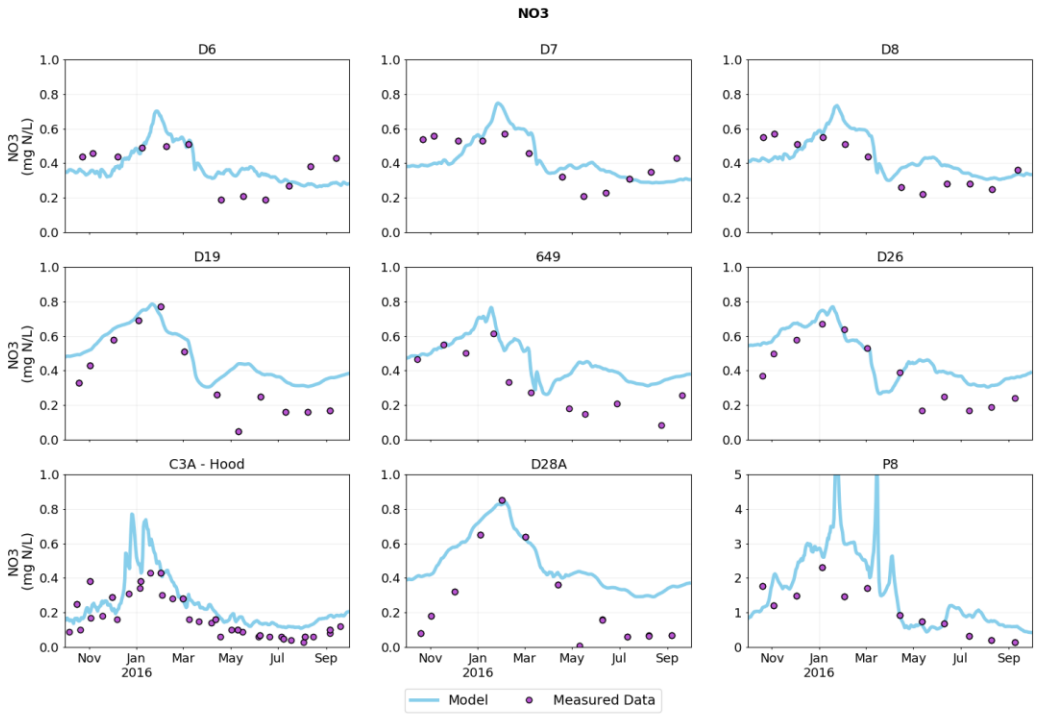

Figure 3.1. WY2016 model validation of nitrate at discrete sampling sites.

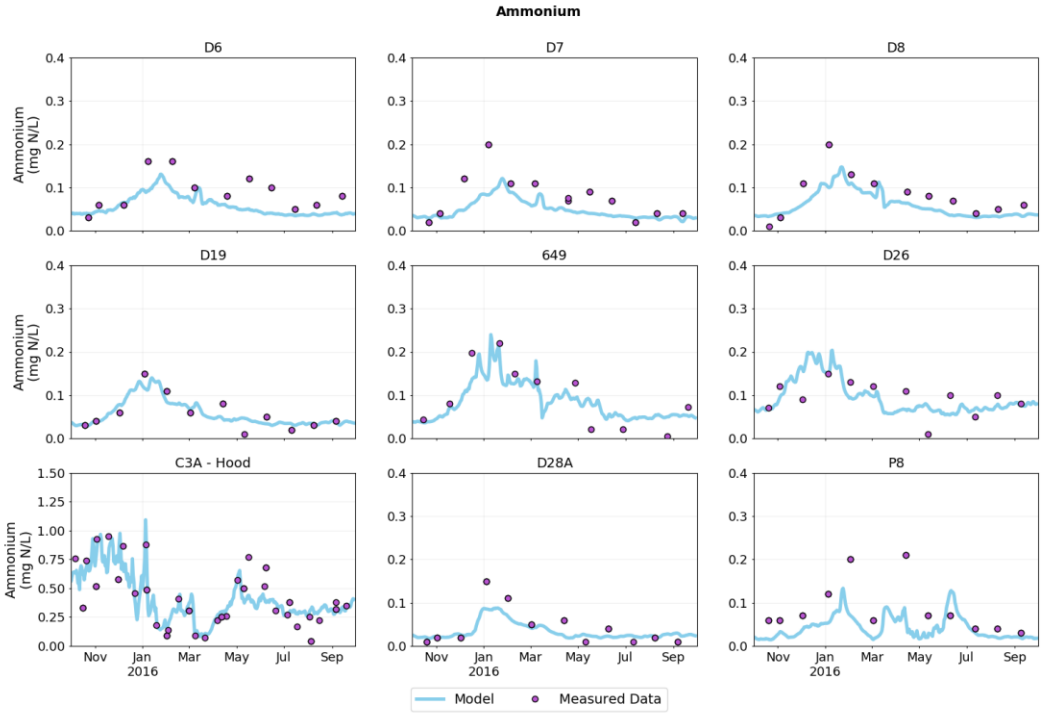

Figure 3.2. WY2016 model validation of ammonium at discrete sampling sites.

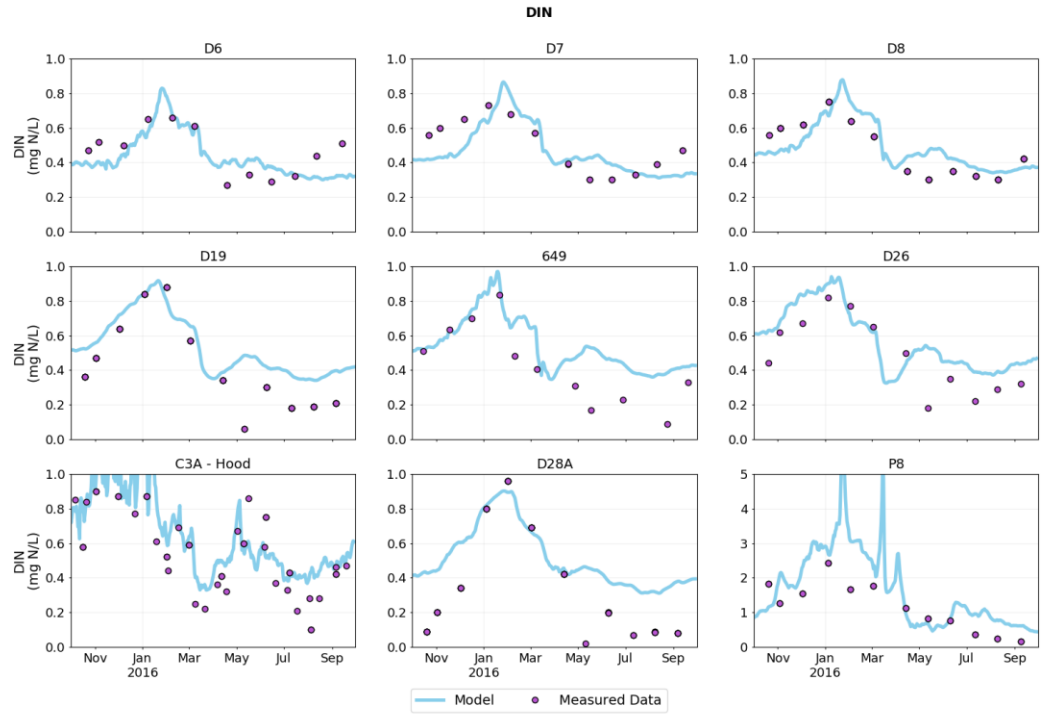

Figure 3.3. WY2016 model validation of dissolved inorganic nitrogen at discrete sampling sites.

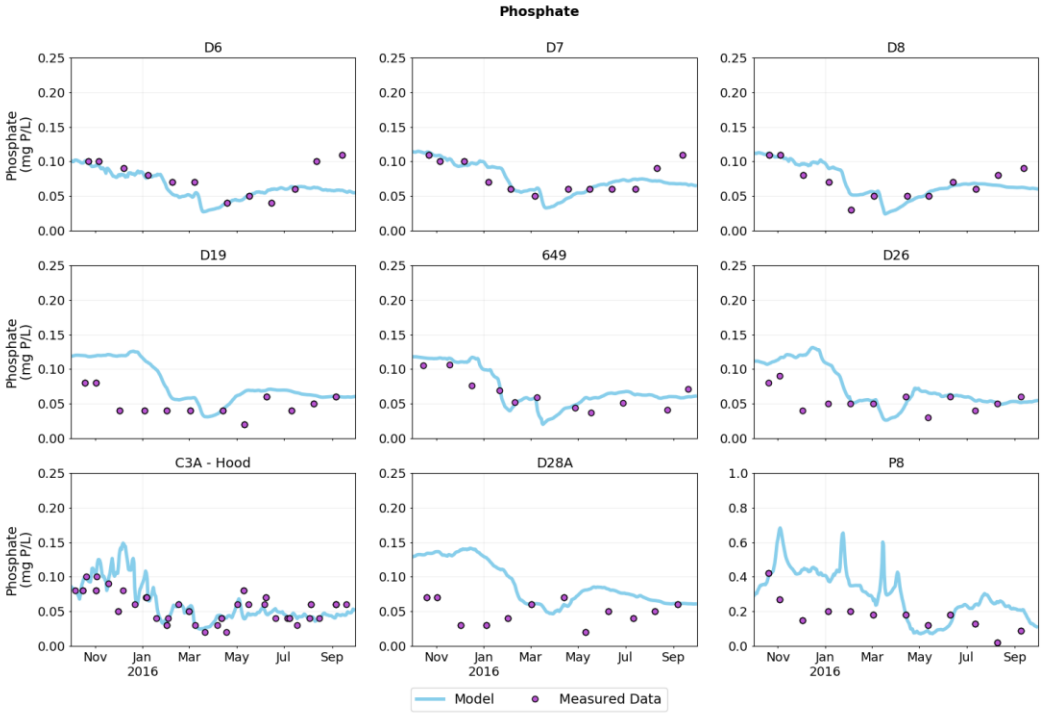

Figure 3.4. WY2016 model validation of phosphate at discrete sampling sites.

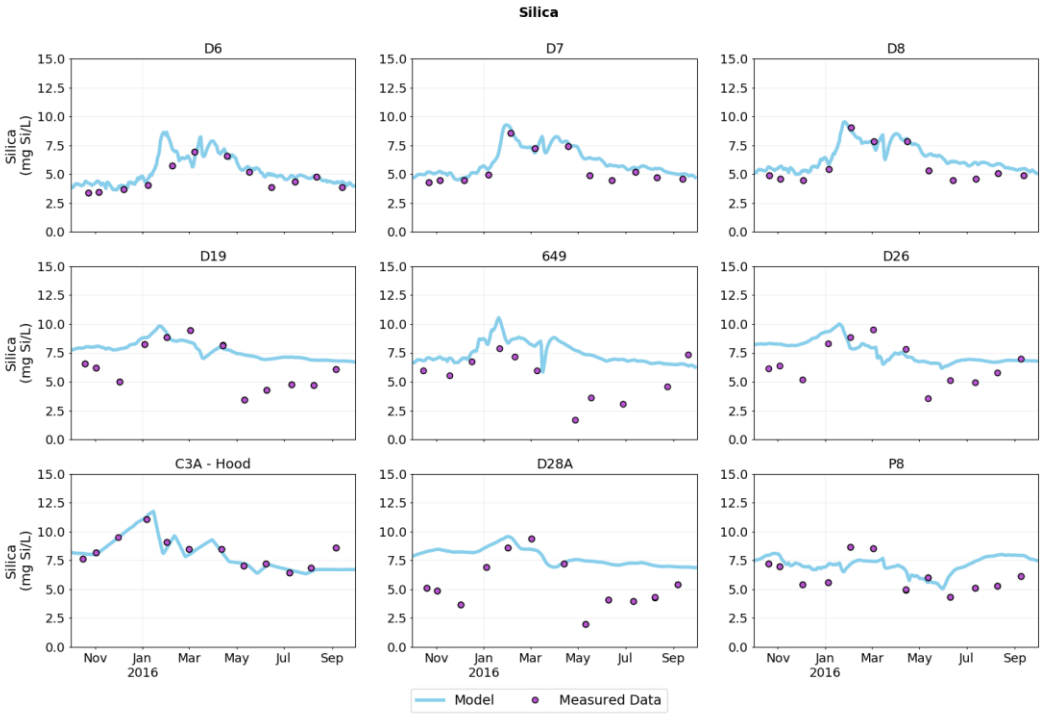

Figure 3.5. WY2016 model validation of silica at discrete sampling sites.

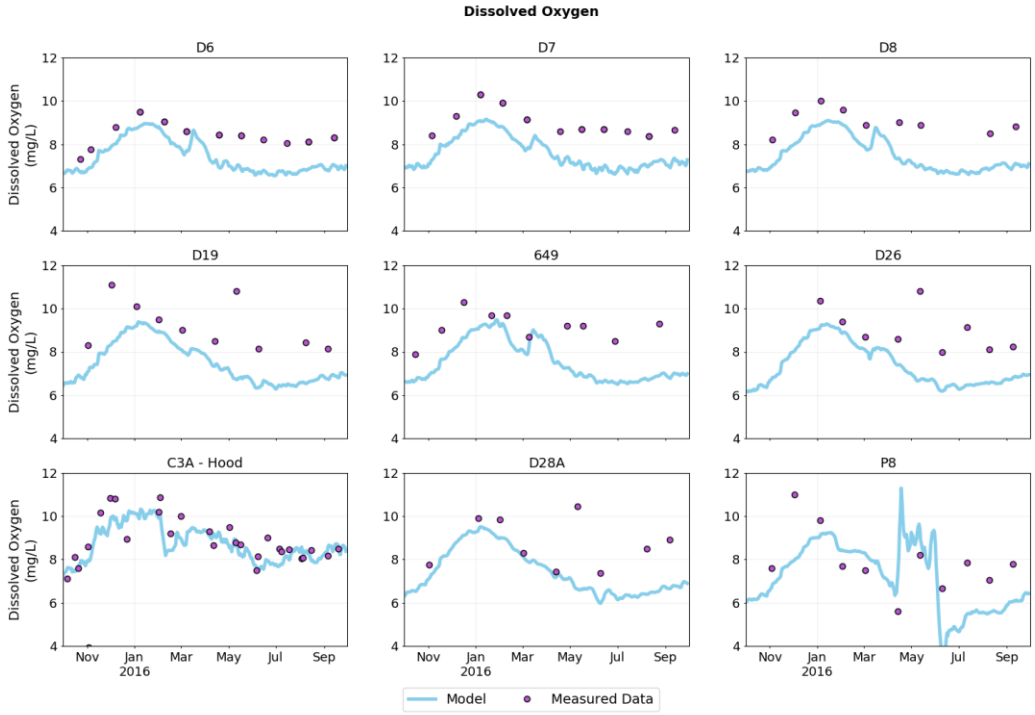

Figure 3.6. WY2016 model validation of dissolved oxygen at discrete sampling sites.

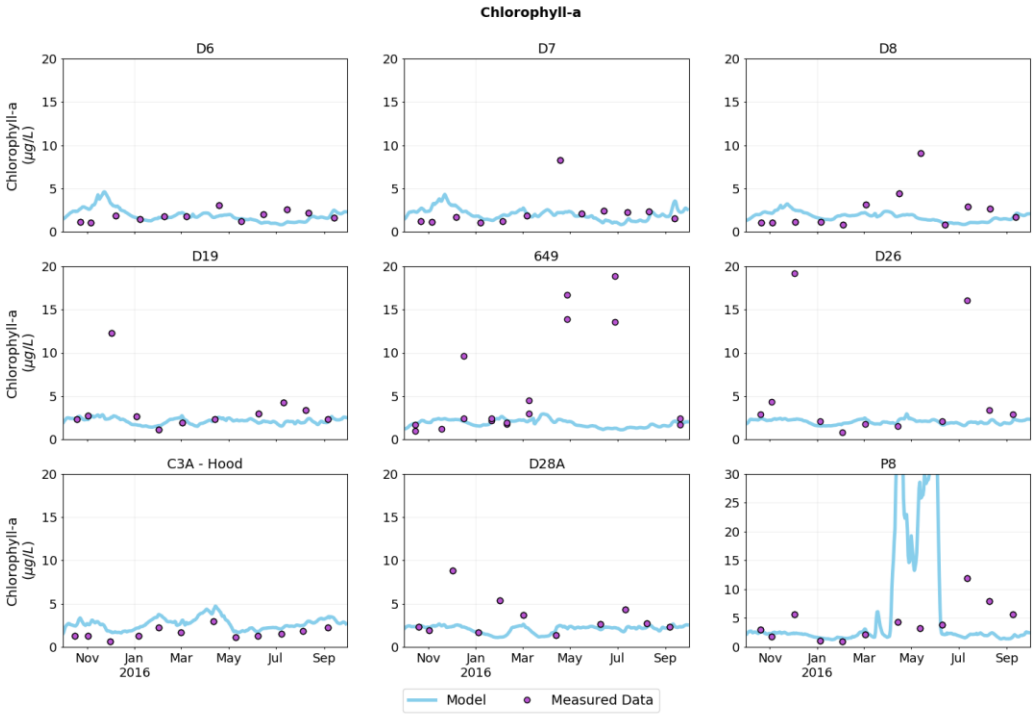

Figure 3.7. WY2016 model validation of chlorophyll-a at discrete sampling sites.

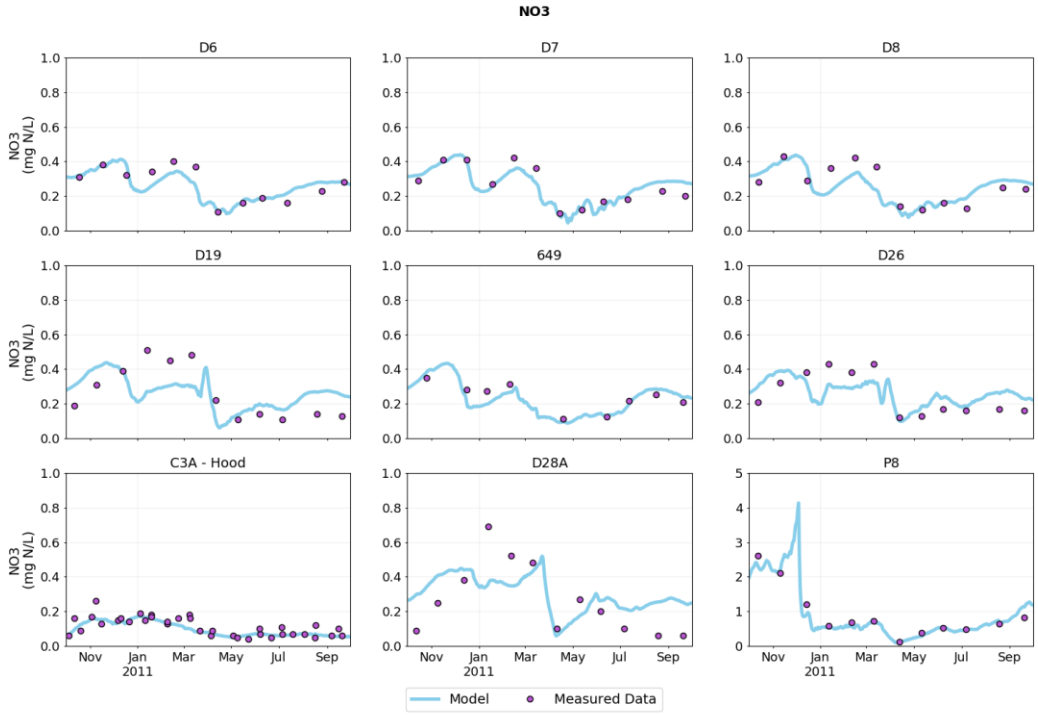

Figure 3.8. WY2011 model validation of nitrate at discrete sampling sites.

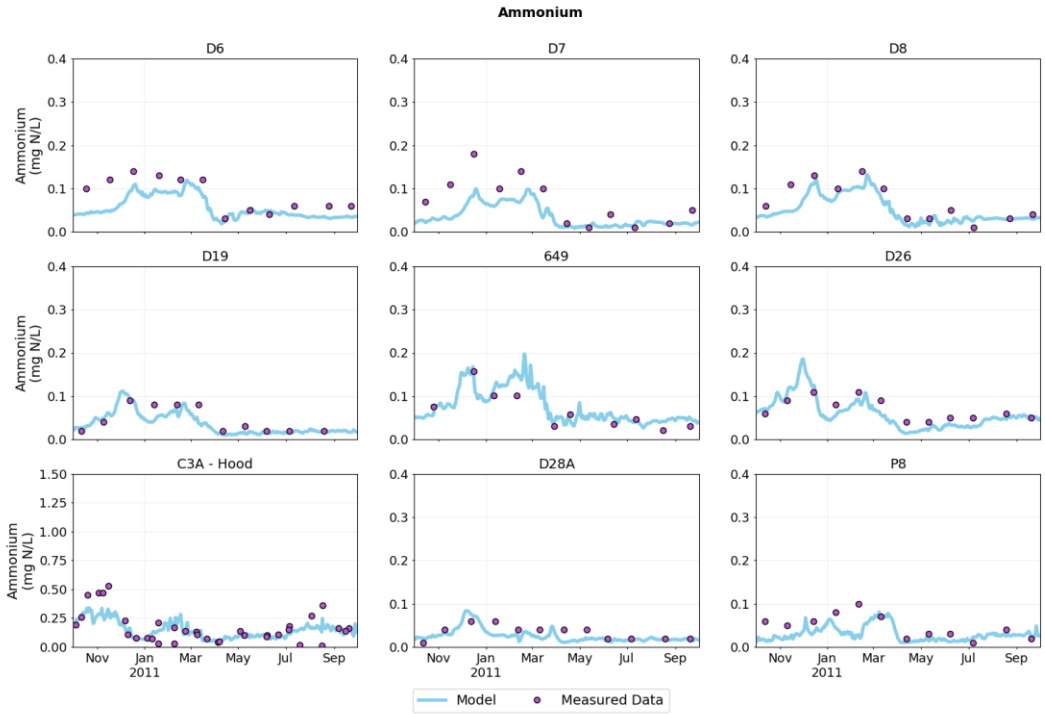

Figure 3.9. WY2011 model validation of ammonium at discrete sampling sites.

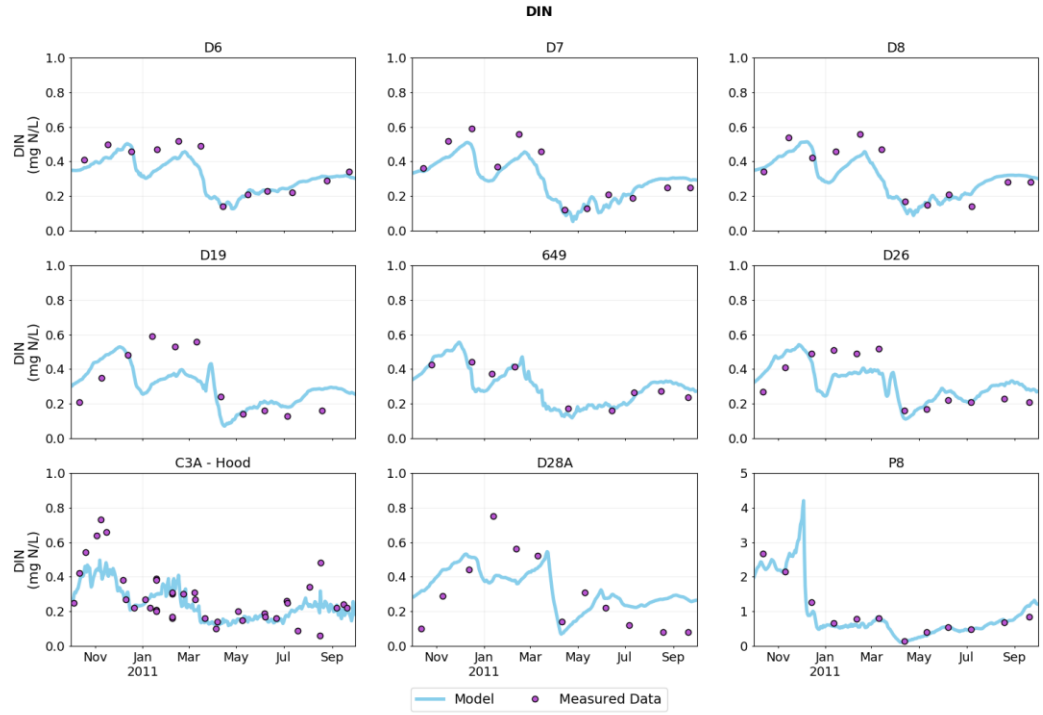

Figure 3.10. WY2011 model validation of dissolved inorganic nitrogen at discrete sampling sites.

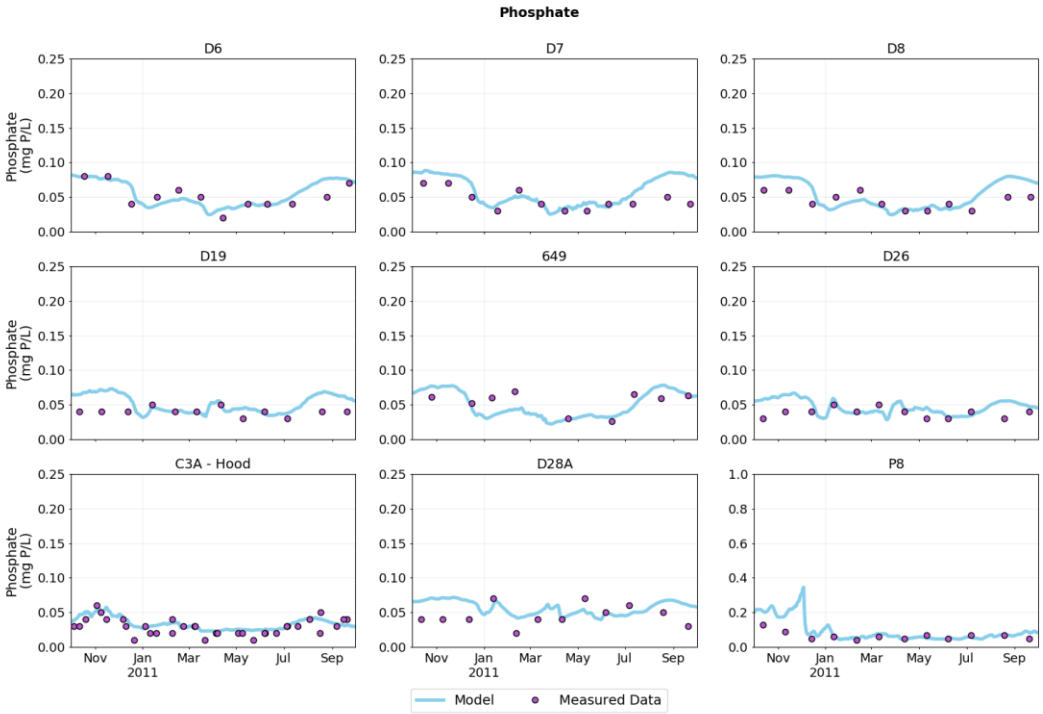

Figure 3.11. WY2011 model validation of phosphate at discrete sampling sites.

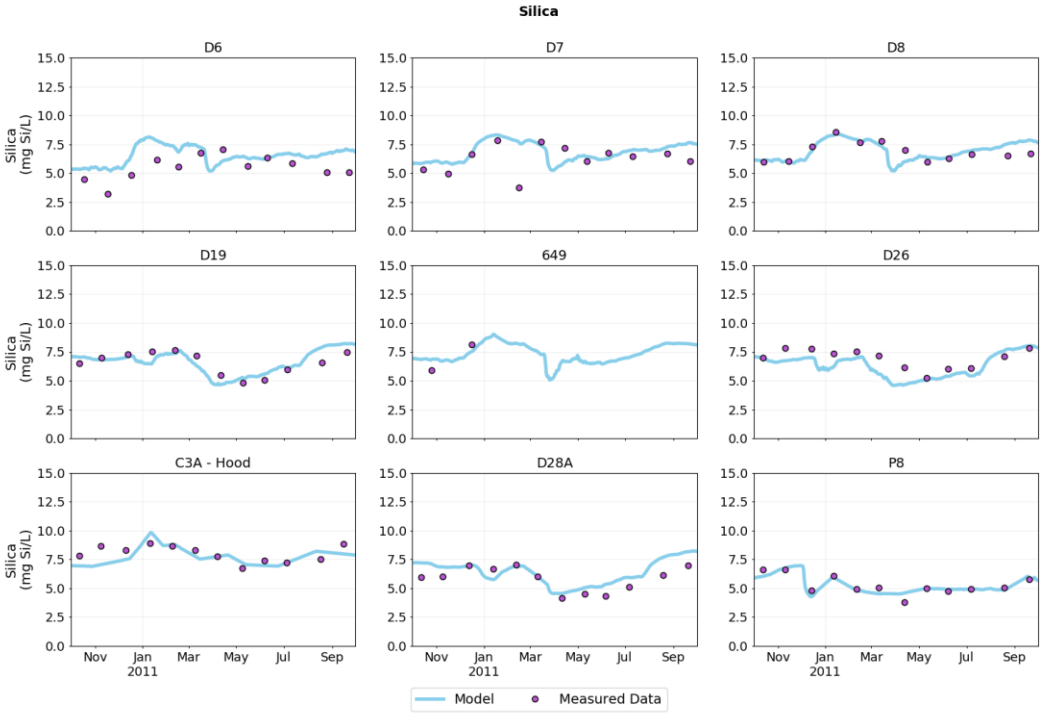

NOTE: Silica data from January 1 - October 1 2011 at Station 649 were flagged during a U.S. Geological Survey quality assurance/quality control check. The flagged data has been omitted from the plots.

Figure 3.12. WY2011 model validation of silica at discrete sampling sites.

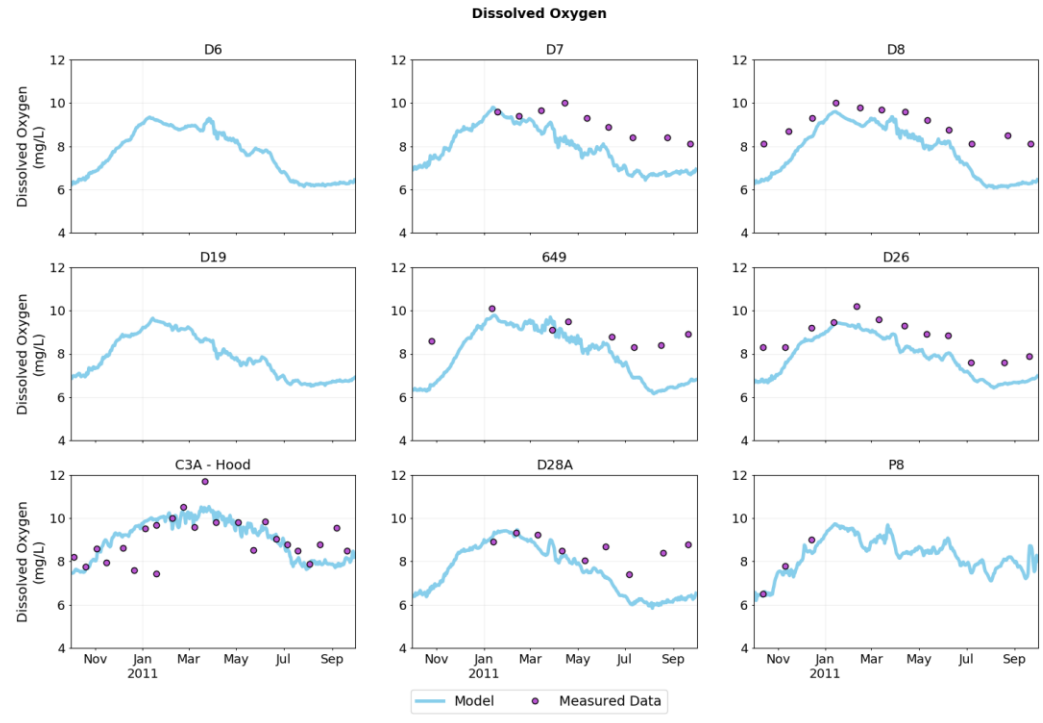

Figure 3.13. WY2011 model validation of dissolved oxygen at discrete sampling sites.

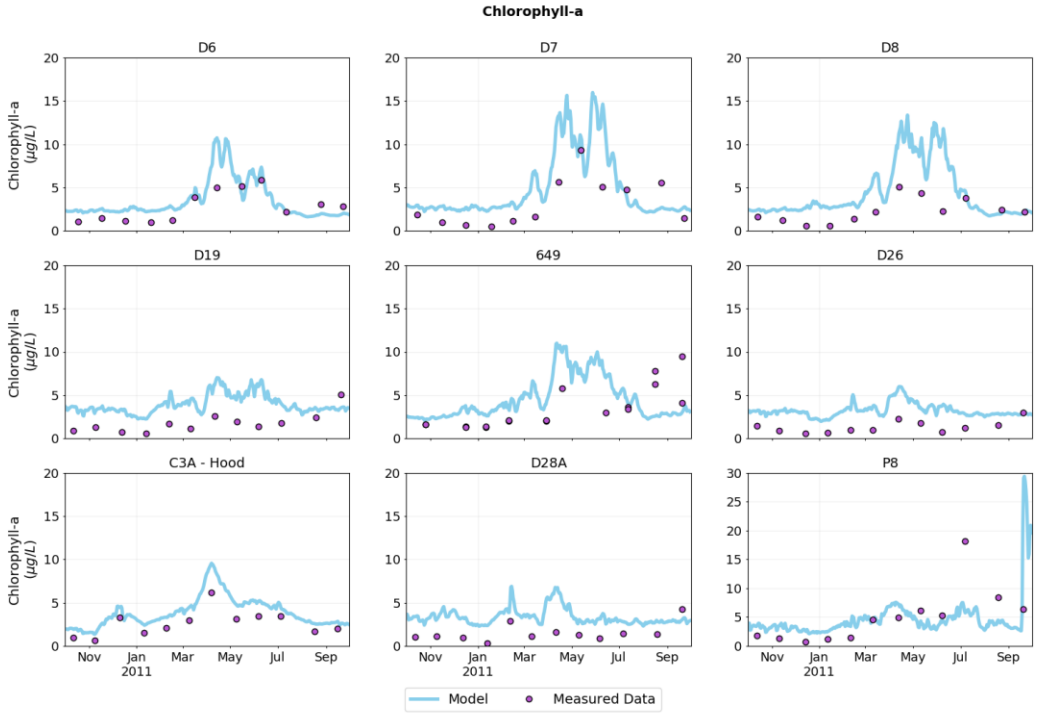

Figure 3.14. WY2011 model validation of chlorophyll-a at discrete sampling sites.

The model captures the seasonal and spatial variations in the observed concentrations of nitrate (Figures 3.1 and 3.8), ammonium (Figures 3.2 and 3.9), and DIN (Figures 3.3 and 3.10) in WY2016 and WY2011. Considering that each parameter varied over a 30-100 fold concentration range over the 2 years and throughout the Delta-Suisun region, the agreement between observed and modeled concentrations indicates that the most important transport and water column processes affecting these state variables are well-represented by the model. Nitrate, ammonium, and overall DIN concentrations in the Delta-Suisun region are influenced by numerous factors, including point sources and nonpoint sources, flow-routing (including water diversions), and transformations in the water column and sediments. The observed seasonal DIN patterns (Figures 3.3 and 3.10), consisting of yearly maximums in winter and lower levels in late spring and summer were generally well represented by the model.

Observed and simulated ammonium levels were relatively low (as a percentage of DIN) throughout the Delta, except in the Sacramento River downstream of the Regional San wastewater treatment plant (C3A), indicating that ammonium loaded from C3A underwent nitrification at relatively fast rates (relative to transport rates within the system), and that this relatively rapid nitrification was well-predicted by the model (Figures 3.2 and 3.9). The observed and simulated late-fall and winter peaks in concentrations of both nitrate and ammonium are likely shaped by two factors. The gradual increases in nitrate and ammonium over Oct-Dec 2015 at all sites, which preceded increases in flow rates, are consistent with the interpretation that they resulted from seasonal, system-wide slow-downs in nitrogen transformation or loss processes (e.g., nitrification; uptake of ammonium and nitrate by phytoplankton or other primary producers; denitrification) due to colder temperatures and shorter days, as previously observed (SFEI 2015). The second cause is likely related to low Sacramento discharge throughout October and November. Decreased river discharge results in slower flushing of nitrogen

loaded from the Sacramento Regional WTP, and the resulting accumulation can produce increased ammonium and nitrate concentrations. The two ammonium concentration minima at C3A in late January and March 2016 coincide with the two major Sacramento River flow peaks, pointing to dilution of C3A's loads by high river flows being the primary cause. The subsequent increase in observed ammonium levels at C3A in late spring (May-June 2016) likely resulted from two factors: 1) decreasing Sacramento River flows, translating to higher ammonium concentrations; and 2) a window of increased loading from C3A (Appendix B, C3A shows a distinct increase in ammonium levels during this time).

Model performance predicting DIN within the central Delta (D26, D19, D28A) varied over time and by station, with concentrations over-predicted in D28A, D26, and D19 during WY2016 (fall, spring-summer), but with substantially better performance in WY2011. Potential explanations for these differences include: overestimating modeled nitrogen fluxes from sediments to the water column (which would have more pronounced effects on concentration during low-flow years, such as WY2016); underestimating modeled phytoplankton production; or DIN uptake by aquatic macrophytes, which can grow to high densities in this region of the Delta, but are not currently represented in the model. Additional work is needed to examine this issue and elucidate the most likely causal factor(s).

While the majority of nutrient model development focused on nitrogen dynamics, tracking phosphate and silicate concentrations can offer additional useful insights into underlying processes. Unlike DIN, measured phosphate concentrations generally reached their maximum levels in summer and fall and were typically at lower levels in winter and early spring (Figures 3.4 and 3.11). This pattern was particularly pronounced in WY2016 in Suisun Bay (D6 through D8) and the central Delta (D26 and D28A). This phosphate signal indicates that fluxes from the sediment to the water column are an important source of phosphorus during summer and fall. Measured phosphate levels were generally between 0.05 - 0.1 mg/L throughout the year, much higher than concentrations that would slow phytoplankton growth. Silicate, an important nutrient for diatom growth, is transported into the system as a natural constituent in runoff and is also recycled from the sediments to the water column. The model captures the general spatial, seasonal, and inter-annual patterns in phosphate and silicate concentrations throughout most of Delta and Suisun Bay and the Sacramento River (Figures 3.4-3.5, 3.11-3.12). The largest deviations between modeled and measured phosphate and silicate concentrations tended to concur in space and time with the largest deviations between modeled and measured DIN concentrations, and may be caused by similar explanations. While multiple potential explanations are being examined through ongoing work, one primary focus is on the role of sediment fluxes, in particular because sediment chemistry and flux data are a major gap throughout the region.

Ambient chl-a concentrations were generally low across the Delta and Suisun Bay throughout most of WY2016 and WY2011, with the exception of several space-time windows with elevated biomass (Figures 3.7 and 3.14). The model reproduces the generally-low chl-a levels in observational data, along with the timing and magnitude of higher chl-a levels at several locations during WY2011. However, the model underestimated chl-a levels in WY2016 during the spring (multiple locations) and fall (in Frank's Tract area). Capturing the bloom magnitude in WY2016 proved challenging because relaxing any set of controlling factors for phytoplankton growth (primarily grazing and light—as indicated earlier there were seldom any nutrient limiting condition periods during the simulation) typically resulted in windows with excessively large biomass predictions that were not supported by the observations. A similar phenomenon (excessively high modeled chl-a values) also occurred when forcings were relaxed for the WY2011 simulation. The current set of phytoplankton growth, grazing, and light extinction parameters

provided the best overall fit across both of the water years. Modeled DO values followed similar seasonal patterns as observed DO, although the model generally under-predicted observations by ~20% (Figures 3.6 and 3.13). The dominant seasonal patterns (across sites and years) are consistent with the variations caused by temperature-driven variations in DO %-saturation, however there were some contribution from temperature-dependent respiration rates. The shortfall in predicted DO concentrations is likely partially attributable to our underestimates of primary production. This underestimation includes both underestimation of phytoplankton during some space-time windows, and the fact that floating and submerged macrophytes (e.g., around the Frank's Tract area), which grow densely in some regions, are not included within the current model.

3.2 High-Frequency Moorings

Figures 3.15 - 3.18 present model results and observations from high-frequency mooring locations at four Delta sites during WY2016 (see Figure 2.15 for site locations; Sacramento River at Freeport [FPT]; Sacramento River above the Delta Cross Channel near Walnut Grove [WGA]), Cache Slough at Ryer Island [CCH], and Sacramento River at Decker Island [DEC]). The results include observed and simulated chl-a, nitrate, DO, and temperature, with modeled values presented for the surface 1 m (no or little vertical variability was observed for predicted values, indicating that the modeled water column was generally well-mixed vertically). Observed light attenuation coefficients (KD) are also presented. These time series of KD at each mooring site were calculated by converting *in-situ* turbidity values to KD using the approach described in Section 2.3.4 and Appendix C. The modeled light limitation factor is included for comparison with KD. The light limitation factor is calculated internally within the model and represents the degree to which predicted phytoplankton growth rates are decreased relative to their maximum growth rate due to light availability (zero indicates total light limitation; one indicates no light limitation). Similarly, the modeled nutrient limitation factor (a quantity indicating to what extent modeled phytoplankton growth is limited by nutrient availability—which could include nitrate, ammonium, ortho-phosphate, etc) is plotted alongside chl-a for reference. The model equations for both these factors can be found within Deltares (2019b).

Depth-averaged light limitation factor values are presented in Figures 3.15-3.18, recognizing that the simulated water column was typically well-mixed at these sites, and that phytoplankton would therefore, on average, be exposed to depth-averaged light levels. Temperature was predicted within the hydrodynamic model, not the water quality model. However, many of the quantitatively-important biogeochemical rates vary strongly with temperature; therefore temperature is included here to provide information about the model's ability to represent seasonal variations in rates.

At Freeport (Figure 3.15), the model shows a close match to the high frequency nitrate data, which aligns with expectations given the Freeport nitrate concentration data were used for the upstream Sacramento River at Verona boundary condition. Considering that the model's Sacramento River boundary is ~30 miles away, this goodness of fit suggests that little transformation (either uptake or denitrification) of nitrate occurs between the boundary (Sacramento at Verona) and Freeport. Chlorophyll-a levels at Freeport are low throughout the year, and the model generally captures the magnitude and seasonal trend. The sharp changes in estimated KDs (increase) and predicted light limiting factor (decrease) during periods of high flow illustrate the strong influence elevated suspended sediment concentrations have on phytoplankton production, with predicted growth rates (depth-averaged) being 80-90% lower than maximum rates.

Observed conditions at Walnut Grove (Figure 3.16) were similar to those ~30 km upstream at Freeport, including elevated KD coinciding with high flows, moderate to low chl-a, and a similar 4-fold difference between high-flow and low-flow nitrate concentrations. Model predictions for light limitation, chl-a, dissolved oxygen and nitrate track observations reasonably well, although the modeled chl-a varied more smoothly than observed chl-a. While at first glance the two stations' observed nitrate concentrations appear similar, some substantial differences emerge when focusing on lower-flow

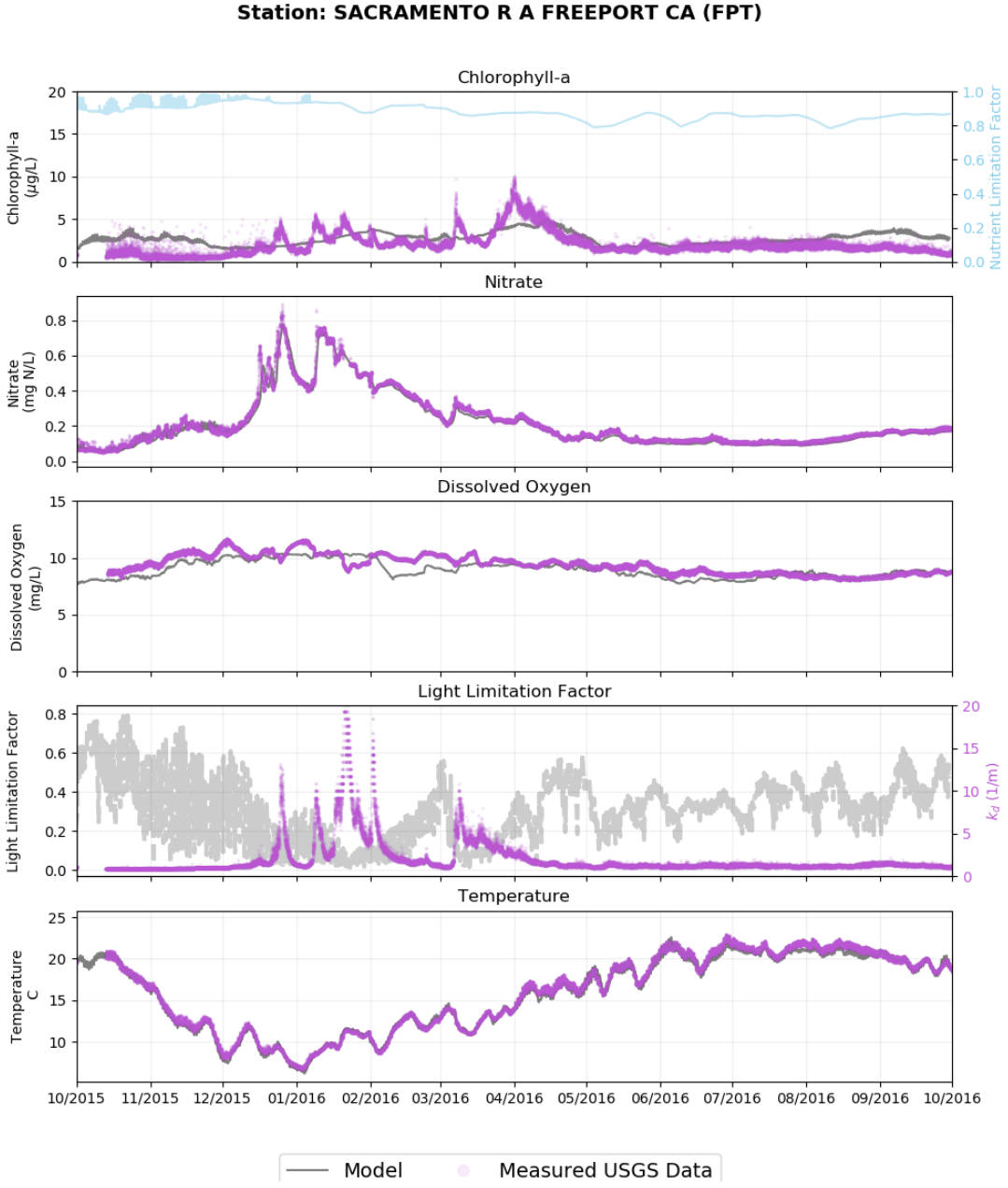

Figure 3.15. Model validation with the high frequency mooring site at the Sacramento River at Freeport

periods. During Nov 2015 and May 2016, WGA observed nitrate concentrations exceeded those at Freeport by ~50% and 30-40%, respectively, consistent with conversion of ammonium discharged by Regional San (released ~0.2 km downstream of Freeport) to nitrate during transit to WGA, along with some nitrate increase related to ammonium flux from the sediments (followed by nitrification; see Kraus

et al., 2017). Predictions agree well with observations at FPT and WGA during these time periods, indicating that the combined effect of those two processes is being well-represented by the model. Robust predictions of nitrate concentration, discharge, and flux at Walnut Grove are particularly important because of this station's proximity to DCC, where large flows (and mass fluxes) are diverted to the interior Delta when the DCC is open.

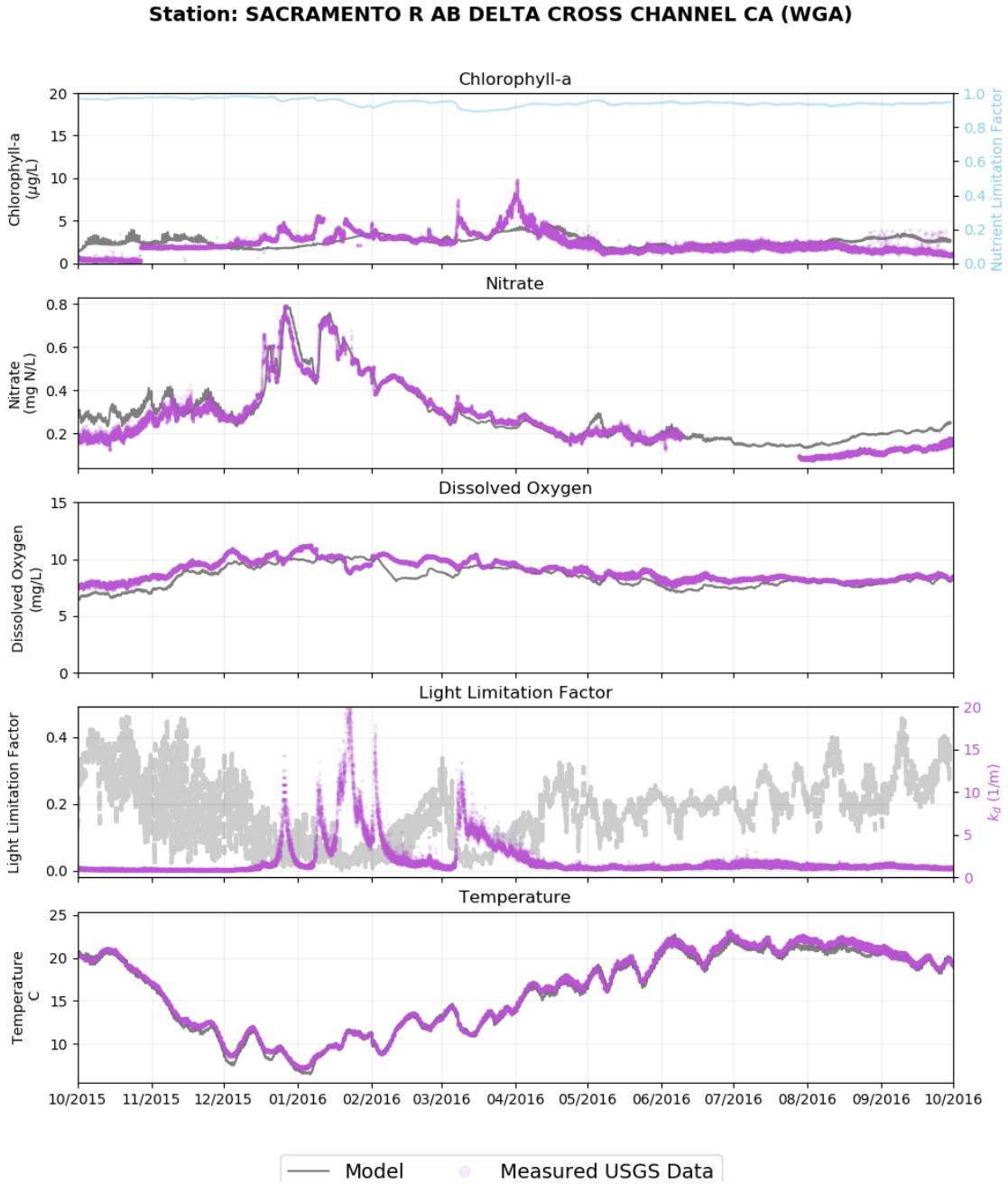

Figure 3.16. Model validation with the high frequency mooring site at the Delta Cross Channel

Observational and model data at the Cache Slough at Ryer Island site are presented in Figure 3.17. The mooring chl-a data highlights the occurrence of short-lived elevated biomass events during fall 2015, along with several elevated biomass events spanning 1-3 weeks during late spring and summer 2016. Simulations did not produce similar events; instead, the model predicted consistently low chl-a

concentrations throughout most of the year at CCH. Modeled nitrate concentrations do, however, track observed nitrate throughout much of the year, although modeled values deviated increasingly from observed values through the spring-summer windows with elevated biomass and during September 2016. Further comparisons of model predictions and high frequency data are explored in Section 3.3 in terms of mass flux, along with some exploration of the relative magnitude or importance of events and deviations. Several factors could be contributing to the deviations between observed and modeled chla and nitrate: limited data on benthic grazer densities; submerged and floating aquatic vegetation, which have a substantial presence in the Cache region, and are not simulated in the current model; and potential limitations of the hydrodynamic model's representation of transport within the Cache region and exchange with the Sacramento River. These potential issues will be further examined and remedied through on-going work.

At Decker Island, modeled nitrate concentrations tracked observations from January through September 2016, but underestimated concentrations by 20-30% during some windows (Figure 3.18). As noted previously (Section 3.1), the model did not capture the observed elevated phytoplankton biomass in spring 2016, a point that is further reinforced by the high frequency data from Decker Island. We see additional bloom activity from the mooring site at Decker Island throughout the summer through August 2016. These activities are also not captured by the model. The observed chl-a signal at Decker appears quite similar -- in terms of timing and concentration -- to observations at CCH (Figure 3.17). On the one hand, the similar chl-a signals might point to a hypothesis that the Cache Slough Complex served as the source of the biomass observed at Decker Island and other down-estuary sites (see Figure 3.7, model comparisons with monthly discrete chl-a observations). On the other hand, however, relative flow rates and mass fluxes must also be considered. For example, the observed nitrate concentrations were substantially higher at Decker Island than at Cache Slough during some times of the year (e.g., fall 2015), and more consistent with most of the flow and mass (at least nitrate mass) being transported from the Sacramento River (i.e., from WGA). Modeled nitrate was consistently lower than measured nitrate (by

about 0.2 mg/L) throughout the fall, but converged with measured nitrate in the winter, around February/March, when freshwater runoff from the Sacramento River peaked.

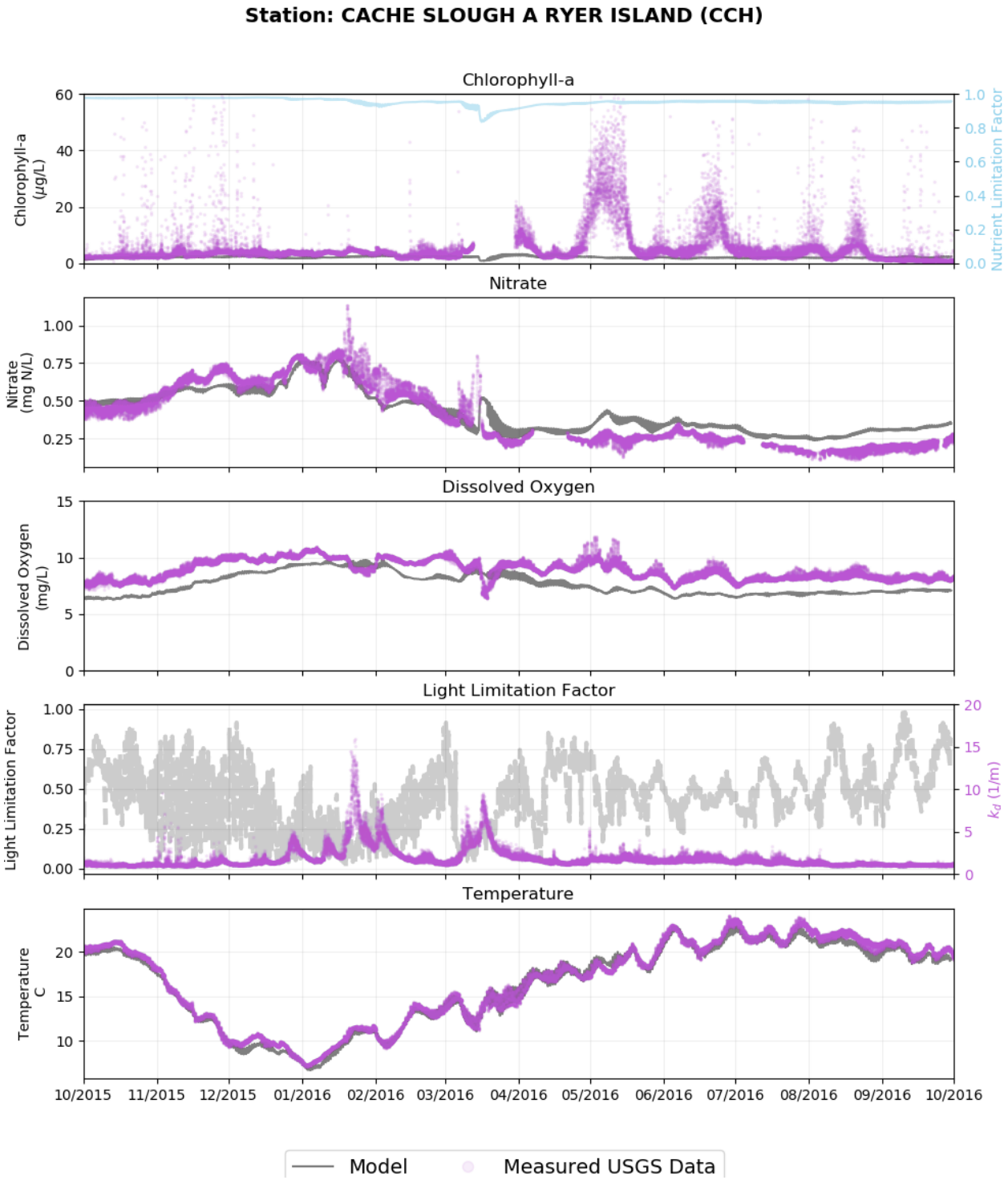

Figure 3.17. Model validation with the high frequency mooring site at Cache Slough at Ryer Island

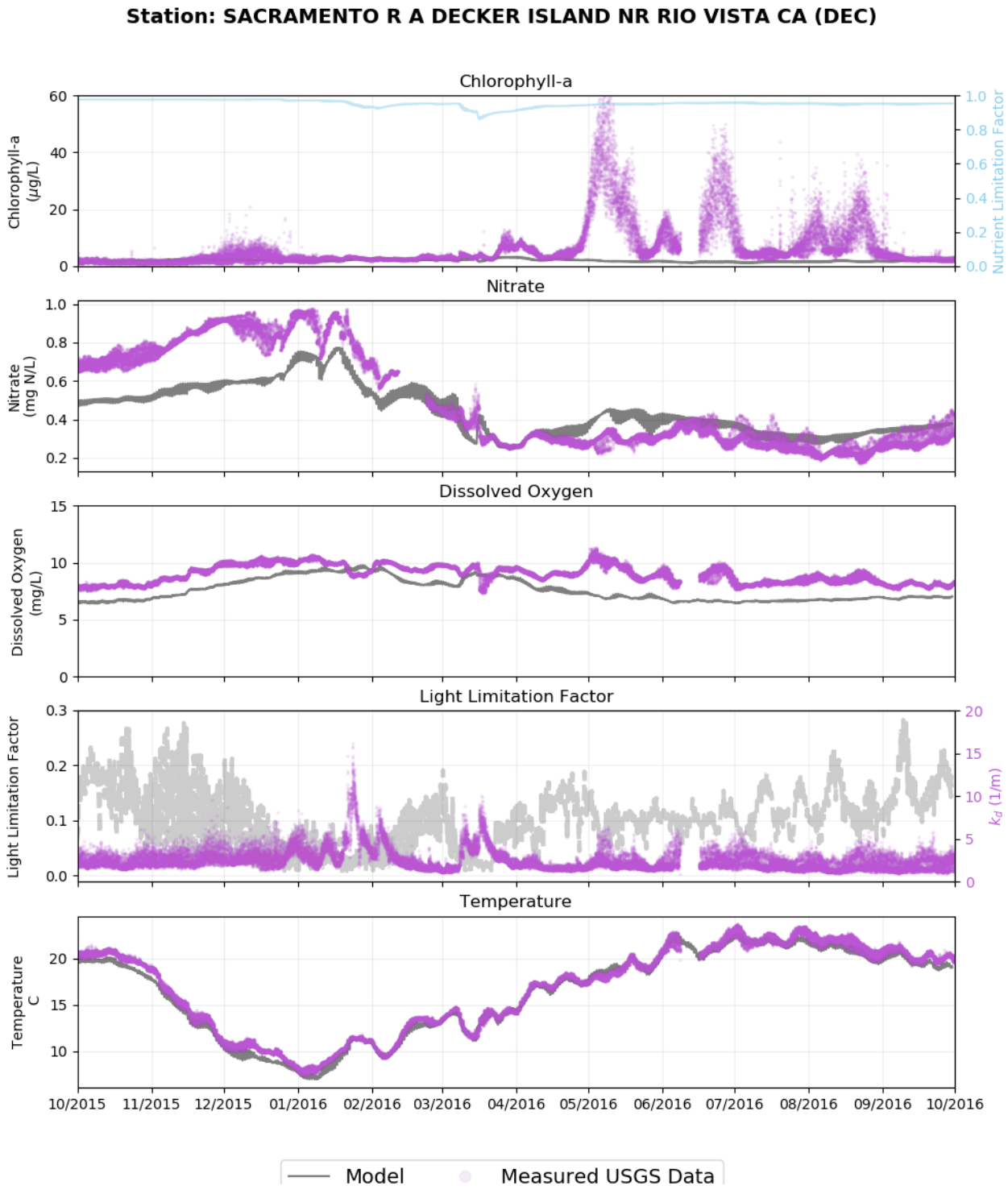

Figure 3.18. Model validation with the high frequency mooring site at Decker Island near Rio Vista

3.3 High-Frequency Flux Measurements

High frequency flux comparisons are presented in Figures 3.19-3.22 for Freeport, the Sacramento River above the Delta Cross Channel (also referred to as Walnut Grove), Cache Slough, and Decker Island, respectively.

As discussed in Section 3.2, the good agreement between observed and modeled nitrate concentrations result in large part from Freeport data's use to develop the northern nitrate boundary condition. The agreement between modeled and measured gives an indication of the very limited net losses or sources from transformation processes in the upper reaches of the Sacramento River (Figure 3.19). Similarly good agreement is observed at Walnut Grove, despite it being 30 km and 1.5 travel days (during low flow) downstream of Freeport. Modeled and measured concentrations also agreed well (Figure 3.20). While modeled chl-a concentrations on-average track measured concentrations at both locations, the model does not reproduce the relatively short-lived chl-a peaks in the observational record, which appear to occur during runoff events, with at least some of that chl-a introduced upstream of the model's Sacramento boundary (and that current boundary conditions apparently do not include). Comparing modeled and measured fluxes offers additional perspective for considering the importance of individual events. Because both discharge (from the hydrodynamic model) and nitrate concentrations (from the biogeochemical model) are used to calculate modeled fluxes, it also offers an additional lens through which to asses overall model performance and confidence in model predictions. At both locations, modeled nitrate fluxes (tidally-averaged and cumulative, bottom two panels) agree well with observations. Chlorophyll-a fluxes also agree well with observations. When the time periods with chl-a spikes are examined through the lens of tidal-averaged and cumulative fluxes (bottom two panels), the deviations between observed and modeled concentrations are minor, with the exception of the deviation introduced during the Mar 2016 high flow event. Interestingly, from April - August 2016, modeled and measured cumulative fluxes again have comparable slopes, indicating that tidally-averaged fluxes agree well during that period (also evident from the tidal-averaged flux plot).

The discussion of predicted and observed phytoplankton biomass in Section 3.1 (Figures 3.7, 3.14) established that the simulations captured the system's generally year-round low-biomass along with several elevated biomass events that punctuated WY2011, but did not reproduce WY2016's sub-regional and weeks-to-month time-scale events identified through monthly discrete monitoring. It is therefore no surprise that the high-frequency chl-a peaks at Cache Slough and Decker Island were also not predicted by the model (Figures 3.21 and 3.22). A comparison of the high-frequency-mooring and monthly-discrete time-series at those sites provides a degree of confirmation or validation of the high frequency-sensor results reliability. The comparison also offers mechanistic context about the characteristic time scales of events, and the scales (time, areal extent, concentration) of events that can be resolved through different monitoring approaches. In addition, germane to assessing model performance, the diverse data sources (high-frequency-observed, monthly-observed, modeled) offer an opportunity to examine the ecological significance of individual events or event-types, and provide information relevant to determining what events or conditions need to be detected through monitoring and reliably predicted by numerical models in order to accurate characterize system behavior. The cumulative chl-a mass flux estimates at Decker Island during WY2016 (Figure 3.22) could be described as having ~3 prominent features or phases: first, a moderate increase (late-Jan: 6-7 Mg increase over 30 days, ~0.2 Mg/d); followed by a second, substantial increase (mid-Mar: 20 Mg increase over 15 days, ~1.3 Mg/d); and then finally, a third, moderate but sustained increase (April through mid-July, 20 Mg

increase over ~100 days, 0.2 Mg/d). The first two phases contributed 50-60% of cumulative annual net chl-a flux to Suisun Bay.

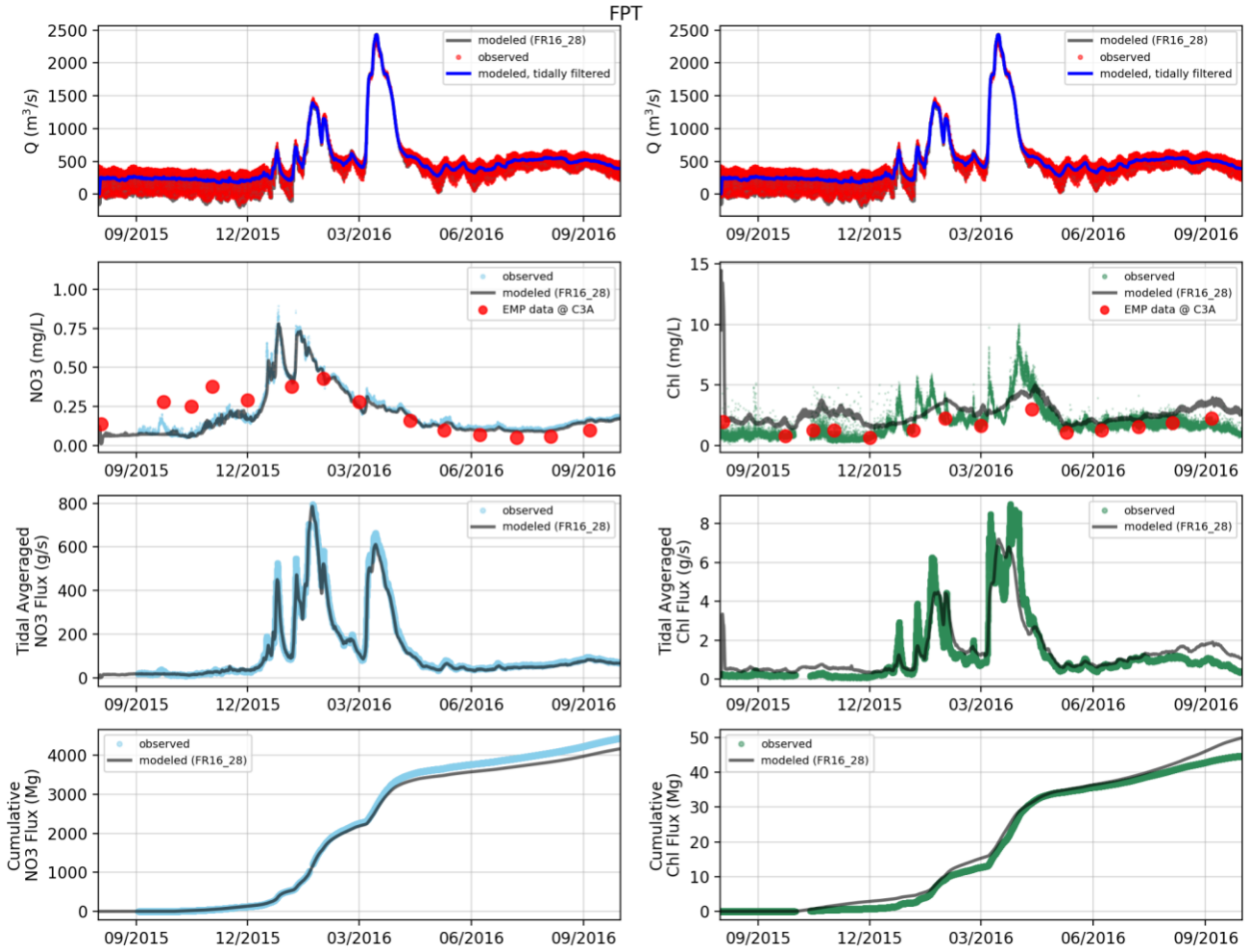

Figure 3.19. Plots of discharge, concentration, instantaneous and cumulative flux of both nitrate and chlorophyll-a at Freeport.

During Jan 2016 (first phase), chl-a concentrations were fairly constant around 2-3 ug/L, however, sharp increases in discharge resulted in increased phytoplankton biomass flux. Through mid- to late-March at Decker (roughly 40% of cumulative annual flux), model tidally-averaged and cumulative fluxes closely tracked the empirical flux estimates, reflecting the close agreement between the model predicted and observed chl-a concentrations throughout that time period.

Although flows decreased sharply between mid-March and early-April (75% decrease), tidally-averaged empirical fluxes remained elevated (Figure 3.22). During that time, the substantially-decreased flows were offset by the modest biomass increase that began in late March and continued into early April March (5-10 ug/L), resulting in the mass flux rate remaining similar. The remaining 40% of the cumulative annual flux was delivered to Suisun Bay at an average rate of 0.2 Mg/d, roughly a factor of 10 lower than the second phase. Of particular note is the fact that the three to four elevated biomass events (i.e., higher concentration of chl-a) during WY2016 occurred during this final phase. However, net export was much lower than during March, despite two to five times greater chl-a concentrations during

the events. In fact, the empirical estimates identify time periods when net chl-a flux was up-estuary (Figures 3.20 and 3.21, tidal averaged flux panel).

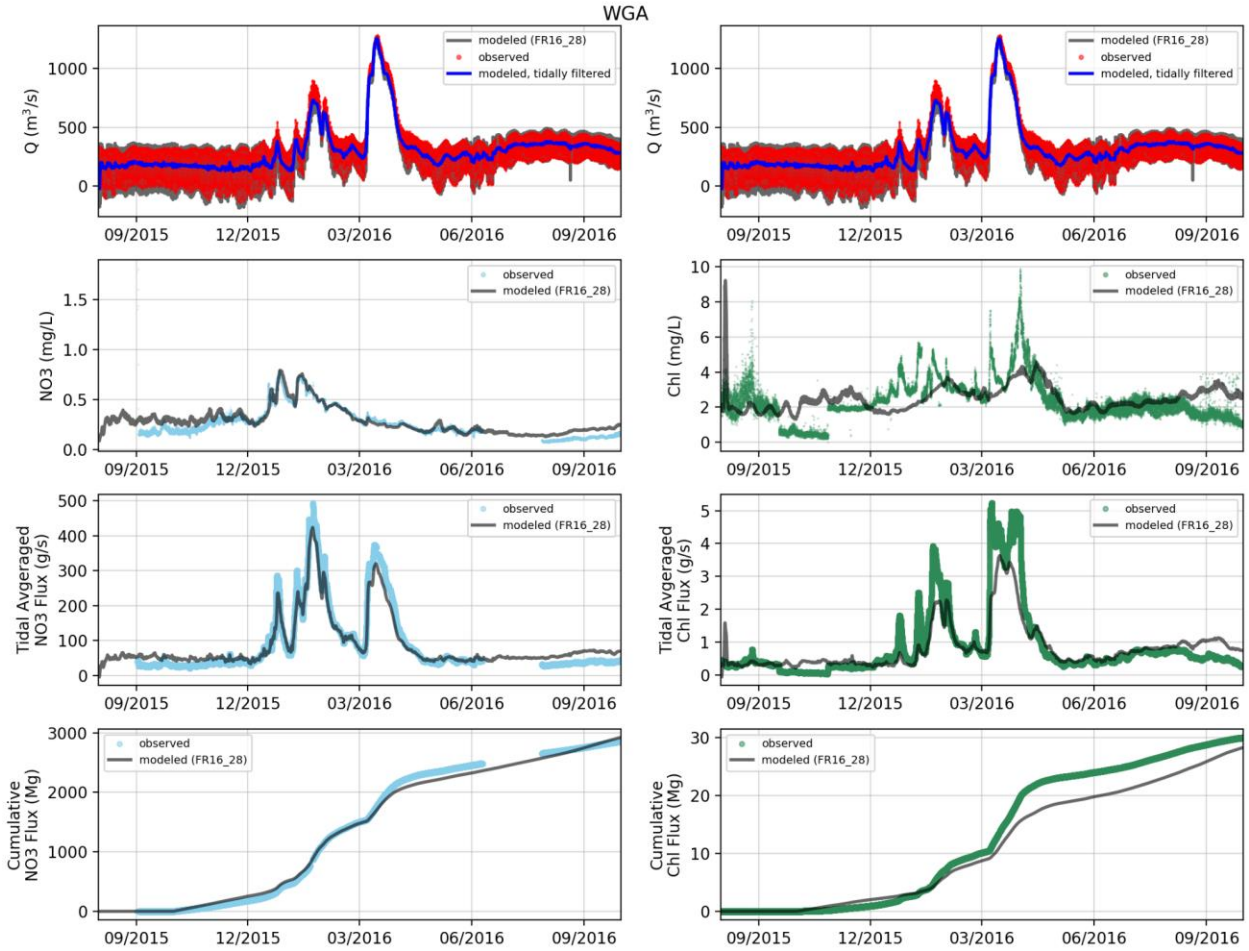

Figure 3.20. Plots of discharge, concentration, instantaneous and cumulative flux of both nitrate and chlorophyll-a above Delta Cross Channel near Walnut Grove.

Empirically-derived mass flux rates were roughly a factor of two greater than modeled fluxes, with the observation's higher baseline and three to four events being the primary reasons for the difference. Over the entire water year, modeled cumulative biomass fluxes past Decker (down-estuary) were 40% lower than observed fluxes (Figure 3.22, bottom right panel). Half of that difference (20% of net annual export) was due to the late March event, with moderately elevated chl-a concentrations (up to 10 ug/L) sustained over 1-2 weeks. The deviations between modeled and observed concentrations during April-August 2016 were responsible for the remaining 20% difference. Some of that difference is simply due to the low predicted baseline chl-a concentration. The prominent events — in terms of concentration (4-10 fold higher concentrations) and duration (7-8 weeks at concentrations greater than 5 ug/L)— therefore contributed a maximum of 20%.

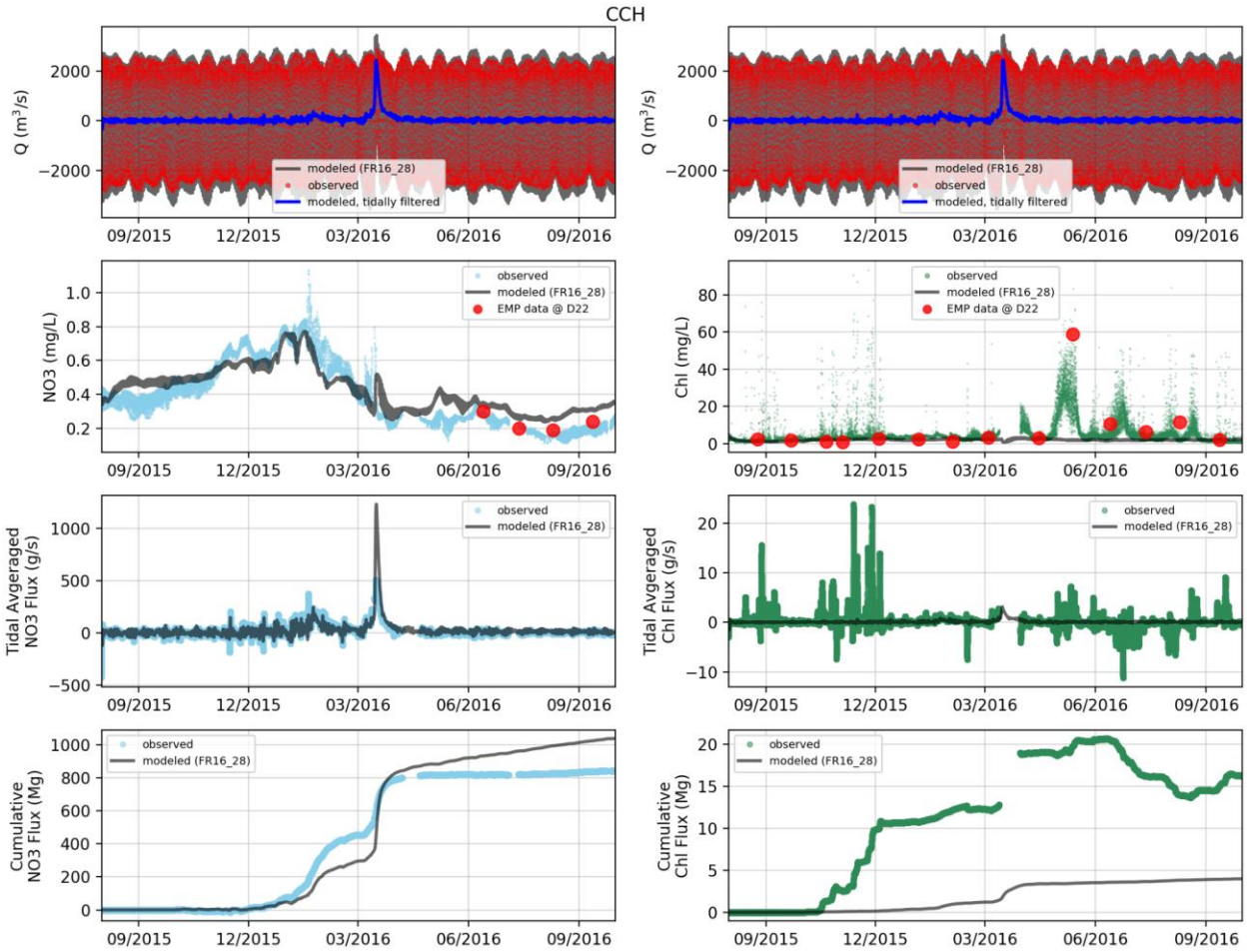

Figure 3.21. Plots of discharge, concentration, instantaneous and cumulative flux of both nitrate and chlorophyll-a above Delta Cross Channel at Cache Slough near Ryer Island.

Modeled and observed nitrate fluxes agreed reasonably well at CCH and DEC (Figure 3.21-3.22). Modeled cumulative nitrate fluxes at Cache Slough aligned closely with observations until mid-January, when they deviated during the high flow event. The model captured the timing of the March event, but underestimated the events integrated flux by ~30%. During April-August 2016, the model over-predicts cumulative flux, which observations suggest had plateaued, resulting in approximately 20% higher annual cumulative flux by the end of the simulation. One potential explanation for this difference is that the model is under-predicting N removal within the Cache Slough Complex (e.g., denitrification, burial, uptake by aquatic vegetation not represented in the model). At Decker Island, the model and data exhibit similar nitrate flux patterns, with the model underestimating annual cumulative flux by ~20%. Notably, the cumulative flux curves have nearly identical slopes from April-August 2016. The bulk of the difference between modeled and measured cumulative flux therefore occurred during the January and March 2016 high flow events. The agreement between modeled and measured fluxes from April-August 2016 is encouraging, given DEC's location at the down-estuary edge of the Delta, and suggests that major components of the simulated N mass-balance provide reasonable approximations of actual losses and recycling upstream.

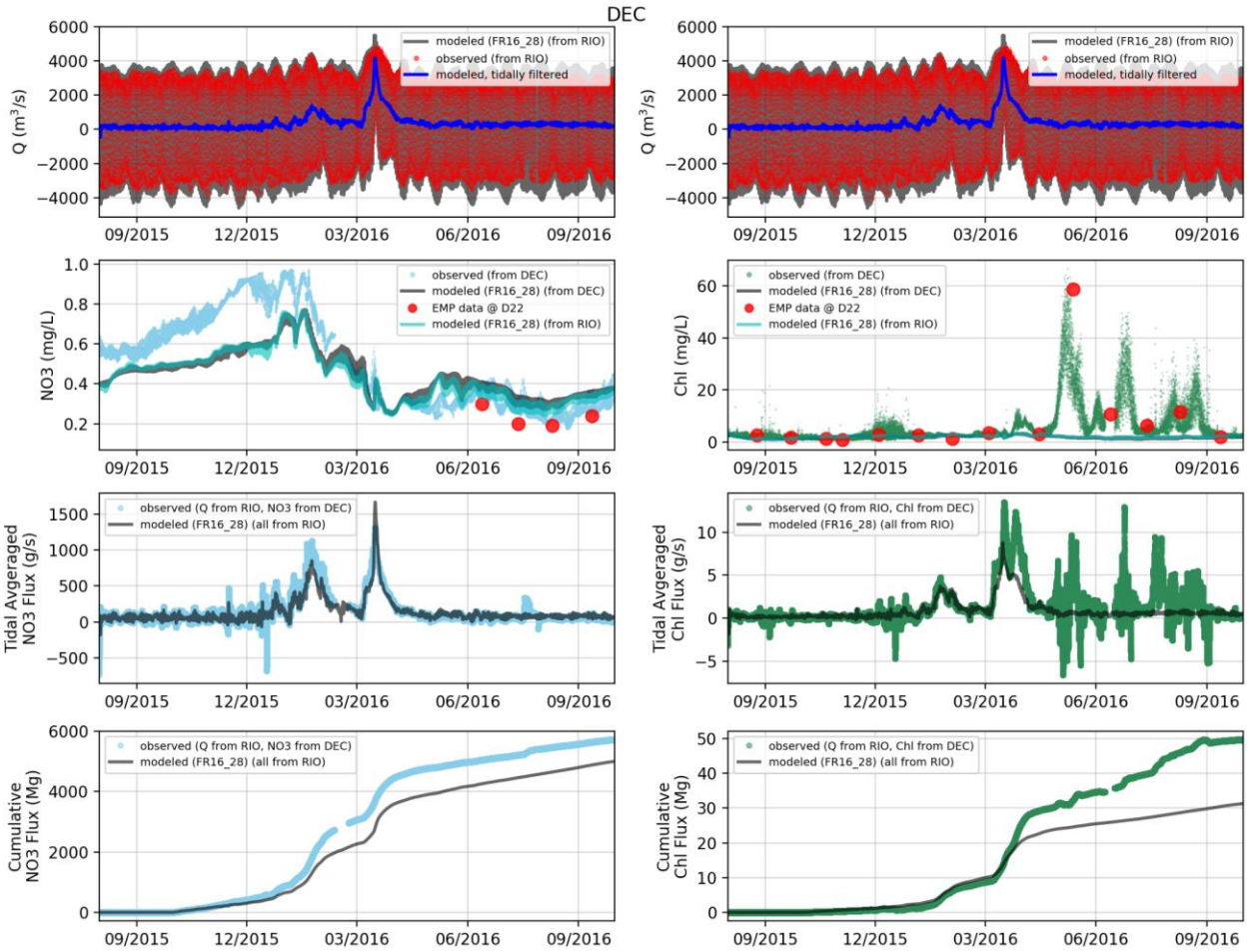

Figure 3.22. Plots of discharge, concentration, instantaneous and cumulative flux of both nitrate and chlorophyll-a at Decker Island.

While a more detailed mass balance analysis is needed to fully determine whether biomass export from the Cache Slough Complex was responsible for the elevated biomass at, and fluxing past, DEC, a preliminary look focusing on mass fluxes offers some useful insights, including for evaluating model performance. Cumulative chl-a flux past DEC totaled ~10 Mg. During the same time period, net chl-a export past CCH was 1-2 Mg. From mid-June through August, another 10 Mg of chl fluxed past DEC; and net fluxes past CCH were -5 Mg (net flux into Cache Slough Complex). The March 2016 flux estimates suggest that, while biomass from the Cache Slough Complex could have seeded production along the lower Sacramento River, net export from the Cache region could only account for a maximum 10-20% of the total export past DEC. During April-August, observations suggest there was net biomass import to the Cache region. A more comprehensive assessment is needed to fully understand the events during spring 2016. From the perspective of evaluating the current model's performance -- although making targeted improvements to the simulation of processes within the Cache region, low predicted phytoplankton production within the Cache region was not the root cause of underestimating biomass down-estuary at CCH. Phytoplankton production is a key management issue in the nSFE, because of the limited supply of high quality food for primary and secondary consumers. Phytoplankton biomass, estimated by measuring chl-a, is often used as a key indicator of ecosystem health in the Delta-Suisun region (gross primary production has also been used in in-depth synthesis studies, e.g., Jassby et al 2002 and Jassby 2008; but chl-a concentration is more readily accessible and therefore more regularly used). The discussion above highlights how viewing the system through concentration-focused vs. mass-flux focused lenses can result in different interpretations. The discussion did not include other important mass balance terms, in particular production rate, grazing rate, mortality, etc.; the model does simulate those processes, and those types of mass balance explorations are planned for subsequent application work using the model. Nonetheless, the comparison of modeled and measured fluxes provides useful context for considering the importance of capturing different types of events.

3.4 USGS Mapping Cruises

Validation plots of the biogeochemical model using USGS mapping cruise data are shown below in Figures 3.23 - 3.34 on four dates (October 21, 2015; April 18, 2016; May 6, 2016; June 9, 2016).

The October 21, 2015 cruise focused on the interior Delta, from the confluence toward Frank's Tract and Stockton. Figure 3.23 shows that the model successfully captures the east-west nitrate gradient (with high nitrate levels greater than 1 mg/L near Stockton and lower levels (less than 0.5 mg/L) moving west toward Suisun Bay. The mapping data of chl-a in the same region (Figure 3.24) shows higher concentrations than the model (greater than 4-10 ug/L vs ~4 mg/L), as well as a trend of increasing chl-a (~10 ug/L) moving east toward Stockton, which is not captured by the model (chl-a is low across the entire region). Oxygen levels are also slightly higher in the measured data than reported by the model by about ~1-2 mg/L (Figure 3.25). The measured data suggests near-saturated conditions, which would be expected with high levels of primary production.

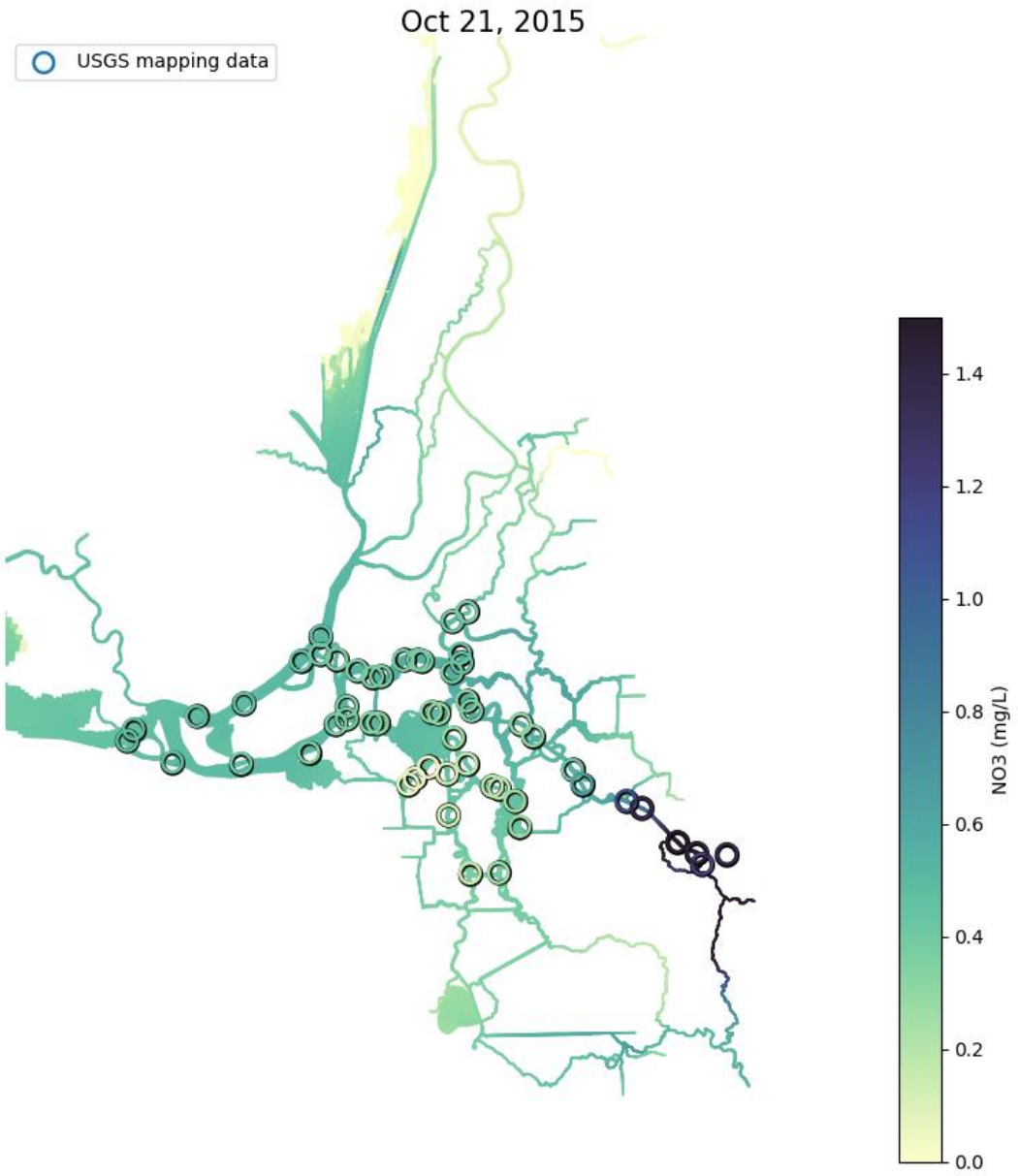

Note: Model results are shown in the map (as a daily and depth-averaged concentration) while the high frequency mapping data is shown as the overlying circles, with circle colors scaled in the same manner as the model results.

Figure 3.23. Model validation with mapping cruise data on October 21, 2015 for nitrate.

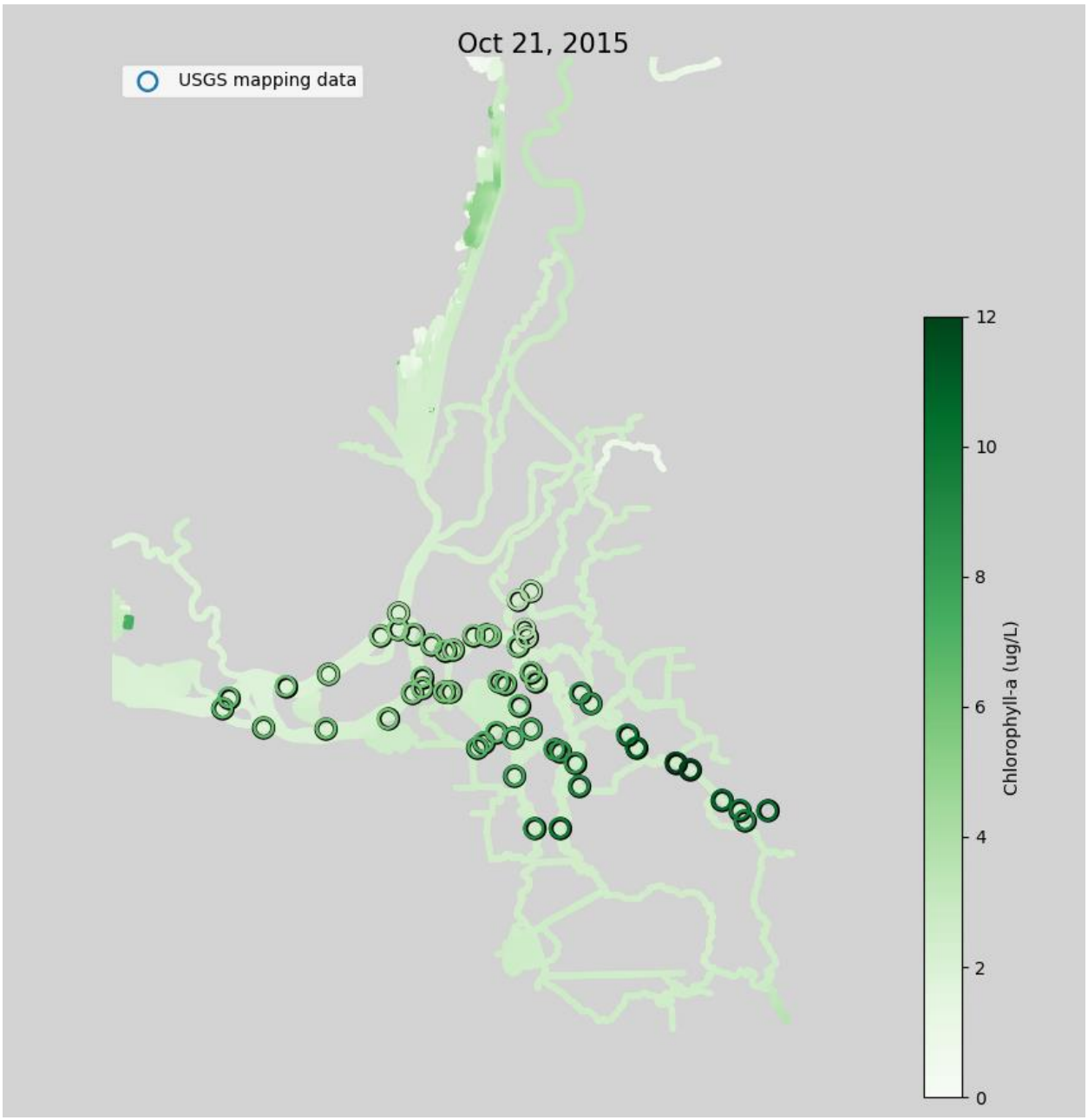

Note: Model results are shown in the map (as a daily and depth-averaged concentration) while the high frequency mapping data is shown as the overlying circles, with circle colors scaled in the same manner as the model results.

Figure 3.24. Model validation with mapping cruise data on October 21, 2015 for chlorophyll-a.

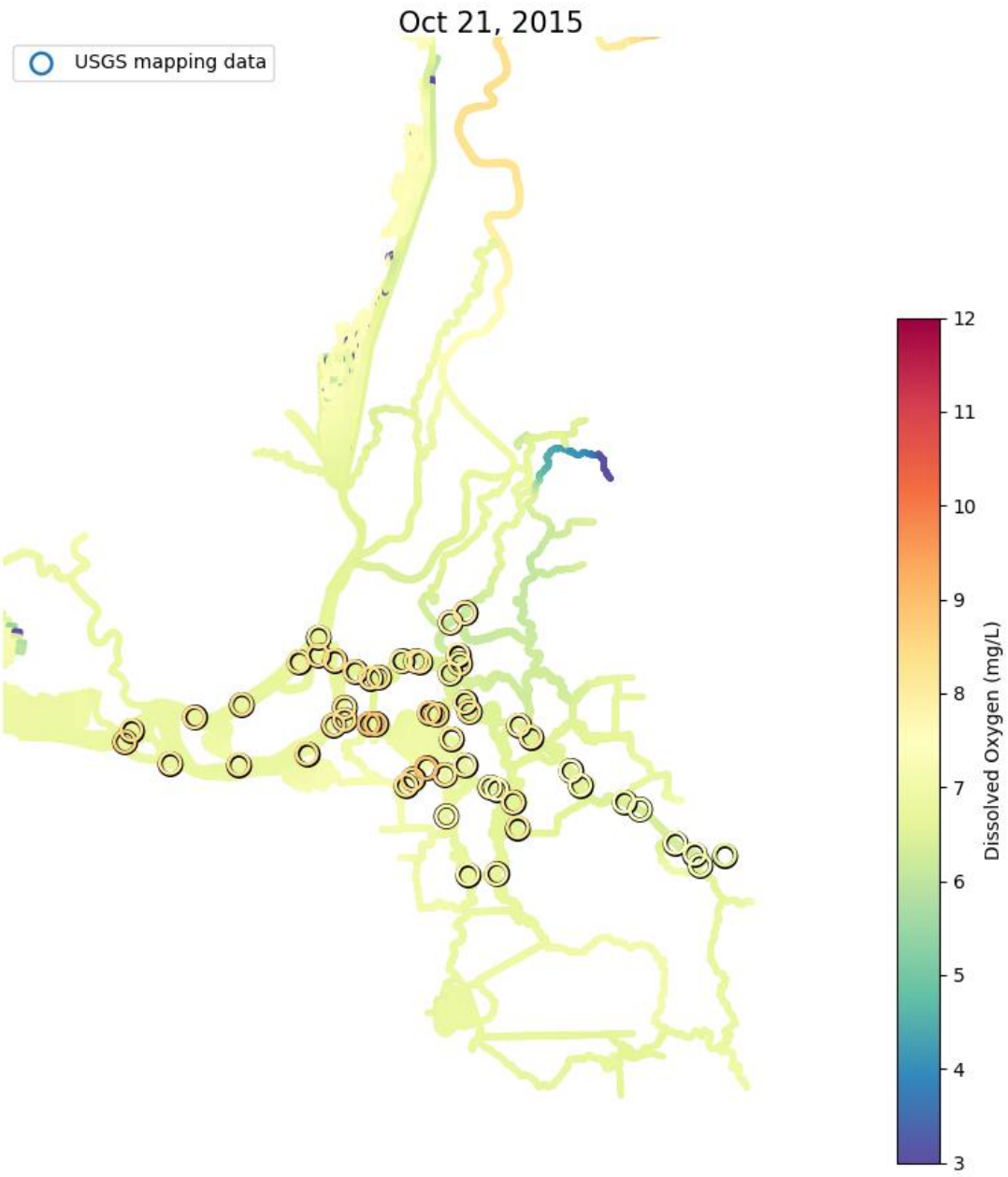

Note: Model results are shown in the map (as a daily and depth-averaged concentration) while the high frequency mapping data is shown as the overlying circles, with circle colors scaled in the same manner as the model results.

Figure 3.25. Model validation with mapping cruise data on October 21, 2015 for DO.

The April 18th, 2016 cruise followed a similar route (interior Delta). The nitrate magnitude and gradient are well-captured by the model, and still evident in the measured data, suggesting this is a year-round persistent gradient (increasing nitrate moving east; Figure 3.26). The model-predicted chl-a shows a strong gradient, with high values near the Stockton Deepwater Ship Channel (greater than 12 ug/L), which sharply decrease moving toward the central Delta to about 4 ug/L. The measured data shows a similar gradient; however, the high chl-a values persistent moving west across the interior Delta, remaining greater than 10 ug/L till around the Frank's Tract region. Overall, the DO levels are on the

same order between the measured and modeled data (~7-9 mg/L), and there is little gradient in the mapping cruise data moving eastward across the interior Delta, which is consistent with the little bloom activity in WY2016.

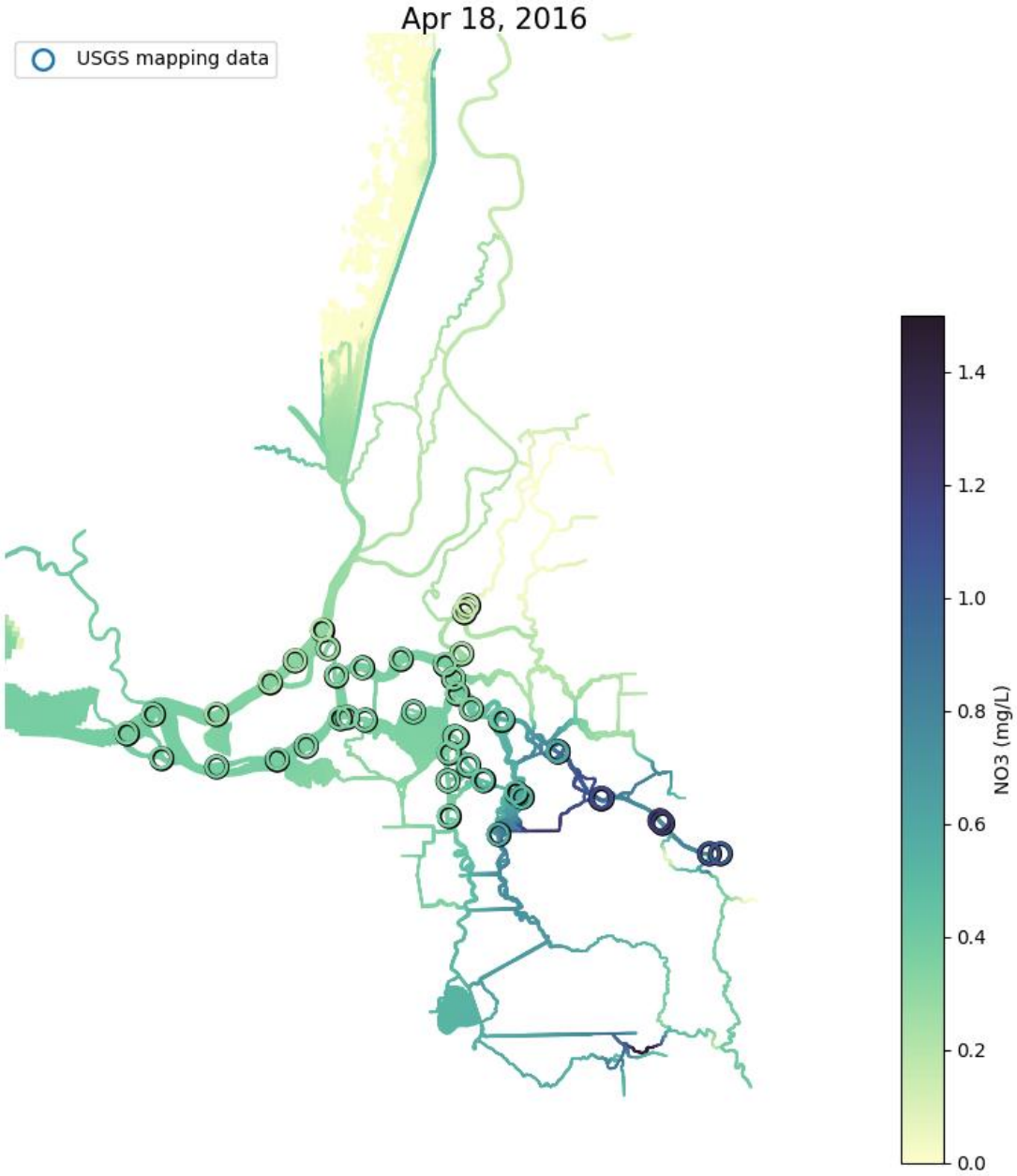

Note: Model results are shown in the map (as a daily and depth-averaged concentration) while the high frequency mapping data is shown as the overlying circles, with circle colors scaled in the same manner as the model results.

Figure 3.26. Model validation with mapping cruise data on April 18, 2016 for nitrate.

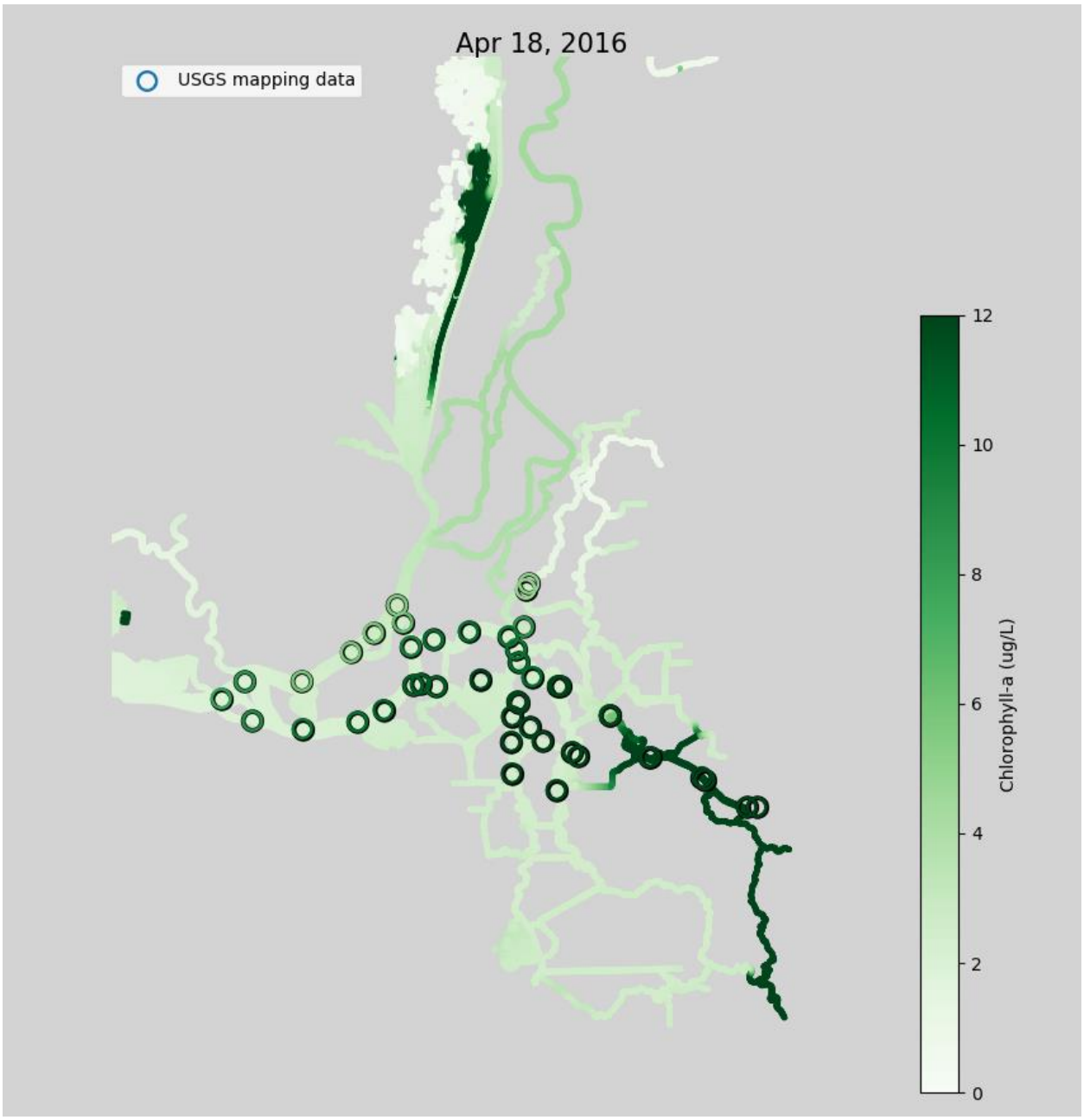

Note: Model results are shown in the map (as a daily and depth-averaged concentration) while the high frequency mapping data is shown as the overlying circles, with circle colors scaled in the same manner as the model results.

Figure 3.27. Model validation with mapping cruise data on April 18, 2016 for chlorophyll-a.

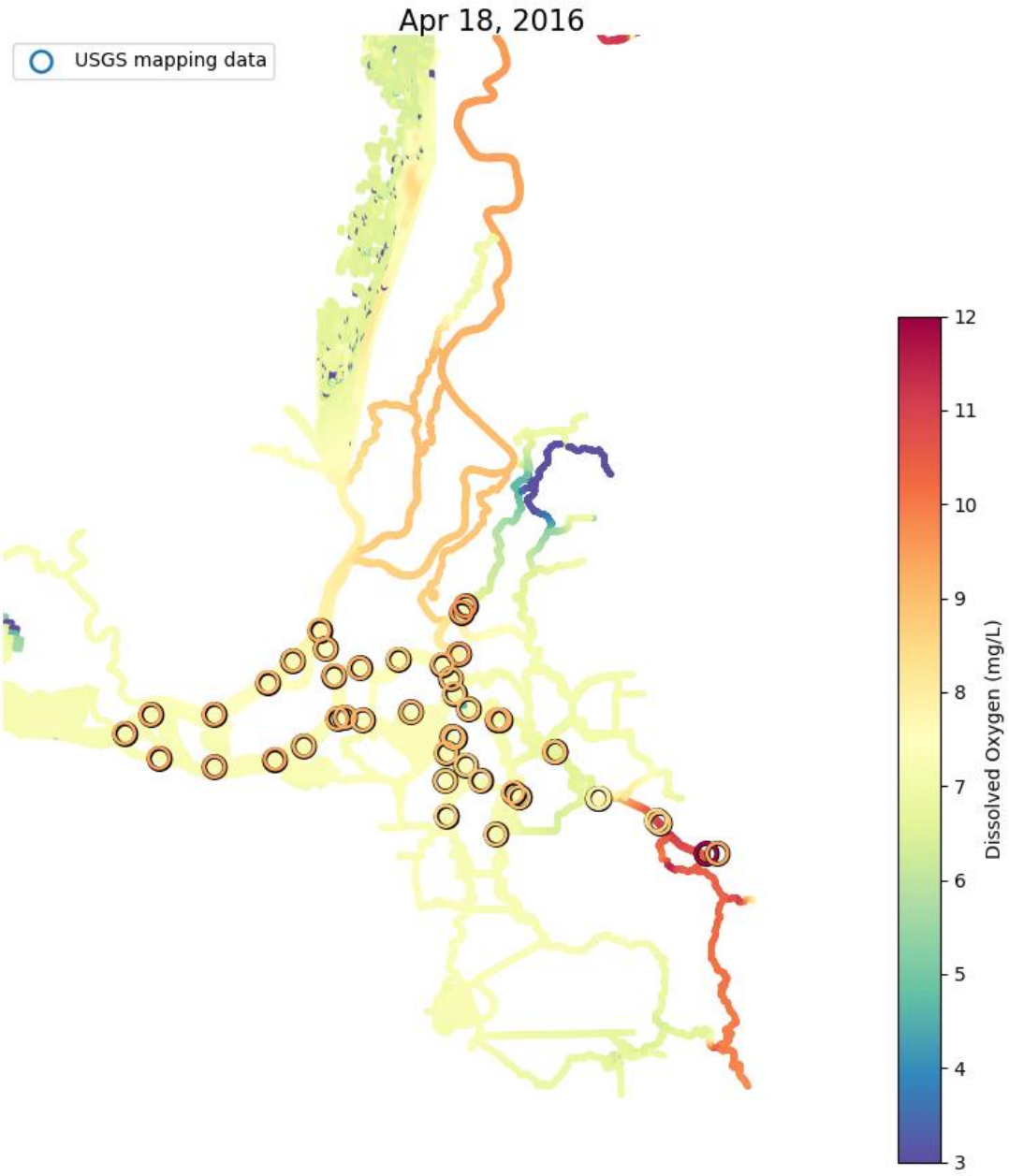

Note: Model results are shown in the map (as a daily and depth-averaged concentration) while the high frequency mapping data is shown as the overlying circles, with circle colors scaled in the same manner as the model results.

Figure 3.28. Model validation with mapping cruise data on April 18, 2016 for dissolved oxygen.

The May 6 and June 9 cruises follow a different track, from Suisun Bay into the lower reaches of the Cache Slough Complex (Figures 3.29 - 3.34). During both the May and June cruise, good alignment in nitrate levels is displayed between the model and observations. The mapping cruise detected little gradient between Suisun Bay and Cache Slough with the exception of lowered nitrate in the Cache Slough Complex itself. The model predicts a similar nitrate magnitude across the Sacramento channel (~0.3-0.5 mg/L) but does not replicate the low nitrate conditions (~0.1 mg/L) in the lower Cache Slough

Complex in May (Section 3.3). The model also under-predicts chl-a by a significant margin. The mapping cruises recorded levels on the order of greater than 5- 12 ug/L while the model predicts ~2-3 ug/L of chlorophyll throughout the main channel, with concomitant underestimation in DO by ~5 mg/L. There is little difference in the mapping cruise data between May and June, suggesting that the gradients and magnitude of nitrate, chlorophyll, and oxygen remain relatively constant throughout the late spring/early summer period.

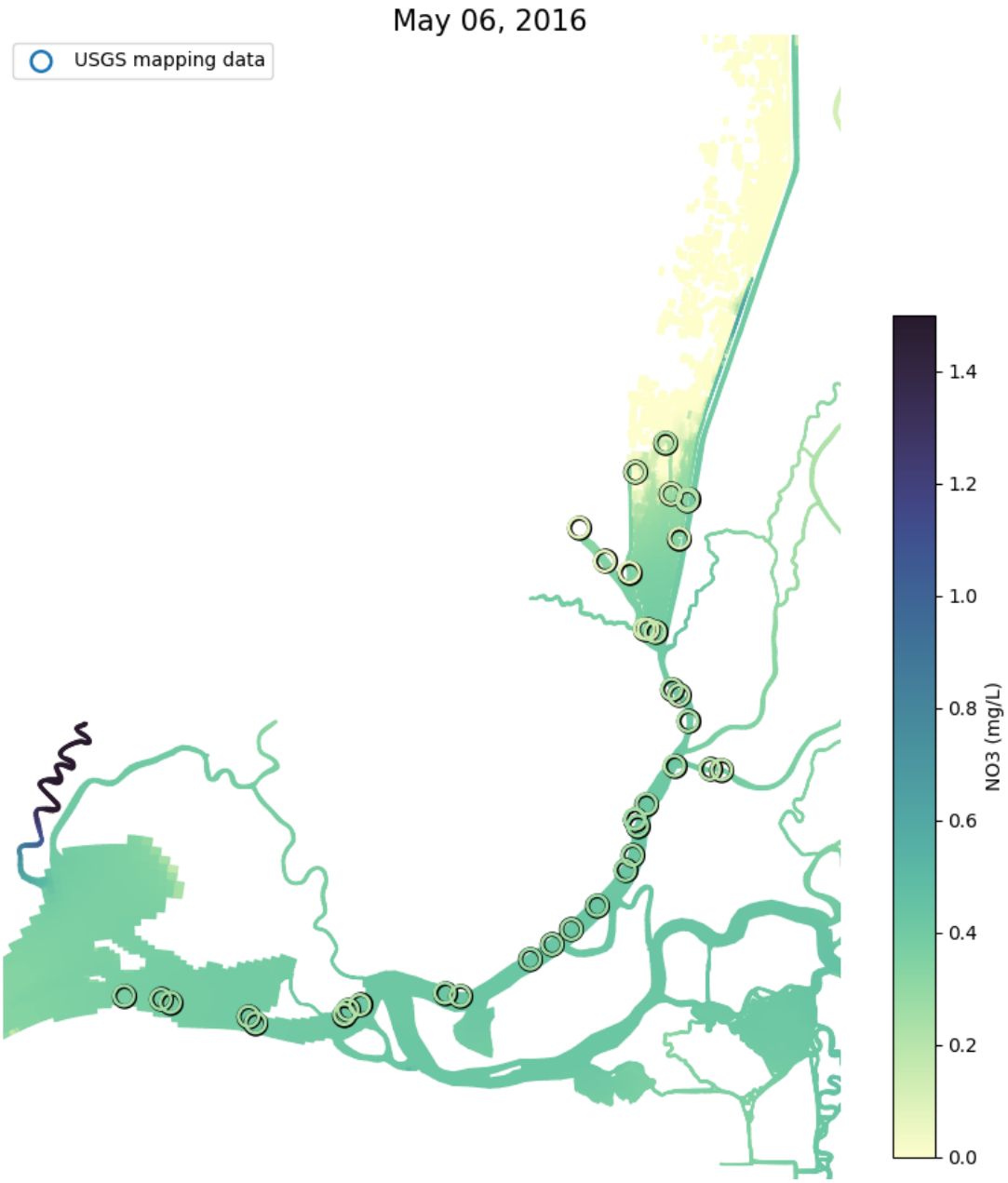

Note: Model results are shown in the map (as a daily and depth-averaged concentration) while the high frequency mapping data is shown as the overlying circles, with circle colors scaled in the same manner as the model results.

Figure 3.29. Model validation with mapping cruise data on May 6, 2016 for nitrate.

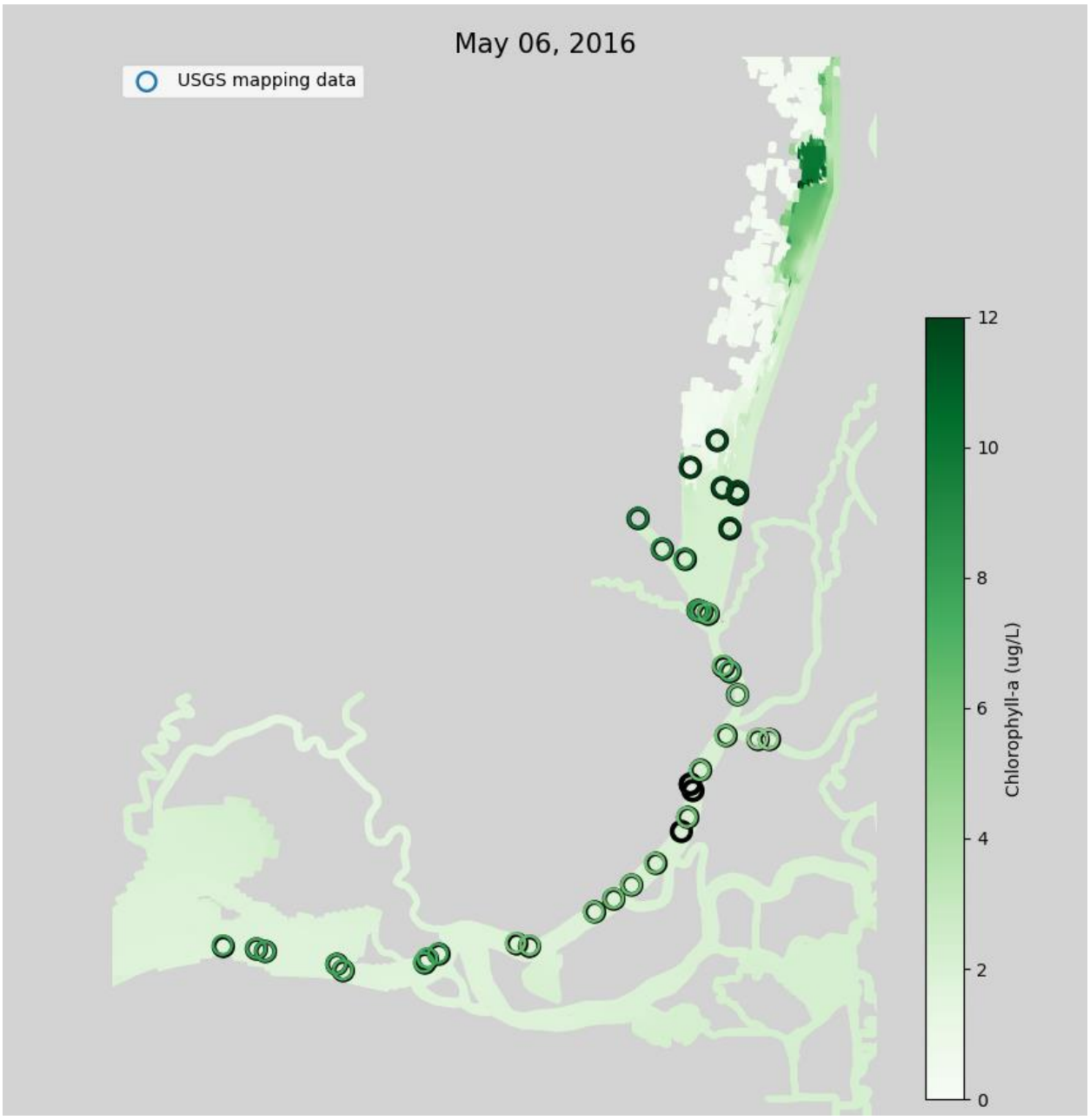

Note: Model results are shown in the map (as a daily and depth-averaged concentration) while the high frequency mapping data is shown as the overlying circles, with circle colors scaled in the same manner as the model results.

Figure 3.30. Model validation with mapping cruise data on May 6, 2016 for chlorophyll-a.

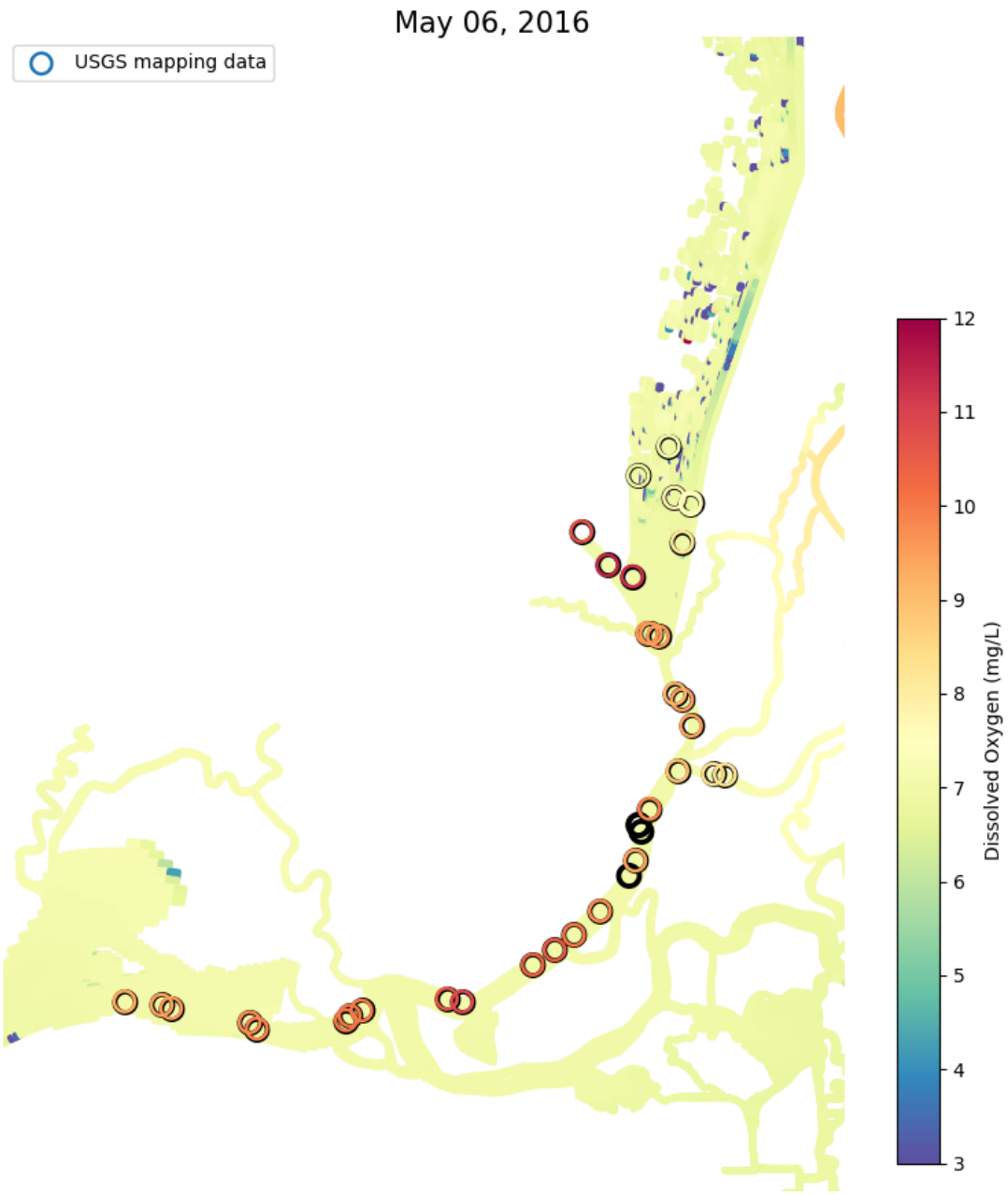

Note: Model results are shown in the map (as a daily and depth-averaged concentration) while the high frequency mapping data is shown as the overlying circles, with circle colors scaled in the same manner as the model results.

Figure 3.31. Model validation with mapping cruise data on May 6, 2016 for dissolved oxygen.

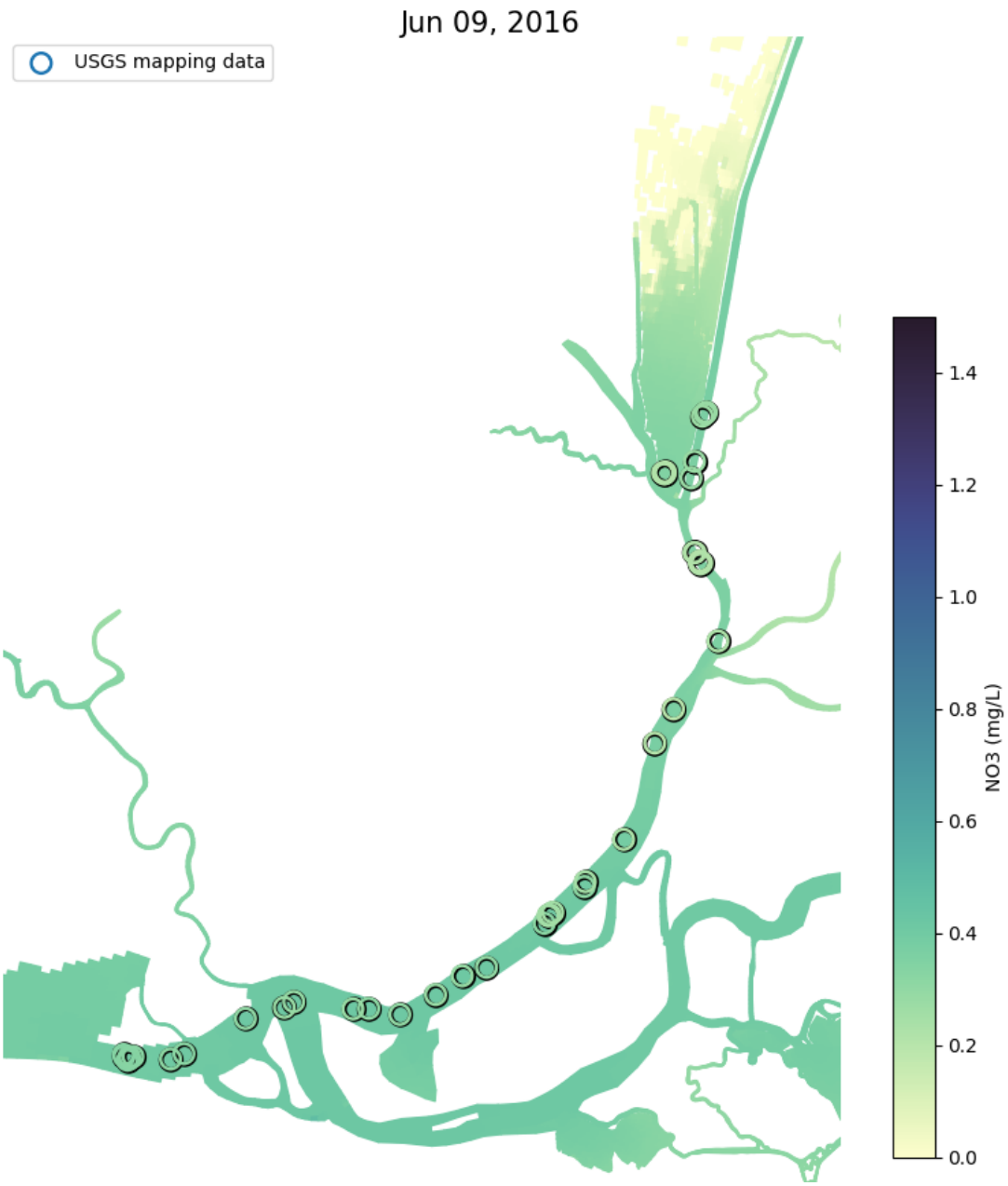

Note: Model results are shown in the map (as a daily and depth-averaged concentration) while the high frequency mapping data is shown as the overlying circles, with circle colors scaled in the same manner as the model results.

Figure 3.32. Model validation with mapping cruise data on June 9, 2016 for nitrate.

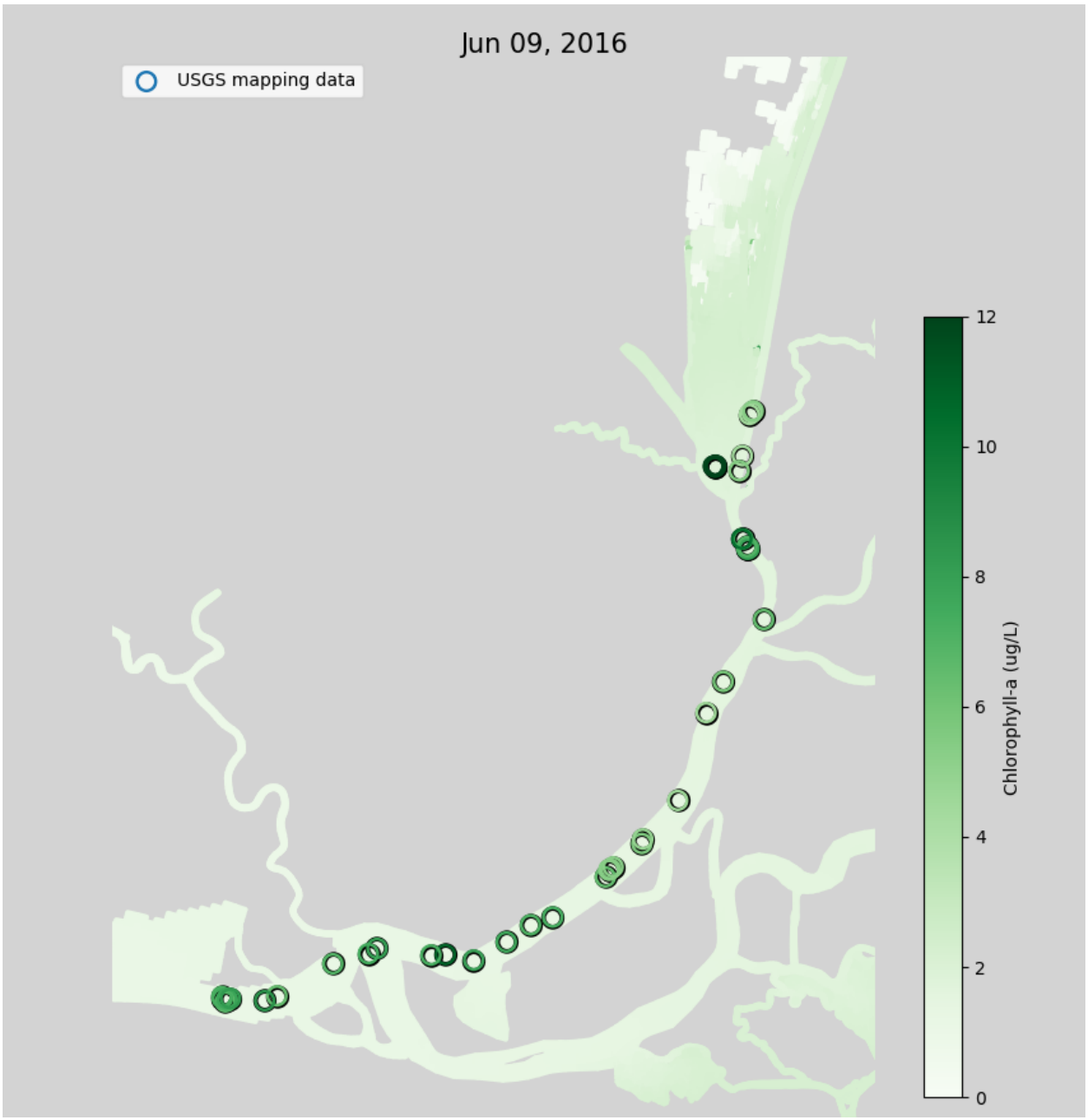

Note: Model results are shown in the map (as a daily and depth-averaged concentration) while the high frequency mapping data is shown as the overlying circles, with circle colors scaled in the same manner as the model results.

Figure 3.33. Model validation with mapping cruise data on June 9, 2016 for chlorophyll-a.

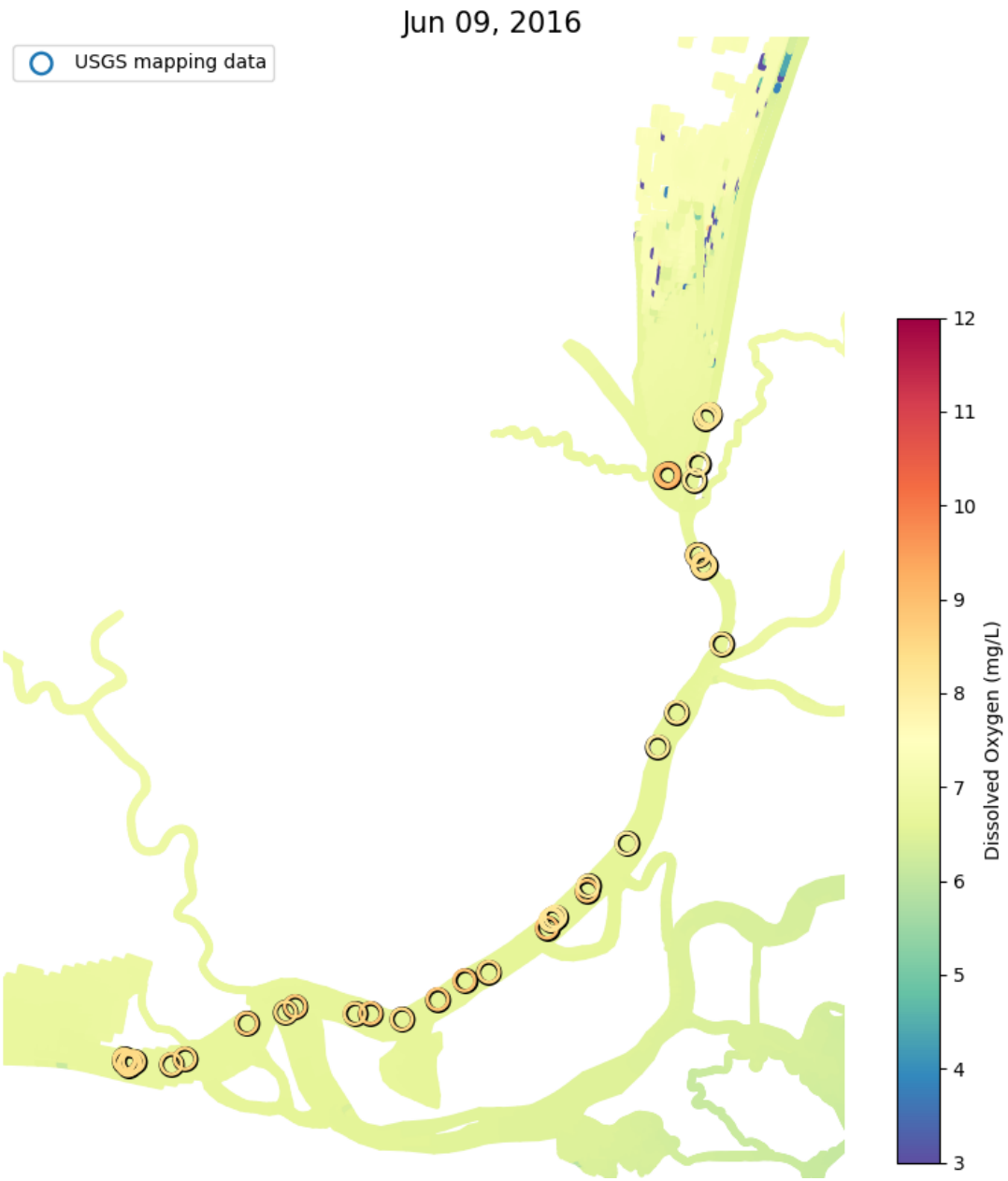

Note: Model results are shown in the map (as a daily and depth-averaged concentration) while the high frequency mapping data is shown as the overlying circles, with circle colors scaled in the same manner as the model results.

Figure 3.34. Model validation with mapping cruise data on June 9, 2016 for dissolved oxygen.

In conjunction with the moored sensor data, overall, the mapping cruises suggest that the May/June bloom originated upstream of Decker Island (potentially even upstream of Cache Slough in the Cache Slough Complex). The potential factors contributing to the model's inability to simulate these blooms were discussed earlier. However, the cruise data also show that the model successfully simulates nitrate gradients on all four dates, which further confirms that the model's inability to simulate the blooms does not severely limit its utility to simulate the large-scale nutrient dynamics in the Delta.

3.5 Grazing

The grazing rates simulated for WY2011 from the SFEI model were compared to the rates used as boundary conditions in the USGS model. These grazing rates effectively represent a grazing pressure imposed on diatoms by benthic grazers (consumption of detritus and other organic matter is out of the scope of the current project). Modeled grazing rates are plotted in both mass units ($gC/m^2/day$) as well as volumetric units ($m^3/m^2/day$) for December 2010, and April and June 2011 in Figures 3.35 – 3.37 respectively. The grazing rates imposed in the USGS model for these months (specified as monthly averages of the volumetric filtration rate) are also shown in these figures. The daily (SFEI) model output of clam diatom consumption ($gC/m^2/day$) was converted to volumetric units by dividing by the corresponding diatom concentration (gC/m^3) in the bottom cell of the water layer. To keep the presentation consistent with the USGS model's imposed grazing rate, the daily (SFEI) model outputs were converted to monthly averages for the months shown in Figures 3.35 – 3.37.

The imposed (USGS model) and simulated (SFEI model) grazing rates show various similarities: relatively low grazing levels in December and higher grazing levels in June. Grazing is generally higher in Suisun Bay, which is dominated by *Potamocorbula* (a saltwater clam) compared to interior Delta and Cache Slough where the freshwater clam *Corbicula* is more prevalent; within Suisun Bay, shallow areas such as Grizzly Bay have greater grazing compared to the channel. Higher grazing rates are present in the central Delta near Frank's Tract and in the northern portions of Old and Middle rivers.

However, there are also important differences: grazing rates are higher in April in the SFEI model in general, while the USGS model does not appreciably differ in the imposed grazing between December and April; moreover, in both April and June, grazing is substantially higher in the SFEI model within the Cache Slough Complex, the San Joaquin River, and the south Delta, and there is also a small but non-zero grazing in the upper Sacramento River in the SFEI model, whereas the USGS model does not impose any grazing in that area.

While there are some inherent uncertainties in comparing these volumetric rates—for example, the SFEI model volumetric rates may over (or under) estimate grazing when the diatom concentrations are under (or over) estimated in the model—the comparison above illustrates that DEB model predictions loosely capture the seasonality (fall to spring changes) imposed in the USGS model. Furthermore, the SFEI model's prediction of chl-a concentrations is generally consistent with observations (see Figure 3.14). This suggests that: 1) the grazing pressure simulated within the model (at least in the areas where there are discrete chl-a measurements) is reasonable; and 2) the uncertainty in the conversion to a volumetric rate is probably small, particularly in June when the watershed-derived organic matter loading is small and much of the organic matter in the system is autochthonous. These results also provide confidence that the balance between top-down control on phytoplankton is appropriately imposed in the model in WY2011. Considering that the top-down control is dynamic in the DEB model, with appropriate initial conditions and the current set of parameters, the model appears to generally provide acceptable time-varying grazing.

These results also show that conditions in WY2016 were unusual due to the March 2016 large freshwater inflow event in Cache Slough Complex that probably reset the grazer balance even if only for one to two growing seasons (see Figures 2.17 and 2.18, the clam populations rebounded by the end of WY2017). Improved grazer measurements in Cache Slough and the south Delta (areas where there is

divergence between the imposed grazing pressure in the USGS model and the SFEI model) will provide more reliable top-down control in the DEB model simulations.

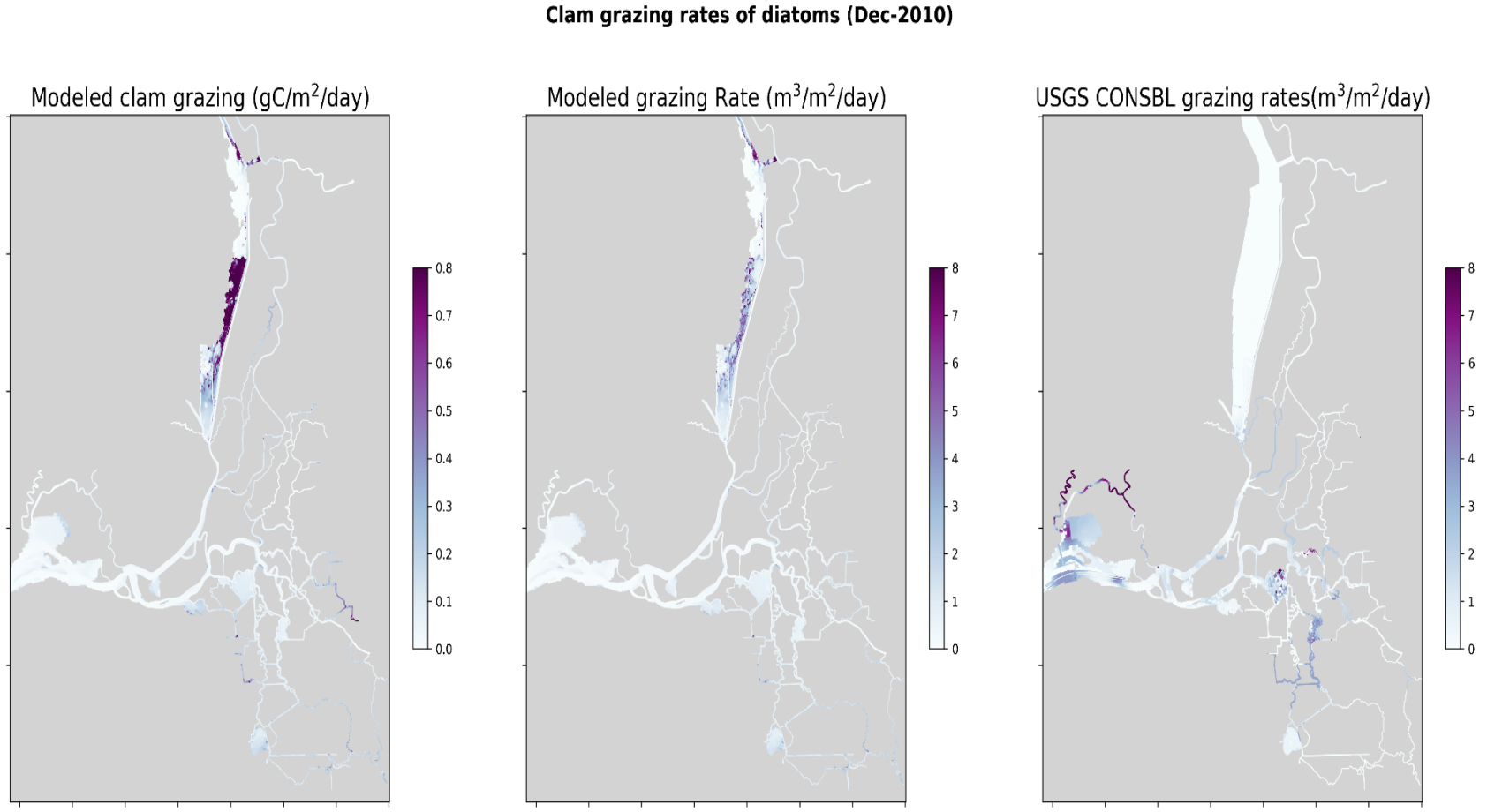

Figure 3.35. WY2011 modelled grazing rates compared to U.S. Geological Survey CONSBL grazing rates (December 2010).

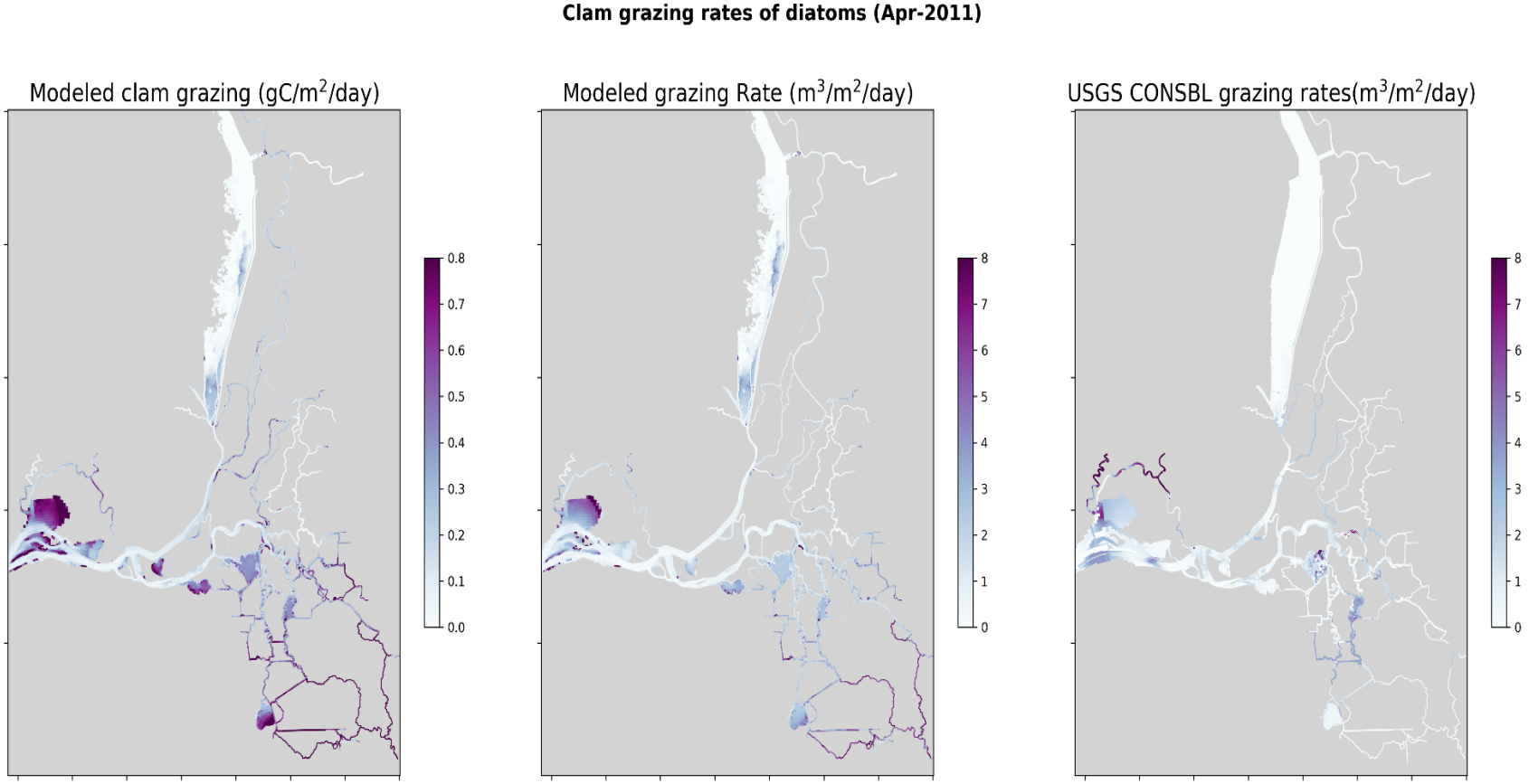

Figure 3.36. WY2011 modelled grazing rates compared to U.S. Geological Survey CONSBL grazing rates (April 2011).

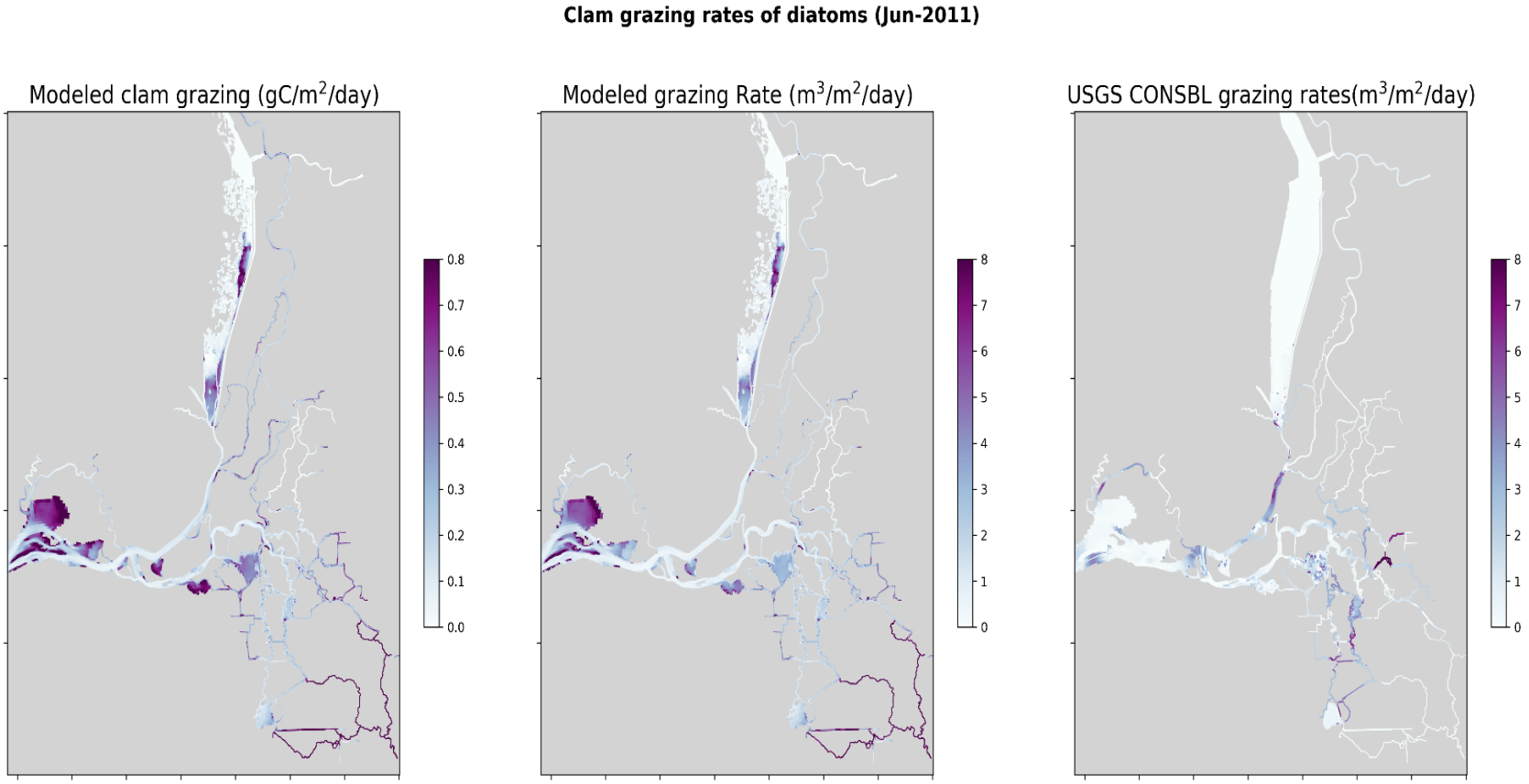

Figure 3.37. WY2011 modelled grazing rates compared to U.S. Geological Survey CONSBL grazing rates (June 2011).

4 Summary

This report described recent work updating the northern San Francisco Estuary Biogeochemical Model (nSFE-BGCMv2), including calibration and simulation across two water years that differed considerably in both their physical forcings (dry vs. wet) and biogeochemical responses (WY2016, WY2011). The model was initialized with spatially-varying concentration fields and clam biomass in order to provide a most-realistic-possible model start, which proved especially important during WY2016 model spin-up because of drought and low-flow conditions during summer and fall 2015. An empirically-derived, space-and-time varying light attenuation coefficient field was also developed to serve as model input for estimating light availability. In addition, refinements were made to the sediment diagenesis and grazing modules, along with tuning of water column rates and calibration/validation of a dynamic grazing model.

To identify the best-current calibration, emphasis was placed on best capturing spatial and seasonal variability across both years for nitrogen cycling and fluxes alongside phytoplankton production and biomass. The model performed well for both water years, especially with regards to predicting seasonal, spatial, and inter-annual variations in DIN concentrations and DIN speciation, and NO3 flux (at locations with appropriate data to calculate observed fluxes). Dissolved inorganic nitrogen is well-captured along the upper Sacramento River, and the general phasing and magnitude of the DIN signal throughout the Delta suggests that the main processes affecting DIN are accurately represented. In terms of phytoplankton production and biomass, the model captures the generally low chl-a concentrations that define the system throughout most of both water years, and also reproduces the key features (approximate timing and magnitude) of a modest bloom event in Suisun Bay in WY2011. As of now, however, the model does not capture several short-lived bloom events in WY2016. The mechanisms precipitating these blooms remains a subject of ongoing inquiry, which makes validating our model's performance difficult. It is possible some of these 2016 bloom events may have originated from stratification events, however, we did not evaluate the correlation between stratification and bloom events within the Delta for this modeling effort. Validation with several high-frequency datasets offered insight into model performance, indicating that the SFEI model can successfully capture large spatial gradients in DIN (moving across the Delta east-to-west) and reliably predict nitrate mass fluxes. There was better agreement between observed and modeled nitrate fluxes than chl-a fluxes, which mainly resulted from the above-noted periods when biomass was not adequately reproduced.

One major focus of upcoming work will be applying the model to extract mechanistic insights, e.g., related to nutrient sources, transport, and fate (cycling, losses, using mass balance approaches); predicting the influence of the Regional San upgrade on ambient nutrient concentrations and fluxes (including exports to Suisun Bay) and subsequent changes in response (e.g., phytoplankton production); and exploring factors or conditions under which phytoplankton production may increase or decrease. As with any model, there also remain uncertainties or areas for continued improvement. Upcoming rounds of model refinements could focus on better capturing the bloom events in spring/summer of WY2016. This work would involve mass balance evaluations to better identify dominant mechanisms (e.g., light limitation, grazing, flushing rates) followed by targeted calibration. That topic, and the mass-balance diagnostic approach, also lends itself to applications related to understanding what conditions could result in higher or lower production in the future. For some applications, there may be benefit to refining the hydrodynamic model (specifically in the Cache Slough Complex). Lastly, the abundance of water column organic nutrient data (DON, PON) in the Delta-Suisun region from long-term EMP

monitoring could make it possible to substantially improve the model's ability to predict organic/detrital carbon and nutrient pools, which would be valuable for exploring food availability.

5 References

Bergamaschi, B.A., Kraus, T.E.C., Downing, B.D., O'Donnell, K., Hansen, A.M., Etheridge, A.B., Stumpner, E.B., Richardson, E.T., Hansen, J.A., Soto Perez, J., Delascagigas, A., Sturgeon, C.L., Von Hoyningen Huene, B.L., and Gelber, A.D. Assessing spatial variability of nutrients, phytoplankton and related water-quality constituents in the California Sacramento-San Joaquin Delta at the landscape scale: 2020 High-resolution mapping surveys: , https://doi.org/10.5066/P90VYUBX.

Bergamaschi, B.A., Downing, B.D., Kraus, T.E.C., and Pellerin, B.A. 2017. Designing a high-frequency nutrient and biogeochemical monitoring network for the Sacramento–San Joaquin Delta, northern California. U.S. Geological Survey Scientific Investigations Report 2017–5058. https://doi.org/10.3133/sir20175058.

Cloern, J.E. 1982. Does the benthos control phytoplankton biomass in south San Francisco Bay? *Marine Ecology Progress Series* 9:191-202.

Crauder, J.S., Thompson, J.K., Parchaso, F., Anduaga, R.I., Pearson, S.A., Gehrts, K., Fuller, H., Wells, E. 2016. *Bivalve effects on the food web supporting delta smelt - A long-term study of bivalve recruitment, biomass, and grazing rate patterns with varying freshwater outflow*. U.S. Geological Survey Report No. 2016–1005, Open-File Report. https://doi.org/10.3133/ofr20161005

Dahm, C.N, Parker, A.E, Adelson, A.E, Christman, M.A, and Bergamaschi, B.A. 2016. Nutrient dynamics of the Delta: effects on primary producers. *San Francisco Estuary and Watershed Science* 14(4).

Deltares. 2019a. D-Flow Flexible Mesh, User Manual: Delft3D Flexible Mesh Suite. Version 1.5.0. January.

Deltares. 2019b. D-Water Quality, User Manual: Delft3D Flexible Mesh Suite. Version 1.1. January.

Downing, B.D., Bergamaschi, B.A., Kendall, C., Kraus, T.E., Dennis, K.J., Carter, J.A. and Von Dessonneck, T.S., 2016. Using continuous underway isotope measurements to map water residence time in hydrodynamically complex tidal environments. Environmental science & technology, 50(24), pp.13387-13396.

Downing, B.D., Boss, E., Bergamaschi, B.A., Fleck, J.A., Lionberger, M.A., Ganju, N.K., Schoellhamer, D.H. and Fujii, R., 2009. Quantifying fluxes and characterizing compositional changes of dissolved organic matter in aquatic systems in situ using combined acoustic and optical measurements. Limnology and Oceanography: Methods, 7(1), pp.119-131.

Downing, B.D., Pellerin, B.A., Bergamaschi, B.A., Saraceno, J.F. and Kraus, T.E., 2012. Seeing the light: The effects of particles, dissolved materials, and temperature on in situ measurements of DOM fluorescence in rivers and streams. Limnology and Oceanography: Methods, 10(10), pp.767-775.

Downing, B.D., Bergamaschi, B.A., and Kraus, T.E.C. 2017. *Synthesis of data from high-frequency nutrient and associated biogeochemical monitoring for the Sacramento–San Joaquin Delta, northern California*. U.S. Geological Survey Scientific Investigations Report 2017–5066. https://doi.org/10.3133/sir20175066

Jassby, A. 2008. Phytoplankton in the upper San Francisco Estuary: recent biomass trends, their causes, and their trophic significance. *San Francisco Estuary and Watershed Science* 6(1).

Kimmerer, W.J. 2006. Response of anchovies dampens effects of the invasive bivalve Corbula amurensis on the San Francisco Estuary foodweb. *Marine Ecology Progress Series* 324:207- 218

Kimmerer, W.J., Ignoffo, T.R., Slaughter, A.M., and Gould, A.L. 2014. Food-limited reproduction and growth of three copepod species in the low-salinity zone of the San Francisco Estuary. *Journal of Plankton Research* 36:722– 735.

Kraus, T.E.C., Bergamaschi, B.A., and Downing, B.D. 2017. *An introduction to high-frequency nutrient and biogeochemical monitoring for the Sacramento–San Joaquin Delta, northern California*. U.S. Geological Survey Scientific Investigations Report 2017–5071. https://doi.org/10.3133/sir20175071.

Kraus, T.E.C., O'Donnell, K., Downing, B. D., Burau, J. R., & Bergamaschi, B. A. (2017). Using paired in situ high frequency nitrate measurements to better understand controls on nitrate concentrations and estimate nitrification rates in a waste water impacted river. Water Resources Research, 53, 8423–8442. https://doi.org/10.1002/2017WR020670

Lesmeister, S., and Martinez, M. 2020. Interagency Ecological Program: discrete water quality monitoring in the Sacramento–San Joaquin Bay–Delta, collected by the Environmental Monitoring Program, 2000–2018. Environmental Data Initiative.

Martinez, M. and S. Perry. 2021. Interagency Ecological Program: Discrete water quality monitoring in the Sacramento-San Joaquin Bay-Delta, collected by the Environmental Monitoring Program, 1975-2020. ver 4. Environmental Data Initiative. https://doi.org/10.6073/pasta/31f724011cae3d51b2c31c6d144b60b0 (Accessed 2021-09-30).

Levesque, V.A., and Oberg, K.A. 2012. *Computing discharge using the index velocity method*. U.S. Geological Survey Techniques and Methods 3–A23.

Lopez, C.B., Cloern, J.E., Schraga, T.S., Little, A.J., Lucas, L.V., Thompson, J.K., and Burau, J.R. 2006. Ecological Values of Shallow-Water Habitats: Implications for the Restoration of Disturbed Ecosystems. *Ecosystems* 9:422–440.

Lucas, L.V., and Thompson, J.K. 2012. Changing restoration rules: Exotic bivalves interact with residence time and depth to control phytoplankton productivity. *Ecosphere* 3(12):1-26.

Lucas, L.V., Cloern, J.E., Thompson, J.K., Stacey, M.T. and Koseff, J.R. 2016. Bivalve grazing can shape phytoplankton communities. *Frontiers in Marine Science* 3:14.

Martyr-Koller, R.C., Kernkamp, H.W.J., van Dam, A., van der Wegen, M., Lucas, L.V., Knowles, N., Jaffe, B., and Fregoso, T.A. 2017. Application of an unstructured 3D finite volume numerical model to flows and salinity dynamics in the San Francisco Bay-Delta. *Estuarine, Coastal and Shelf Science* 192:86–107.

Paerl, H.W. Controlling eutrophication along the freshwater–marine continuum: dual nutrient (N and P) reductions are essential. *Estuaries and Coasts* 32(4):593-601.

Paraska, D.W., Hipsey, M.R., and Salmon, S.U., 2014. Sediment diagenesis models: Review of approaches, challenges and opportunities, Environmental Modelling and Software, 61: 297-325, doi: http://dx.doi.org/10.1016/j.envsoft.2014.05.011

Pellerin, B.A., Bergamaschi, B.A., Downing, B.D., Saraceno, J.F., Garrett, J.A., and Olsen, L.D. 2013. *Optical techniques for the determination of nitrate in environmental waters: Guidelines for instrument selection, operation, deployment, maintenance, quality assurance, and data reporting.* U.S. Geological Survey Techniques and Methods 1–D5.

Peterson, David H., John F. Festa, and T. John Conomos. "Numerical simulation of dissolved silica in the San Fancisco Bay." Estuarine and Coastal Marine Science 7.2 (1978): 99-116.

Petter, G., Weitere, M. Richter, O. and Moenickes, S. 2014. Consequences of altered temperature and food conditions for individuals and populations: a dynamic energy budget analysis for Corbicula fluminea in the Rhine. *Freshwater Biology* 59(4):832-846.

Ruhl, C.A., and Simpson, M.R. 2005. *Computation of discharge using the index-velocity method in tidally affected areas, 1–41*. U.S. Geological Survey.

Schraga, T.S., and Cloern, J.E. 2017. Water quality measurements in San Francisco Bay by the US Geological Survey, 1969–2015. *Scientific Data* 4(1):1-14.

Schraga, T.S., Nejad, E.S., Martin, C.A., and Cloern, J.E. 2020, *USGS measurements of water quality in San Francisco Bay (CA), beginning in 2016 (ver. 3.0, March 2020)*. U.S. Geological Survey data release. https://doi.org/10.5066/F7D21WGF.

SFEI (San Francisco Estuary Institute). 2015. *Characterizing and quantifying nutrient sources, sinks and transformations in the Delta: synthesis, modeling, and recommendations for monitoring*. SFEI Contribution No. 785. San Francisco Estuary Institute, Richmond, CA.

SFEI 2018a. *Hydrodynamic and Water Quality Model Calibration and Application in San Francisco Bay*. SFEI Contribution No. 913. San Francisco Estuary Institute, Richmond, CA.

SFEI. 2018b. *Delta-Suisun Biogeochemical Model Development: Year 1 Progress*. SFEI Contribution No. 960. San Francisco Estuary Institute: Richmond, CA.

SFEI. 2019a. *Delta-Suisun Biogeochemical Model Development: Year 2 Progress*. SFEI Contribution No. 961. San Francisco Estuary Institute: Richmond, CA.

SFEI. 2019b. *Hydrodynamic Model Development Report: Sacramento-San Joaquin River Delta and Suisun Bay (Water Year 2016)*. SFEI Contribution No. 964. San Francisco Estuary Institute: Richmond, CA.

SFEI. 2019c. *Wind Over San Francisco Bay and the Sacramento-San Joaquin River Delta: Forcing for Hydrodynamic Models*. SFEI Contribution No. 937. San Francisco Estuary Institute: Richmond, CA.

SFEI. 2020a. *Changing nitrogen inputs to the northern San Francisco Estuary: Potential ecosystem responses and opportunities for investigation*. SFEI Contribution No. 1006. San Francisco Estuary Institute: Richmond, CA.

SFEI. 2020b. *San Francisco Bay Numerical Modeling: FY2020 Update, Draft Report*. SFEI Contribution No. 1006. San Francisco Estuary Institute: Richmond, CA.

SFEI. 2020c. *Delta Biogeochemical Model, WY2016: Progress Update*. SFEI Contribution No. 1021. San Francisco Estuary Institute: Richmond, CA.

Troost, T.A., Wijsman, J.W., Saraiva, S., and Freitas, V. 2010. Modelling shellfish growth with dynamic energy budget models: an application for cockles and mussels in the Oosterschelde (southwest Netherlands). *Philosophical Transactions of the Royal Society of London Series B, Biological Sciences* 365(1557):3567–3577.

Troost, T.A., Desclaux, T., Leslie, H.A., van Der Meulen, M.D., and Vethaak, A.D. 2018. Do microplastics affect marine ecosystem productivity? *Marine Pollution Bulletin* 135: 17-29.

Vroom, J., van der Wegen, M., Martyr Koller, R.C., and Lucas, L.V. 2017. What determines water temperature dynamics in the San Francisco Bay-Delta system? *Water Resources Research* 53:9901–9921.

Wagner, R.J., Boulger, R.W., Jr., Oblinger, C.J., and Smith, B.A. 2006. *Guidelines and standard procedures for continuous water-quality monitors—Station operation, record computation, and data reporting*. U.S. Geological Survey Techniques and Methods 1–D3.

Wilde, F.D. 2018. *Field Measurements*. U.S. Geological Survey Techniques of Water-Resources Investigations, Book 9, Chap. A6.

Zierdt Smith, E.L, Parchaso, F., and Thompson, J.K., 2021, A spatially and temporally intensive sampling study of benthic community and bivalve metrics in the Sacramento-San Joaquin Delta (ver. 2.0, May 2021): U.S. Geological Survey data release, https://iep.ca.gov/Science-Synthesis-Service/Monitoring-Programs/EMP.